LEAD-FREE ORGANOMETALLIC PEROVSKITE CHARACTERIZATION FOR ENVIRONMENTALLY FRIENDLY SOLAR CELLS

by

İbrahim Şimşek

BS. in Chemical Engineering, Yıldız Technical University, 2011

Submitted to the Institute of Environmental Sciences in partial fulfillment of

the requirements for the degree of

Master of Science

in

Environmental Sciences

Boğaziçi University

2015

“The real voyage of discovery consists not in seeking new landscapes, but in having new eyes.”

Marcel Proust

ACKNOWLEDGEMENTS

First of all, I would like to offer my gratitude to my thesis supervisor Assoc. Prof. Burak Demirel, who dedicated his time for counseling, motivation and endless support. It was an honor for me to work with him during my graduate thesis, which was a great work to broaden my horizons and to have opportunity to see from different angles.

I would like to offer my special thanks to my thesis committee members, Assoc. Prof. Burak Demirel, Prof. Miray Bekbölet and Prof. Ramazan Yıldırım for their time and contributions.

I warmly thank to my dear colleagues; Dr. Amrita Mandal Bera, Dan Ralf Wargulski, Pascal Becker, Klara Sucher and Sergiu Levcenco for their endless support, help, and friendship.

I am very grateful to my supervisors in the Helmholtz Zentrum Berlin für Materialieren und Energy; Prof. Dr. Marcus Bär, Dr. Regan Wilks and Dr. Thomas Unold.

I have special thanks to Selen Solak who is mentoring me and directing me to go in the path which is decorated with solar cells.

I would like to thank to my family and my friends for their love and encouragement during this thesis.

LEAD-FREE ORGANOMETALLIC PEROVSKITE CHARACTERIZATION FOR ENVIRONMENTALLY FRIENDLY SOLAR CELLS

Solar energy is rapidly emerging to take place of the conventional energy sources due to its cheap and clean energy advantages. It is very important to obtain energy from solar cells for Turkey as well, since Turkey's nearly half of the energy sources are imported. One of the best way to accomplish this is using lead-free Perovskites in solar cells.

The goal of this study was to investigate the preparation and the material characterization methods of the lead-free organometallic Perovskite layers, which were obtained from the reaction of methyl ammonium iodide and various tin halide salts with the help of different polar-aprotic solvents. Applying this kind of Perovskite material prevents the lead-Perovskite's lead-originated environmental harms, which can show up when the solar panels complete their commercial lifetimes. It is very well known that the potential lead (Pb) exposure can cause decreased fertility, nerve disorders, high blood pressure and memory or concentration problems in human beings. In addition, replacement of DMF, which is usually used in literature with DMSO, prevents potential carcinogen effects of the solvent by inhalation, which may occur in the preparation phase of Perovskite layer.

In order to acquire homogenized lead-free perovskite layer for the experimental use, one step method, two step method and solid state method were applied in this study. After development of a homogenized lead-free Perovskite layer step, the layer was ready to be used with hole transport materials (HTM), blocking layers, back contact and front contact in order to obtain a high-efficient solar cell with Perovskite layer. At the end of the research, different kinds of the Perovskite were successfully synthesized and characterized by different material characterization methods. Since all the layers of solar cells need to be optimized separately, electrical characterization was not included in this work as a goal.

ÇEVRE DOSTU GÜNEŞ HÜCRELERİ İÇİN KURŞUNSUZ ORGANOMETALİK PEROVSKİTE KARAKTERİZASYONU

Güneş enerjisi, ucuz ve temiz enerji olması avantajlarıyla, alışılagelmiş enerji kaynaklarının yerini almak için hızlı bir yükseliş gösteriyor. Güneş hücrelerinden enerji üretmek de enerjisinin neredeyse yarısını ithal eden Türkiye için çok önemlidir. Bunu gerçekleştirmenin en iyi yollarından biri de güneş hücrelerinde kurşunsuz Perovskite kullanımıdır.

Bu çalışmanın amacı, metilamonyum iyodür (MAI) ile çeşitli kalay halojenür tuzlarının tepkimelerinden farklı polar-aprotik çözücülerin de yardımıyla elde edilen kurşunsuz ve organometalik Perovskitelerin hazırlanma ve kararterizasyon metotlarını tetkik etmektir. Bu tür bir Perovskite üretimi, kurşun-Perovskitelerin -güneş panellerinin ticari ömürleri bittiğinde ortaya çıkabilecek- kurşun kaynaklı çevresel zararlarını engeller. Zira olası kurşun maruziyeti doğurganlığın düşmesine, sinir hastalıklarına, yüksek kan basıncına ve hafıza ya da konsantrasyon problemlerine sebep olabilir. Ayrıca, literatürde genellikle kullanılan DMF'in DMSO ile değiştirilmesi, Perovskite tabakasının üretimi aşamasında oluşabilecek çözücü solunumlarının olası kanserojen etkilerini engeller.

Deneysel kullanım amacıyla homojenleştirilmiş kurşunsuz Perovskite üretimi için, tek adım metodu, iki adım metodu ve katı hal metodu uygulandı. Homojenleştirilmiş kurşunsuz Perovskite tabakası geliştirildikten sonra, tabaka; boşluk iletim malzemesi (HTM), blokaj tabakası, ön kontak ve arka kontak ile birlikte yüksek verimli Perovskite tabakalı güneş hücresi elde etmeye hazır hale getirilmiştir. Araştırma sonucunda farklı türde Perovskite türleri başarıyla sentezlenerek, malzeme karakterizasyon metotlarıyla karakterize edilmişlerdir. Güneş hücrelerini tüm tabakalari ayrı ayrı optimize edilmesi gerektiğinden elektriksel karakterizasyon bu çalışmada yer almamaktadır.

TABLE OF CONTENTS

ACKNOWLEDGEMENTS iv
ABSTRACT v
ÖZET vi
TABLE OF CONTENTS vii
LIST OF FIGURES ix
LIST OF TABLES xiii
LIST OF SYMBOLS/ABBREVIATIONS xiv
1. INTRODUCTION 1
2. LITERATURE SURVEY 4
2.1. Economic Direction of Photovoltaic Technology 4
2.1.1. Levelized Costs of Electricity 4
2.1.2. Feed in Tariff in Turkey 8
2.2. Photovoltaic Effect 9
2.3. Perovskite 10
2.4. Perovskite Solar Cells 11
2.5. Challenges 15
2.5.1. Stability 16
2.5.2. Material Limitations 17
3. MATERIALS AND METHODS 19
3.1. Materials of the Experiment 19
3.1.1. Methylammonium Iodide 19
3.1.2. Tin Halide Salts 20
3.1.3. Etched FTO Glasses 20
3.2. Experimental Work 21
3.2.1. Reaction Methods 21
3.2.1.1. One Step Method 21
3.2.1.2. Two Step Method (Sequential Deposition) 22
3.2.1.3. Solid-state Reaction Method 23
3.2.2. Coating Methods 24
3.3. Structural Characterization of the Materials 27

3.3.1. X-Ray Diffraction 28
3.3.2. Scanning Electron Microscope 29
3.3.3. Ultraviolet-Visible Spectroscopy 30
3.3.4. Photoluminescence Imaging 31
3.3.5. Current-Voltage (I-V) Curves 32
4. RESULTS AND DISCUSSION 33
4.1. One Step Method 33
4.1.1. Tin (II) Iodide 33
4.1.2. Tin (II) Chloride 35
4.2. Two Step Method (Sequential Deposition) 40
4.3. Solid State Reaction Method 40
4.3.1. Tin (II) Iodide 41
4.3.2. Tin (II) Bromide 44
4.3.2.1. Tin (II) Bromide for Different Reaction Temperatures 47
4.3.2.2. Tin (II) Bromide for Different Weight Concentrations 49
4.3.2.3. Tin (II) Bromide for Different MAI Concentrations 50
4.3.3. Tin (II) Chloride 51
4.4. Solvent Changing 54
4.4.1. Acetone 54
4.4.2. Dimethyl Sulfoxide (DMSO) 55
4.5. Further Investigations 58
4.5.1. Effects of the Glass Surface 59
4.5.2. Simulated Chemical Vapor Deposition 60
4.6. Overall Evaluation of the Experimental Work 62
5. CONCLUSIONS AND RECOMMENDATIONS 65
REFERENCES 66
APPENDIX: ELECTRICAL CHARACTERIZATION 73

LIST OF FIGURES

Figure 1.1. Comparison of OSC and PSC efficiency on the same time span 2

Figure 2.1. Scheme of the photovoltaic effect 9

Figure 2.2. Singular crystal and simulated lattice structure of Perovskite 11

Figure 2.3. Solid-state mesoscopic solar cell and SEM pictures of the cross-section 12

Figure 2.4. Certified solar cell efficiency chart 13

Figure 2.5. Cross-sectional SEM image of the device and color changing of Perovskite ($CH_3NH_3SnI_{3-x}Br_x$) for different bromide numbers 15

Figure 2.6. Scheme for the unification challenge of solar cells 16

Figure 3.1. Nitrogen filled glovebox 19

Figure 3.2. Different types of etched FTO glasses 21

Figure 3.3. Perovskite solutions which are prepared with different tin halide salts; $SnCl_2$, $SnBr_2$ and SnI_2 22

Figure 3.4. Schematic presentation of the two step method 22

Figure 3.5. Schematic presentation of the solid state reaction 23

Figure 3.6. Color changing in solid state reaction, before reaction, after reaction 23

Figure 3.7. Working principle of spin coaters 24

Figure 3.8. SCS spin coater 25

Figure 3.9. Different coating methods 25

Figure 3.10. Layers of the Perovskite solar cell 26

Figure 3.11. Back contact evaporator for gold or silver 27

Figure 3.12. Bragg reflection according to his law 28

Figure 3.13. Schematic shown of the SEM, EDS mapping 29

Figure 3.14. Transmittance, Reflectance measurements of the Uv-Vis Spectroscopy 30

Figure 3.15. Schematic shown of the Photoluminescence Imaging 31

Figure 4.1. XRD patterns for the experimental $MASnI_3$ and the reference 34

Figure 4.2. SEM images of the experimental $MASnI_3$ crystals 34

Figure 4.3. XRD pattern of the product from MAI and $SnCl_2$ 36

Figure 4.4. XRD patterns from the literature for different Perovskites: $MASnI_3$ and $MASnCl_3$ 36

Figure 4.5. XRD patterns of the experimental polycrystalline Perovskite 38

Figure 4.6. SEM images of the experimental polycrystalline $MASnI_{3-x}Cl_x$ crystals 38

Figure 4.7. PL result for the mixed Cl-I based tin Perovskite sample 39

Figure 4.8. Degraded chlorine based tin Perovskite 39

Figure 4.9. Image of tin (II) chloride for the sequential deposition method 40

Figure 4.10. XRD pattern for the experimental $MASnI_3$ of solid state reaction 41

Figure 4.11. SEM images of the experimental $MASnI_3$ crystals of solid state reaction 42

Figure 4.12. Prepared $MASnI_3$ by the solid state reaction method 42

Figure 4.13. Prepared $MASnI_3$ crystals of solid state reaction while annealing 43

Figure 4.14. PL result for the pure iodine tin Perovskite of the solid state reaction 43

Figure 4.15. XRD pattern for the experimental $MASnIBr_2$ of solid state reaction 44

Figure 4.16. SEM images of the experimental $MASnIBr_2$ crystals 45

Figure 4.17. PL result for the Br-I mixed tin Perovskite of the solid state reaction 46

Figure 4.18. Uv-Vis pattern for the experimental $MASnIBr_2$ of solid state reaction 46

Figure 4.19. Uv-Vis pattern for the bromine-iodine mixed tin Perovskites 46

Figure 4.20. XRD patterns of the $MASnIBr_2$ for different reaction temperatures 47

Figure 4.21. Final product selectivity due to the reaction temperature 48

Figure 4.22. XRD patterns for the Br-I combinations of the tin Perovskite 49

Figure 4.23. Final product selectivity due to the concentration of the precursors 49

Figure 4.24. The investigation for the effects of different MAI concentrations 50

Figure 4.25. XRD patterns of the experimental $MASnI_{3-x}Cl_x$ for solid state reaction 51

Figure 4.26. Life-time comparison of the same Cl-I mixed tin Perovskite sample 52

Figure 4.27. SEM images of the experimental $MASnI_{3-x}Cl_x$ crystals 52

Figure 4.28. EDX images of the $MASnI_{3-x}Cl_x$ crystals of solid state reaction 53

Figure 4.29. Undissolved precursor of the bromide based tin Perovskite 54

Figure 4.30. Partial solubility of the precursors in acetone 55

Figure 4.31. XRD pattern for the tin bromide Perovskite produced with DMSO 56

Figure 4.32. Final product selectivity due to the concentration of the precursors 57

Figure 4.33. SEM images of the experimental $MASnIBr_2$ crystals 57

Figure 4.34. PL result for the Br-I tin Perovskite which is produced with DMSO 58

Figure 4.35. SEM images of the $MASnIBr_2$ crystals on FTO 59

Figure 4.36. SEM images of the $MASnIBr_2$ crystals on titania 60

Figure 4.37. Low-budget CVD method simulation 61

Figure 4.38. SEM images of the $MASnI_3$ crystals of simulated CVD 61

Figure A.1. Spiro-MeOTAD and gold back contact coatings 74

Figure A.2. Electrical characterization under the solar simulator 75

LIST OF TABLES

Table 2.1. Hypothetical levelized cost of electricity 6

Table 2.2. Economic comparison of the dispatchable and intermittent technologies 7

Table 2.3. Feed in Tariff policy of Turkey for renewable energy plants 8

Table 4.1. Experimental band gap energy results 62

LIST OF SYMBOLS/ABBREVIATIONS

Symbol	Explanation
Å	Angstrom
AM	Air Mass
BESS	Battery Energy Storage System
c-Si	Crystalline Silicon
CdTe	Cadmium Telluride
CIGS	Copper Indium Gallium Selenide
CVD	Chemical Vapor Deposition
DMF	Dimethyl Formamide
DMSO	Dimethyl Sulfoxide
DSSC	Dye-Sensitized Solar Cell
E_g	Band Gap Energy, eV
EMRA	Energy Market Regulatory Authority
ETM	Electron Transport Material
FiT	Feed in Tariff
FTO	Fluorine doped Tin Oxide
HOMO	Highest Occupied Molecular Orbital
HTM	Hole Transport Material
IARC	International Agency for Research on Cancer
Imec	Interuniversity Microelectronics Centre
LCOE	Levelized Cost of Electricity
LUMO	Lowest Unoccupied Molecular Orbital
MACl	Methyl Ammonium Chloride
MAI	Methyl Ammonium Iodide
$MAPbI_3$	Methyl Ammonium Lead Triiodide
OSC	Organic Solar Cell
PL	Photoluminescence
PV	Photovoltaic
PSC	Perovskite Solar Cell
SEM	Scanning Electron Microscope

SSC	Silicon Solar Cell
ssDSSC	Solid State Dye-Sensitized Solar Cell
TCO	Transparent Conductive Oxide
Uv-Vis	Ultraviolet-Visible Spectroscopy
wt	Weight, g
XRD	X-Ray Diffraction

1. INTRODUCTION

Solar energy has great theoretical potential and it is considered as the most important renewable energy source with its unlimited access. Aside from the very occasional solar eclipse, the sun is a reliable source of energy that the human race can depend on for the next five billion years.

The amount of solar energy received per day is a thousand times greater than the energy needs of the world and this natural potential waits to be used. Especially, the photovoltaic (PV) systems, which directly transform the sunlight into electricity, seem to have a significant importance in this pursuit of alternative energy sources (Dennler et al., 2009). For the purpose of generating electricity, solar energy has a great advantage upon the fossil fuels, which is being environmentally friendly.

According to a PV report of UK Trade & Investment from 2012, PV technology has the fastest growing market in the global range and it has the largest amount of investment among the renewable energy sources (UK Trade & Investment, 2012). However, the cost of PV system is high and it depends not only on the technological improvements, but also on installation, projecting, operation and finance.

The first generation PV technology, which is based on inorganic semiconductors (particularly single crystal and polycrystalline silicon cells), have been commercially available for the past 50 years. Crystalline silicon-wafer based (c-Si) solar cells are used predominantly in order to achieve direct conversion of sunlight energy into electricity. The production and operation cost of c-Si solar cells has fallen to a point, where sunlight can now compete with fossil fuels in some parts of the world.

Whether the decrease rate of the cost or even the current cost of c-Si solar cells is sustainable, there are still so many open questions about solar technology. This has led to increased research and development exertions in alternative solar cell technologies that may lead to further cost reductions and wider adoption of solar energy production. Thin-film solar

cell technology is one of the promising progeny of these efforts, which can be considered as second generation, and it has been studied extensively as an alternative to the sumptuous first generation PV systems.

At the end of the first decade of the 21st century, scientists gave to the idea of using Perovskite for the manufacture of dye-sensitized solar cell (DSSC) a shot. These solar cells can reduce the expense of PV systems, they can be potentially produced in high volumes, and they are more flexible than the conventional silicon solar cells (SSC).

On the other hand, the first trials of Perovskite based solar cells were made of methyl ammonium lead triiodide ($MAPbI_3$), which was toxic due to its lead (Pb) content. However, they converted solar energy into electricity with 3.8% efficiency at their first shot. Now, the lead-Perovskite solar cell produced by Yang et al. (2014) notched up 19.3% efficiency, which was good enough to compete with traditional silicon based solar cells (Green et al. 2014). Different efficiencies can be seen in Figure 1.1 for organic solar cells (OSC) and Perovskite solar cells (Burn and Meredith, 2014).

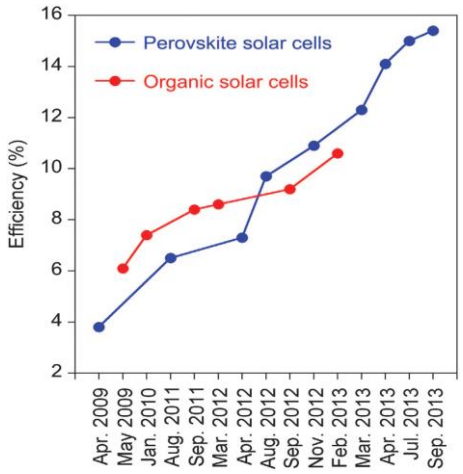

Figure 1.1. Comparison of OSC and PSC efficiency on the same time span (Burn and Meredith, 2014).

After these advancements, the most important imperfection of the lead-Perovskite solar cell was the lead based toxicity. At that point, the structure engineering grabbed the flag. While changing Perovskite structure with another substitute, a few necessary substitution properties should be considered; e.g. toxicity, feasibility, attainability and stability. In our

case, exchanging lead with tin would definitely remove the toxicity. Lead and tin are at the same periodical group, which means that their chemical properties are similar; that makes the exchange theoretically feasible. Tin is cheaper than lead and it is easily reachable; these make tin attainable. Therefore, the stability of tin Perovskite after exchange will be the main subject of this work.

In addition, dimethylformamide (DMF) is the most common solvent for Perovskites in literature. During preliminary research, we observed that tin (II) chloride salt could be dissolved in acetone easily; but the other salts could not, and chloride including tin Perovskite was known to be more efficient than the others. Therefore, with possible solvent exchange, the product can be made environmentally friendly even at the production point, since DMF is classified as a possible carcinogen by the International Agency for Research on Cancer (IARC) and DMF exposure have been associated with many reports of liver disease and damage on developing fetus. In addition, dimethylsulfoxide (DMSO) is also a less-harmful alternative to DMF.

In summary, a small step for metallic exchange procedure has taken recently; with a little deficiency, lead has been exchanged with tin. Improvement methods for exchange are still being developed. When the lead-Perovskite based device has reached the 15% efficiency, first tin-Perovskite based device has been recorded as 5.73% efficiency, which is a good start. This starting point reenergized the solar cell field and now the scientist believe that the tin-Perovskite can reach the record of lead-Perovskite solar cells and possibly surpass. On the other side, lead-Perovskite researches are ongoing as well, because they had started in 2008 and within this short period of time they had tremendous improvements. Lead Perovskites will be used as perfect templates for tin-Perovskite based solar cells. However, if the lead-free Perovskites cannot be as successful as the lead contained ones, lead Perovskites will be in use as plan B. In any case, Perovskites are very new and very promising materials, so it seems that they are worth investigating.

Thus, the preliminary aim of this research is to improve the coverage of the Perovskite layer and to obtain the best theoretical efficiency consequently. Although this application will be environmentally friendly by itself, the efforts will be given to try to make it less harmful even during its production stage.

2. LITERATURE SURVEY

The literature survey section consists of economic direction of photovoltaic technology photovoltaic effect, the properties of the Perovskite material, and the working principles of Perovskite PV systems. The design characteristics and challenges of these devices will also be discussed.

2.1. Economic Direction of Photovoltaic Technology

Energy generation technologies can be separated into two main headings: dispatchable generating technologies and intermittent ones. Dispatchable technologies include energy production systems that has stored resources and are ready to produce electricity when it is required. Coal, gas-combined-cycle and nuclear plants can be given as examples.

On the other hand, intermittent technologies are more renewable ones, but the reason why they are called intermittent is that their sources can be interfered by nature. For instance, wind speed can change in a day, solar energy can be hindered by clouds as well although it is already limited by daytime, etc. It is also possible to turn the intermittent technologies into dispatchable technologies by the help of the battery energy storage systems (BESS) (Teleke et al., 2010).

Two main factors will be determinative on the economic direction of the PV systems; Levelized Costs of Electricity (LCOE) and Feed-in Tariff policies.

2.1.1. Levelized Costs of Electricity

With the help of the contemporary technology systems, there are many kinds of energy production processes. On the other hand, for the competitiveness of those processes, there are some parameters, which are gathered in some specific assessment methods. The levelized costs of electricity is the most recent and the most promising assessment method because of that it can also consider carbon price, which is necessary for the protection of the environment. Carbon price is also being argued by the developing countries because of that

it is a penalty for the side-product of the cheap energy production; while developing, the most important compound is energy for them.

As a simple definition, LCOE is the estimation of "levelized cost" per megawatt-hour (MWh) energy provided. It is used for measuring the real total (capital and operating costs) life-cycle costs of a particular generating process per MWh energy provided. Because of that investments are affected by inflation and rate of interest, the assessment should be held properly with the consideration of the economic lifetime of the plant as well (Akyüz et al., 2009).

According to LCOE, it is costly to turn intermittent technologies into dispatchable technologies at the moment. But, during the peak hours, which are the times when the unexpected electricity demand occurs (e.g. when air conditioners are more necessary in the summer), it is more economic to use the intermittent technology for this excessive-demand instead of the conventional technologies. LCOE can be defined as;

$$LCOE = \frac{I_0 + \sum_{t=1}^{n} \frac{A_t}{(1+i)^t}}{\sum_{t=1}^{n} \frac{M_{t,el}}{(1+i)^t}} \quad (2.1)$$

Where;

LCOE	Levelized cost of electricity (Euro/kWh)
I_0	Investment expenditures (Euro)
At	Annual total costs (Euro in year t)
$M_{t,el}$	Produced quantity of electricity in the respective year (kWh)
i	Real interest rate (%)
n	Economic operational lifetime (year)
t	Year of lifetime (1, 2, ...n)

The annual total costs consist of fixed and variable costs, which are coming from the operation of the process, service, maintenance, insurance payments, carbon prices and repairs (Fraunhofer, 2013).

Joskow (2011) has reported some numerical examples for the proper usage of LCOE as shown in the Table 2.1., making the following assumptions;

- There are 3,000 hours for the peak period, which is in daytime, and there are 5,760 hours for the off-peak period per year,
- The off-peak demand amount equals to 50% of the peak demand amount,
- Generating capacities are utterly enough to meet the demands,
- The wholesale market prices are $90/MWh for the peak period and $40/MWh for the off-peak period.

Table 2.1. Hypothetical levelized cost of electricity (Joskow, 2011).

	Dispatchable	**Intermittent**
Construction + fixed O&M costs ($/MW/year)	300,000	150,000
Operating cost ($/MWh)	20	0
Capacity factor	90 %	30 %
MWh/MW/year	7,884	2,628
Levelized cost ($/MWh)	58.1	57.1

As can be seen from Table 2.1., although the dispatchable technologies have higher capacity factor, they are not as competitive as the intermittent ones due to their higher construction and fixed costs. Since that they are renewable energy sources, there is no fuel usage for the intermittent technologies and that makes a big difference in the operating costs (Dağdaş, 2005).

Moreover, depleting fossil fuel amounts of the world will increase the fuel prices in the future and operating costs will be even higher when the carbon price is included because of the global warming issue. If all these factors are taken into an account as well, the intermittent technologies will be more attractive (Joskow, 2011).

When the example is elaborated in the Table 2.2, it can be clearly seen that the dispatchable technologies can be exchanged with intermittent ones.

Table 2.2. Economic comparison of the dispatchable and intermittent technologies (Joskow, 2011).

	Dispatchable all cases	**Intermittent Case 1**	**Intermittent Case 2**	**Intermittent Case 3**
Peak period MWh supplied	3,000	0	50	2,628
Off-peak period MWh supplied	4,884	2,628	2,578	0
Revenues $/MW/year	465,360	105,120	107,620	236,520
Total cost $/MW/year	457,680	150,000	150,000	150,000
Profit $/MW/year	7,680	(-44,800)	(-42,380)	86,520

Let us choose the competitive intermittent technologies against to dispatchable ones; we can set solar power plant as the intermittent case 3, which produces all the electricity in the peak period, and as case 1 and 2, we can use two wind farms for the off-peak period, thus we have the same total yearly costs for the comparison. Also, although the total supplied electricity amounts are the same, the supplied electricity amounts are different for the different periods of the wind farms in order to observe the profit difference.

When the information given in Table 2.2. is examined, it can be easily evaluated that this is an extreme (sort of the worst case) scenario. As it can be seen, there is no wind for the wind turbines in daytime or the wind is too calm to move the generators. There are just 50 hours utilizable wind for the intermittent case 2, which can give an idea about the location of the system. This system must be in a desert. Another scenario would be a chillier location, where the wind speed is higher enough to move the wind turbines, but most probably the sunlight intensity would be lower for that location and compensate the income from the wind turbines by the lesser profit of the solar plant. Thus, one can tell the simulation more or less works adequately (Joskow, 2011).

LCOE has an increasing popularity for the investors, because the levelized cost of electricity is a very detailed assessment method, which is peculiar to the desired location.

However, the most significant property of it is to take expenses, carbons costs and feed-in-tariffs into account.

2.1.2. Feed in Tariff in Turkey

The most important step for the renewable energy law was taken on 29th of December 2010 in the Turkish Parliament. Electricity demand was growing more than 6 % and in order to satisfy this demand, Turkey was importing around 70% of energy resource, since it had no large oil and gas reserves, although it had abundant renewable energy potentials. In order to liberalize the energy market and to encourage investors to undertake renewable energy projects, the new law with No. 6094 "Amendment of the Law on Utilization of Renewable Energy Resources for the Purpose of Generating Electrical Energy" was brough into force by the Turkish government. The Energy Market Regulatory Authority (EMRA) took the regulatory responsibility for the sector by the allowance of the Ministry of Energy and Natural Resources (Yüksel, 2011). The feed in tariff policy for Turkish renewable energy power plants is given in Table 2.3.

Table 2.3. Feed in Tariff policy of Turkey for renewable energy plants (Yüksel, 2011).

Power source of generating facility	**Feed-in tariff ($/MWh) for first 10 years of operation**
Hydraulic	73
Wind	73
Geothermal	105
Solar	133
Biomass (including landfill gas)	133

These Feed in Tariffs (FiT) are not only lower than other countries, but they are also superficial. For example, as can be seen in Table 2.3., there is no difference between solar PV energy and solar thermal energy or between on-shore wind energy and off-shore wind energy. In the legislation draft, proposed FiT for solar PV systems was €250 for each MWh electricity and there were FiTs for wave, current and tidal energy as well, but they were not mentioned in the regulation. Finally, the most deficient article is about the FiT validity

duration; according to the legislation, the FiT is valid just for 10 years, whereas it was 10+10 years (with higher tariff rate in the first 10 years) in the draft (Yüksel, 2011).

The first licensing period of Turkey was designed for 600 MW of solar project for 27 regions, which are announced by EMRA partner of the Ministry of Energy and Natural Resources. With the incentives for domestically-manufactured components, FiT for per MWh photovoltaic plant electricity is $200 and $225 for per MWh electricity of concentrating solar plants, but this extra incentive will be valid just for first 5 years and can be used for the projects which will be ready before December 31, 2015 (Yüksel et al., 2013).

2.2. Photovoltaic Effect

The photovoltaic effect is the changeover process of the sunlight energy into electricity by the semiconductor materials. An electron of the semiconductive active material leaps to the lowest unoccupied molecular orbital (LUMO) from the highest occupied molecular orbital (HOMO) when the solar cell is illuminated by photons. The excited electron, which can be seen in Figure 2.1., heads for the electron transport material (ETM), while the hole heads for the hole transport material (HTM) in order to complete the circuit after the electron energy is used as an electricity. For the purpose of electricity production, photon energy should be higher than the HOMO and LUMO energy difference, which is called as band gap energy (E_g).

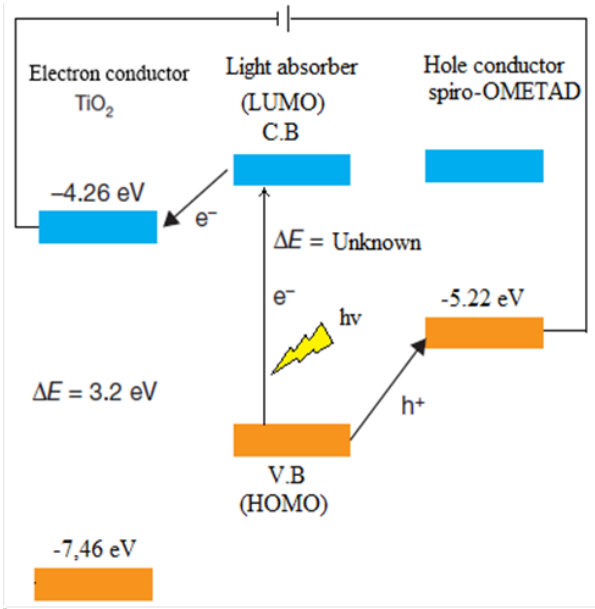

Figure 2.1. Scheme of the photovoltaic effect (Chung et al., 2012).

Band gap energy is a distinctive material property and it is directly related with the optical and electrical properties of the materials (Goswami et al., 2000).

2.3. Perovskite

In 1893, German Mineralogist Gustav Rose discovered the first Perovskite mineral ($CaTiO_3$) in the Ural Mountains of Russia and gave the name of Russian Mineralogist Lev Perovski to it. Today, as natural and synthetic, many type of Perovskites are known with its ABX_3 structure and the most copious one is the magnesium silicate Perovskite ($MgSiO_3$) in the earth's mantle (Gao et al., 2014).

Lead and tin halide synthesis methods are known since 1893, yet, compared to them, crystallographic studies on Perovskite are pretty new. The first synthetic Perovskite production was made by Christian Møller in 1957 (Møller, 1957). But that Perovskite structure was cesium lead halide, which had a $CsPbX_3$ (X=Cl, Br or I) chemical formula. He also monitored that these Perovskites had photoconductive properties, so they could be used as semiconductors.

Recently, Chung et al. (2012) processed $CsSnI_3$ Perovskite as a hole conductor and recorded 8.5% efficiency (Chung et al., 2012). On this device, active material was molecular Ruthenium-based sensitizer, but now that the Perovskite itself was also a strong photo absorber in the visible range, the source of charge carriers were not clear (Chung et al., 2012). In 1978, Dieter Weber made a cation exchange and cesium substituted with methylammonium cation ($CH_3NH_3^+$). He obtained the first three dimensional organic-inorganic hybrid (organometallic) Perovskite (Grätzel, 2014).

Generic crystal structure of cubic metal halide Perovskite is shown in Figure 2.2. for ABX_3 structure. Green spheres in the figure represent A, which is methylammonium ($CH_3NH_3^+$) in our case, grey spheres which are in the middle of grey octahedrons represent B, which is lead or tin, and purple dots represent X halides (Cl, Br or I).

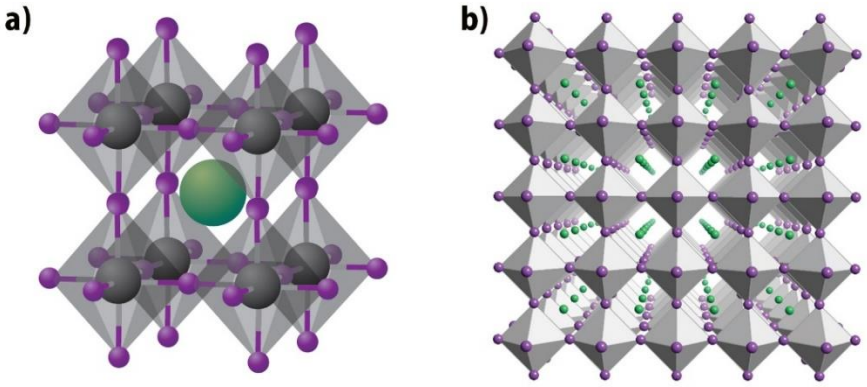

Figure 2.2. Singular crystal (a) and simulated lattice (b) structure of Perovskite (Gong et al., 2013).

Recent researches shows that increasing in the size of A causes the increase of the band gap energy of ABX_3; replacing Pb with Sn decreases band gap energy of ABX_3; and as X changes from I to Br to Cl, the band gap energy will increase (Gong et al., 2013).

2.4. Perovskite Solar Cells

Among the emerging thin-film solar cell technologies, solution processed, organic-inorganic Perovskite thin film based solar cells have recently demonstrated dramatic increases in power conversion efficiency. Such cells promise to combine extremely low production costs with high efficiency and therefore break the existing paradigm.

To date, the highest efficiencies have been achieved with mixed methyl ammonium organometallic halide Perovskites, in particular $CH_3NH_3PbI_{3-x}Cl_x$, absorber layers. These solar cells are composed of complex, stacked thin-layer structures. Typically, each layer plays a specific role, e.g., electron conductor, light absorber, hole-conductor or contact layer. The overall device performance depends not only on the qualities of the individual layers, but also on the interfaces formed between them.

Miyasaka and co-workers has reported the first lead-Perovskite absorber based solar cell, which had 3.8% efficiency (Miyasaka et al., 2009). Two years later, Park et al. (2011) increased the efficiency up to 6.5% (Park et al. 2011). However, in their devices, both Miyasaka and Park groups were using liquid electrolyte, which could erode the Perovskite

structure. Thus, the corrosive property of the electrolyte was limiting the life-span of the device to a couple of minutes (Park, 2013).

After few trials, the liquid electrolyte has been substituted with a solid-state hole-transporting material (HTM). Kim et al. (2012) recorded 9.7% PCE with spiro-MeOTAD as a hole-transporter, whose cross-sectional SEM images can be seen in Figure 2.3. (Kim et al., 2012).

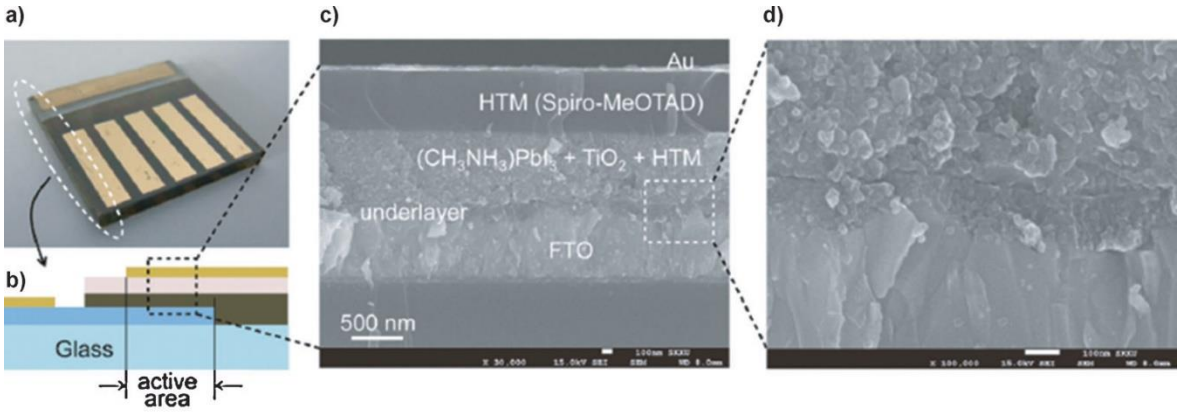

Figure 2.3. Solid-state mesoscopic solar cell (a, b) and SEM pictures of the cross-section (c, d) (Kim et al., 2012).

Then, Lee et al. (2013) used the insulating Al_2O_3 scaffold instead of semiconducting TiO_2 film. They achieved 10.3% PCE record and then, the record was improved to 12.3% efficiency by the same group (Lee et al., 2013). Doing so developed the stability and increased the conversion efficiency at the same time. At this point, Perovskite solar cell (PSC) was a simulation of the solid-state dye sensitized solar cell (ssDSSC) (Grätzel, 2014).

Then, it became clear from the studies of Etgar et al. (2012) that the Perovskite could also be used as a hole conductor. Despite the fact that these 'HTM-free' devices had only around 5% conversion efficiency initially, they had many advancements in recent years. Today, PSC devices are still using the HTM-free mesoscopic, showing great stability under long-term light soaking (1000 h under full sunlight) (Grätzel, 2014). After a series of the shifts, the efficiencies jumped from around 10% to a certified 17.9% and uncertified 19.3%, respectively (Service, 2014). The updated record of the solar cell efficiencies can be followed from the National Renewable Energy Laboratory chart given in the Fig 2.4.

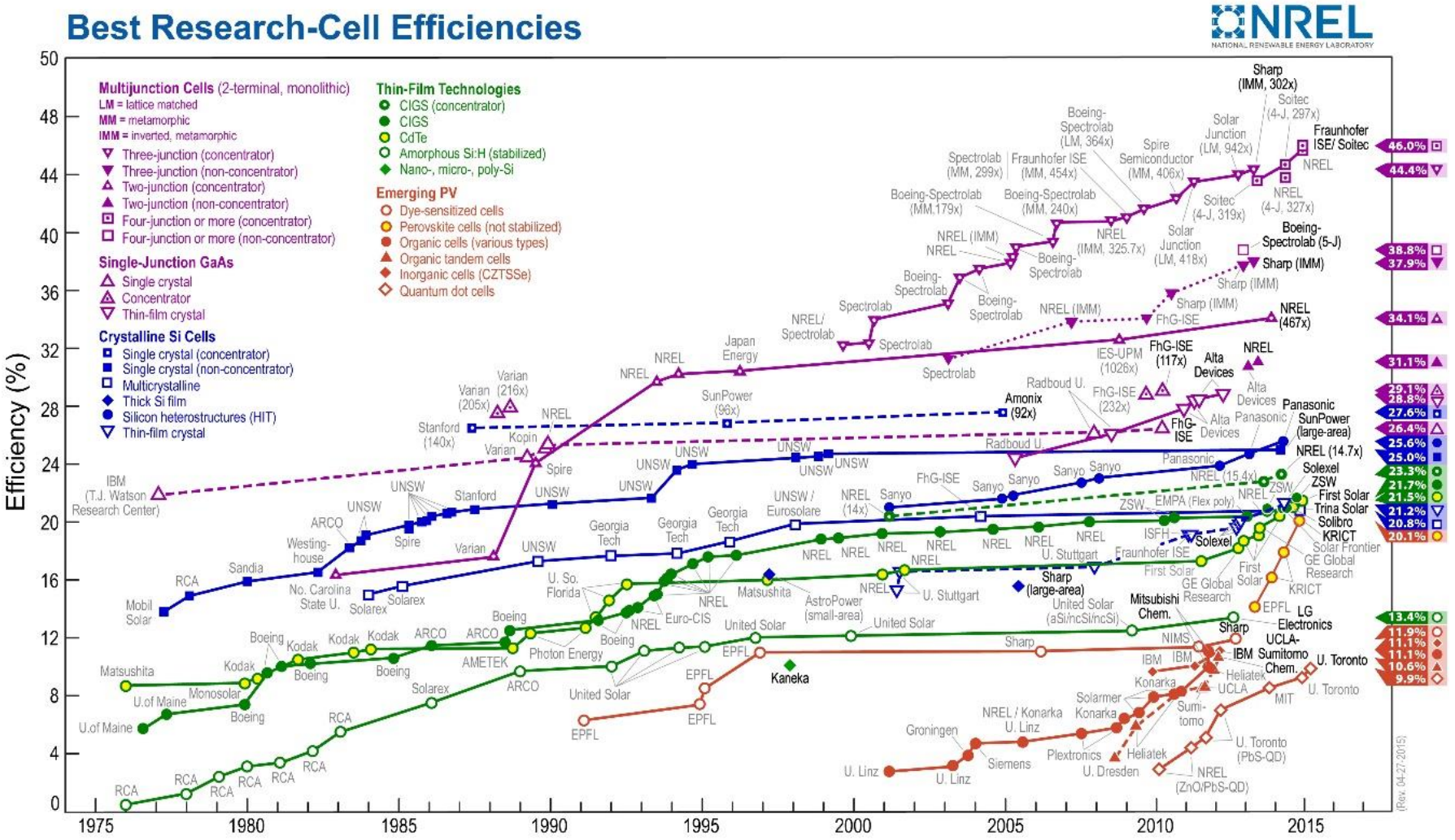

Figure 2.4. Certified solar cell efficiency chart (NREL, 2015).

But the real challenge has already begun; replacing lead with another non-toxic or less-toxic metal idea made the tape rewind. Although Henry Snaith, a physicist at the University of Oxford and one of the leaders in the field, stated that the coal combustion originated annual lead emission was more harmful than a 10-terawatt array of lead based Perovskite solar cells; the notables of the field believed that completely non-toxic material would be better for the environment (Peplow, 2014). Instead of lead, other than tin and germanium, members of the group 14 metals could also be used. Yet, as atomic numbers decrease in the group 14, the stability of the 2+ oxidation state also decreases. It should be taken into account that the higher stability is one of the most important parameters that the solar energy field sought (Yin et al., 2014).

There have been Pb-Sn mixed Perovskite studies conducted, but, they cannot be called completely 'Lead-free'. Recent research of Ogomi et al. (2014) showed that the different ratio of mixed Pb-Sn metal Perovskite was giving a chance for tuning of the solar material's band gap energy between Pb and Sn band gap energy spectra. Yet the same study stated that iodide based pure tin Perovskite ($CH_3NH_3SnI_3$) did not display any important photovoltaic properties, and there should be a little Pb-Perovskite in the cell in order to stabilize Sn in its 2+ oxidation state. According to this research, the Perovskite, which had a 1:1 Pb/Sn ratio ($MASn_{0.5}Pb_{0.5}I_3$), showed the best performance with 4.18% efficiency until that time (Ogomi et al., 2014).

Recently, Snaith et al. (2014) has firstly reported that they produced a device with the completely lead-free Perovskite ($CH_3NH_3SnI_3$) as photoactive material with greater than 6% efficiency. The key point was obtaining the Perovskite under inert atmosphere in a glovebox. Because of the fact that the reaction was also too sensitive, the Dimethylformamide (DMF) solvent was used after degasification. By spin coating at 2000 rpm for 45 seconds, the dark brown $CH_3NH_3SnI_3$ Perovskite layer was obtained. This result also shows that the Pb-based Perovskite is not unequaled material for solar cells; in other words, lead can be exchanged.

At the same time, Kanatzidis et al. (2014) was working on lead-free tin Perovskite photovoltaic solar cells and their device was coated with Lead-free solution-processed solid-state Perovskite ($CH_3NH_3SnI_3$) by the spin coater. Instead of iodide, different bromide

concentrations -which were also environmentally friendly- were also used and investigated simultaneously. For different numbers of bromide in the Perovskite, the different transparency was observed, which was important for both efficiency and usage of tandem layers. Color and transparency changes of this mixed halide Perovskite can be seen in Figure 2.5 (Kanatzidis et al., 2014).

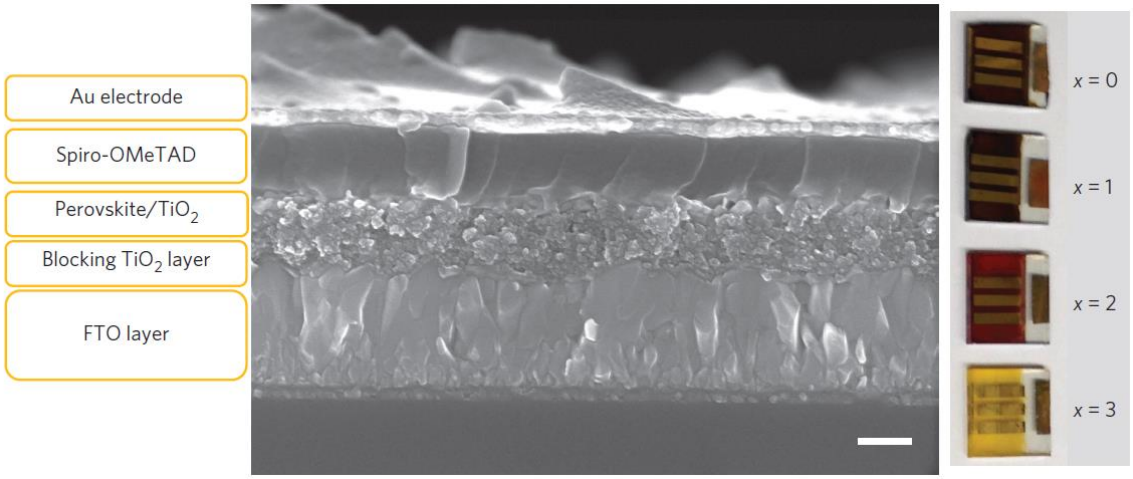

Figure 2.5. Cross-sectional SEM image of the device and color changing of Perovskite ($CH_3NH_3SnI_{3-x}Br_x$) for different bromide numbers (Kanatzidis et al., 2014).

The research of Kanatzidis et al. (2014) was significant because of the fact that iodine based tin Perovskite was not unique for solar cells. Besides, more significant fact was the efficiencies of mixed halides (5.48% for $CH_3NH_3SnI_2Br$ and 5.73% for $CH_3NH_3SnIBr_2$) were higher than that of the pure iodide one's (5.23%), but pure bromide's efficiency (4.27%) was not at the same conditions. The expectation for chloride mixed efficiency was higher as the results were observed from lead-based Perovskites.

2.5. Challenges

With new generation solar cells, single crystals and deposited thin films took all attention on them because of their optical and electrical properties. Mostly, in order to obtain high quality single crystals, crystals are grown from the melt phase of the material. But, it is not applicable for the methylammonium-based Perovskites, because organic ammonium cations decompose at comparatively lower temperatures (<250 °C). Thus, hybrid organic-inorganic Perovskites are prepared by solution chemistry methods, but generally, crystals

which are grown from solution chemistry techniques, have poor quality for the device application; they are small or inadequate (Mitzi et al., 1998).

As can be seen in Figure 2.6., there are three different goals to acquire for the solar cells; low-cost process, high efficiency and high stability.

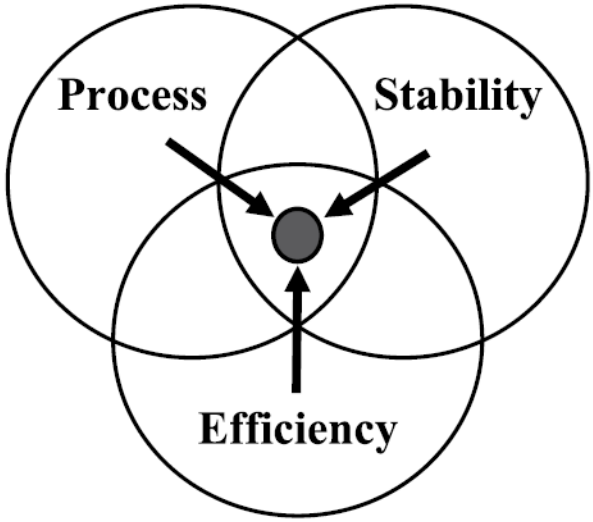

Figure 2.6. Scheme for the unification challenge of solar cells (Krebs, 2008).

As comparison with traditional inorganic solar cells, organic solar cells are cost effective products, but they are inadequate when the efficiency and stability are questioned (Krebs, 2008).

2.5.1. Stability

Instability of solar cells can take place because of degradation of the active material and oxidation of the metal electrode. That makes these components a variable of the hypothetical lifetime function. There are some common degradation factors of materials, which can be physical, chemical and mechanical. In other words, there are intrinsic and extrinsic factors. The experiment atmosphere directly affects the extrinsic factor. For instance, Perovskite solar cells are easily affected by moisture because of the fact that its methylammonium iodide precursor is hygroscopic. That is why the Perovskite experiments are run in the glovebox, which is filled with nitrogen (Jørgensen et al., 2008).

Perovskite solar cells overcame the efficiency problem as well as cost effectiveness, however, the stability is still a decisive issue because of their moisture and oxygen sensitivity. Wang et al. (2015) reported that pure lead iodine perovskite starts to degrade at 55% of moisture and the presence of oxygen makes it irreversible. However, there has not been any report published yet, which reports harmful moisture ratio for tin perovskites in the literature. Solving the stability problems will be great improvement for the dealing with the energy demand of the developing world.

2.5.2. Material Limitations

In addition to amorphous silicon, polycrystalline silicon, microcrystalline silicon, solar PVs include cadmium telluride, copper indium selenide/sulfide and other rare materials. Recent previews of material researches about the terawatt-level development of photovoltaics show that crystalline silicon resources would not be a limitation for the silicon PV technologies, but the reserves of silver may be a problem. According to the same review, when the utility of the silver (Ag) as top electrode has an alternative, there will not be any other limitation for the crystalline silicon solar cells (Feltrin and Freundlich, 2008).

Kamp et al. (2011) reported that 40% of cell processing costs consist of expensive Ag paste usage (Kamp et al., 2011). Rehman and Lee (2014) stated that Ni/Cu plating process could be used instead of Ag contact. This decreases the used silver amount, but it is also close to regular process costs because of the complex plating process. The appealing parts of it are to increase the efficiency because of the low contact resistance and to be used as a silver alternative (Rehman and Lee, 2014). Appleyard (2012) reported that Interuniversity Microelectronics Centre from Belgium achieved 20% efficiency with copper contact, whereas silver one was with 19.5% efficiency. It was also reported that the copper deposition could be done from chemical solutions in galvanic processes, which were cheaper and more suitable for high rate deposition (Appleyard, 2012).

When the thin film PV technology is questioned, because of the tellurium (Te) and indium (In) unavailability, -the most prominent members of the thin film PVs- cadmium telluride (CdTe) and copper indium gallium selenide (CIGS) thin cells are not promising in

the long run. Also, putting zinc oxide (ZnO) electrodes instead of indium tin oxide (ITO) makes multi-terawatt production possible, but because of their comparatively low efficiency, the thin film PVs need more surface area which is another limitation. Germanium (Ge) is another limiting material for the multi-junction concentrator cells, but gallium substitution would solve the problem (Jacobson and Delucchi, 2010).

Wadia et al. (2009) investigated the yearly obtained electricity amount from 23 different PV technologies, which were produced with the limiting materials, and whether they would cover whole demand or not. Also, they calculated the minimum $/W cost of the materials for each of the 23 PV technologies. Finally, they reached the conclusion, which was that there was a "Major opportunity for fruitful new research and development based on low cost and commonly available materials" such as FeS_2, CuO,Cu_2S, and Zn_3P_2 (Wadia et al., 2009).

With the light of these reviews, it can be securely stated that there is no material limitation for the Perovskite solar cells.

3. MATERIALS AND METHODS

In this study, because of the fact that the tin-Perovskite producing reaction is very sensitive to moisture and oxygen, the whole experimental procedure is performed in German product, Mbraun brand, nitrogen (N_2) filled glovebox seen in Figure 3.1.

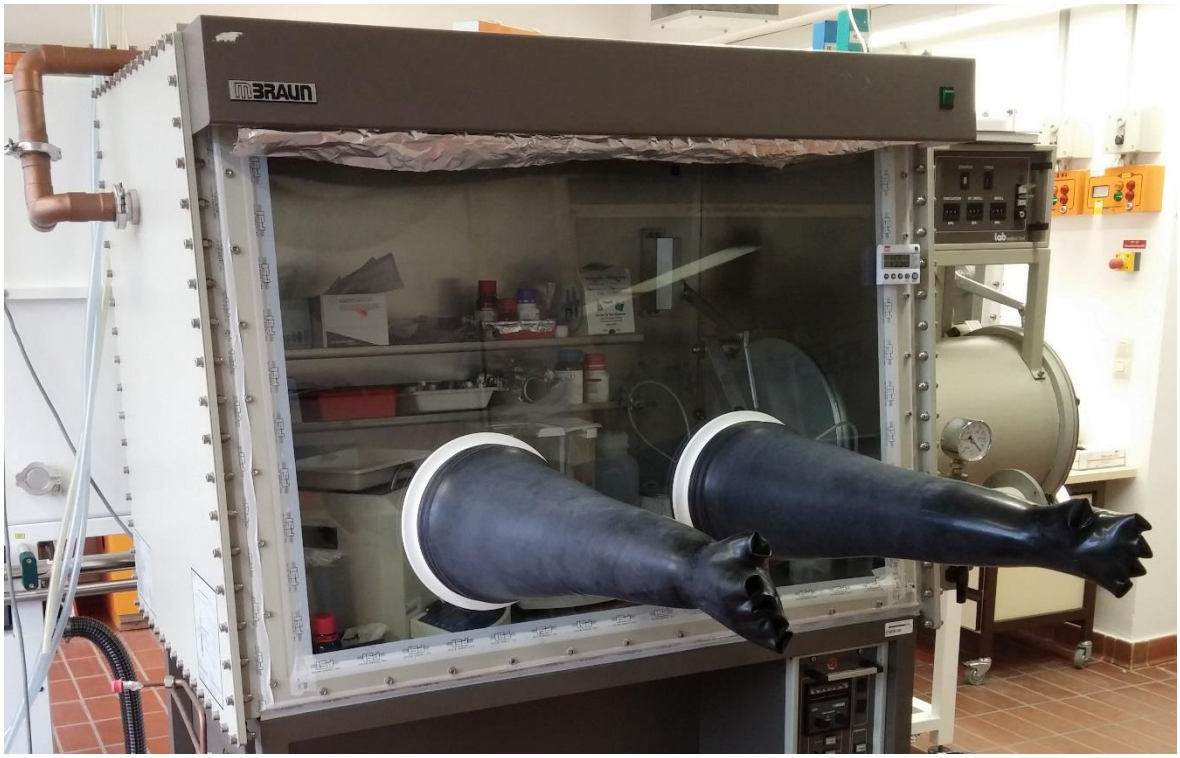

Figure 3.1. Nitrogen filled glovebox.

The experimental stage of this study was conducted under supervision of Prof. Dr. Marcus Bär, who is a professor of the Brandenburg University of Technology and the Head of Young Investigator Group at the Helmholtz-Zentrum Berlin.

3.1. Materials of the Experiment

3.1.1. Methylammonium Iodide

Methylammonium iodide (CH_3NH_3I) salt, which has 158.97 g/mole molecular weight, is used as a precursor for metal-halide Perovskites. MAI can be formed by the reaction of

27.86 mL methylamine (CH_3NH_2) (40% in methanol) and 30 mL of hydroiodic acid (57 wt % in water) in 250 mL round bottomed flask at 0 °C for 2 h with stirring. The precipitated MAI solid can be obtained by evaporation of methanol at 50 °C for 1h.

Then, the produced MAI should be washed with diethyl ether three times by stirring for 30 minutes for each wash and should be dried at 60 °C in vacuum oven for 24 h in the end (Park et al. 2011). Since MAI is hygroscopic material, it should be sealed in the inert atmosphere in order to keep it away from moisture and oxygen.

As a precursor, 100 g methylammonium iodide with Dyesol brand of Australia is procured and used in this study.

3.1.2. Tin Halide Salts

Tin halides have similar structures with lead halides (Abrahams and Demetriou, 2000). Thus, the products of tin halides and MAI are similar with the ones of lead halides and MAI as well. Though, there are not satisfying number of reports about tin halide perovskites in the literature. Tin halides can be prepared by adding solid tin shots into hydrohalic acids such as hydroiodic acid (HI), hydrochloric acid (HCl), and hydrobromic acid (HBr) (Nara and Adachi, 2011).

In this study, Sigma Aldrich 100 g tin (II) chloride ($SnCl_2$) in poly bottle, Alfa Aesar 5 g tin (II) bromide ($SnBr_2$) in glass bottle, and Alfa Aesar 5 g tin (II) iodide (SnI_2) in glass bottle were used for the experiments

3.1.3. Etched FTO Glasses

In order to investigate the active material properly and to standardize the deviation, Solaronix Perovskite Kit glasses are used. There are combinations of fluorine doped tin oxide (FTO) layered glasses with blocking titania layer and scaffolding titania layer, which can be seen in Figure 3.2. The dimension of the glasses are 20 mm x 20 mm.

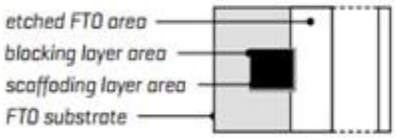

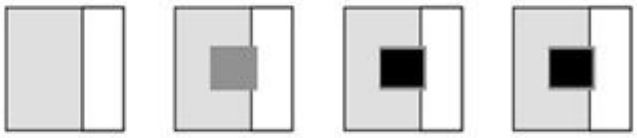

	Etched FTO	Blocking Layer	Scaffolding Layer (600 nm)	Scaffolding Layer (300 nm)
Etched FTO Electrodes, 16 pcs.	✔	-	-	-
Blocking Layer Electrodes, 16 pcs.	✔	✔	-	-
Scaffolding Layer Electrodes, thin, 16 pcs.	✔	✔	✔	-
Scaffolding Layer Electrodes, ultra-thin, 16 pcs.	✔	✔	-	✔

Electrode size: 20 x 20 mm
Active area: 6 x 6 mm

Figure 3.2. Different types of etched FTO glasses (http://www.solaronix.com/documents/solaronix_materials.pdf).

3.2. Experimental Work

The experimental work is mainly consisted of three main sections, which explain reaction methods, coating methods and structural characterization methods. The final product may differ for each of the reaction methods.

In addition, different physical or chemical characteristics of each materials may change the coverage ratio, which is vital for the efficiency of PV devices. Therefore, the investigation of these parameters is vital as well.

3.2.1. Reaction Methods

3.2.1.1. One Step Method. In this method, the reaction occurs in the solution. The precursors, MAI and tin halide salt, are mixed equimolarly in proper, polar aprotic solvent (DMF, DMSO or Acetone) as between 40-60 % by weight. Then, the dissolved precursors react and form the active material solution. After 20 minutes stirring at 80-120 °C, greenish yellow ($SnCl_2$), orange ($SnBr_2$) and dark yellow (SnI_2) Perovskite solutions are obtained, which can be seen in Figure 3.3.

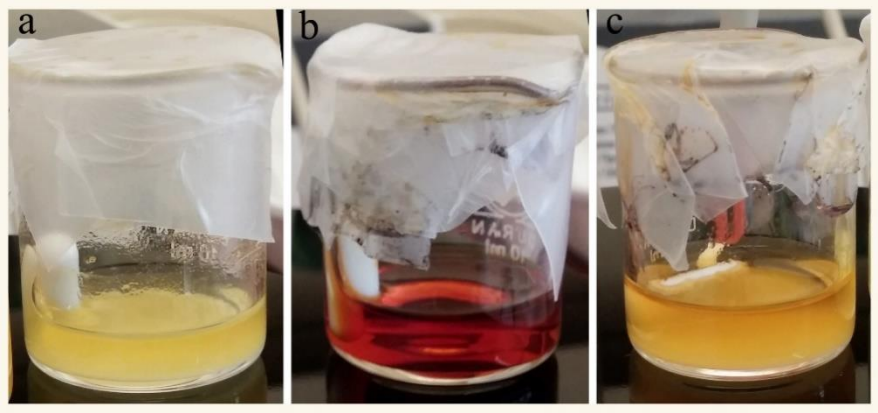

Figure 3.3. Perovskite solutions which are prepared with different tin halide salts; (a) $SnCl_2$, (b) $SnBr_2$ and (c) SnI_2.

In order to attain high coverage on glass, the prepared solution should be spin coated on hot glasses, which are at same temperature with the solution. The spinning rate of spin coater should be 2000 rpm, but it can be adjusted to have thinner or thicker layers. About 45 seconds spinning time is enough. Finally, the coated glass is annealed to form Perovskite crystals. Annealing is a heat treatment method, which improves the mechanical properties of the materials. For the crystalline case, annealing coarsens the crystal size and increases the coverage ratio as well.

3.2.1.2. Two Step Method (Sequential Deposition). This method includes a second step in which the reaction goes on. In the first step, one of the precursors (tin salt in this case) is coated on glass and the glass is annealed to dry. In the second step, the coated glass is dipped into the solution, which is prepared with the other precursor (methylammonium iodide in this case). The whole procedure can be seen in Figure 3.4. (Burschka, 2013).

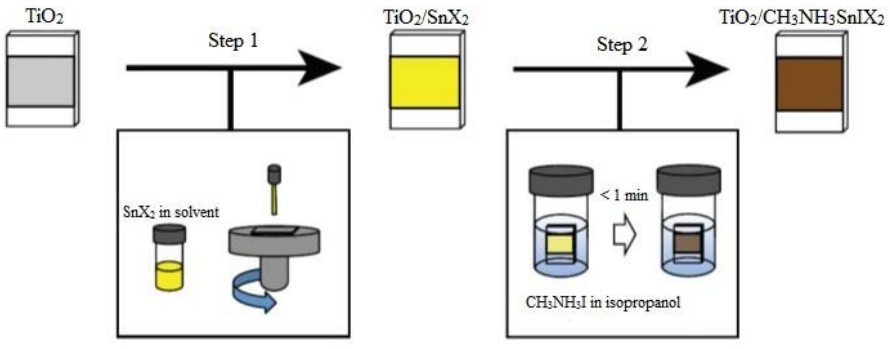

Figure 3.4. Schematic presentation of the two step method (Burschka, 2013).

The key point is the selection of solvent (one of the polar protic solvent, e.g. isopropanol). The second step should be done meticulously, because the solvent should not dissolve the first layer in order to have a good coverage. Dipping time depends on thickness of the first layer. Sometimes, the reaction may not take place at the bottom of the layer because of unreachability of the second solution. Finally, the coatings are annealed at 80°C. Compared to the one step method, this method gives a better coverage ratio. Also, because of the polar protic solvent, the crystal size is bigger than the ones obtained in the one step method.

3.2.1.3. Solid-state Reaction Method. This method, which can be seen in Figure 3.5, is very similar to the one step method. The only difference is that the reaction occurs without use of any solvent. Equimolar precursors are grounded and mixed in a bottle. Then, the sealed bottle is heated at 100 °C for 20 minutes.

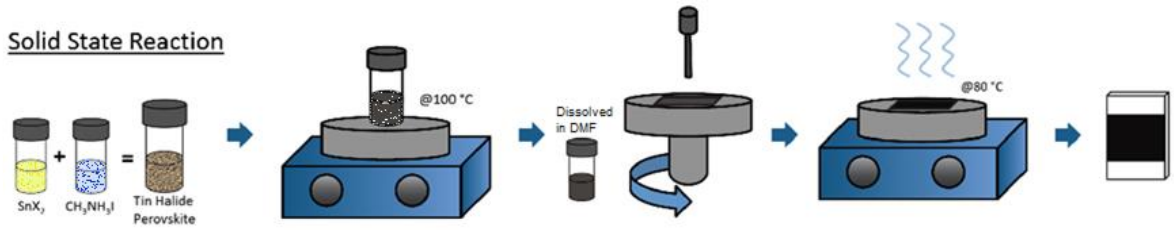

Figure 3.5. Schematic presentation of the solid state reaction.

Changing color, which can be seen in Figure 3.6., indicates that the reaction occurs even during grounding of the white colored precursors and without any solvent.

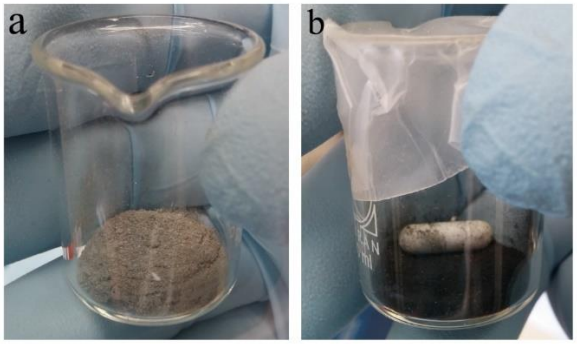

Figure 3.6. Color changing in solid state reaction, (a) before reaction, (b) after reaction.

In the end, the obtained Perovskite is ready to dissolve in a solvent and to coat on glass. The spin coating and annealing conditions are identical with the one step method. The advantage of this method is to attain bigger Perovskite crystals in the end, most probably, because of that the intermediate molecule amount is already higher in the solution than the one in the one step method.

3.2.2. Coating Methods

Spin coaters use centrifugal force in order to deposit the sol-gel type coating materials uniformly. As spinning rate increases, solid particles in the sol-gel solution stick to the substrate and solvent evaporates easily. The working principle of the spin coater can be seen in Figure 3.7. On the other hand, spinning rate of the spin coater and the viscosity of solution affect the film homogeneity and thickness.

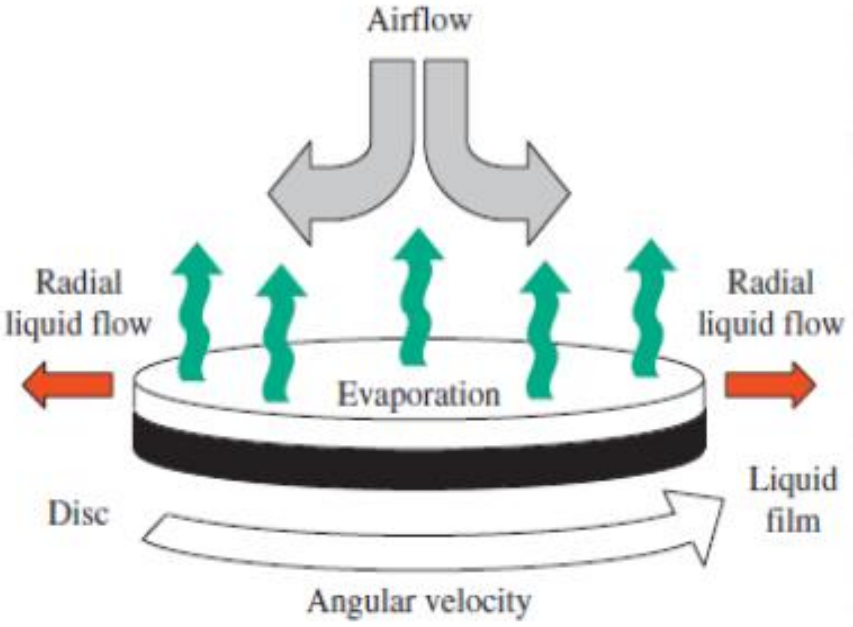

Figure 3.7. Working principle of spin coaters (Pivrikas, 2011).

After many trials, the optimum spinning rate and solution viscosity can be found. For this investigation, Specialty Coating Systems (SCS) G3P-8 model programmable spin coater from USA is used as seen in Figure 3.8. It can rotate up to 9.999 times in a minute and can store up to 30 programs with up to 20 steps each.

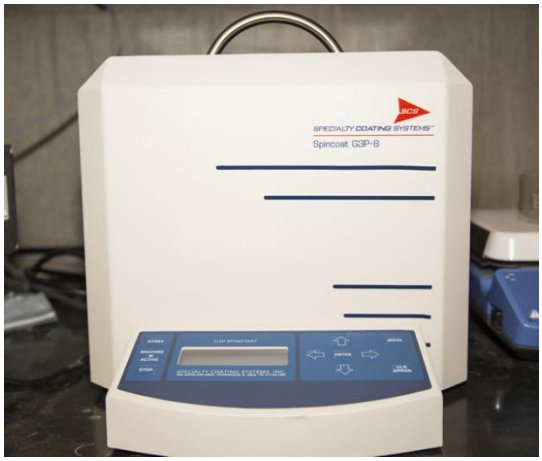

Figure 3.8. SCS spin coater.

In fact, there are already 4 different known coating methods, which can be seen in Figure 3.9. (Gao et al., 2014). The first coating method (a) is spin-coating. In Figure 3.9. (b), two-step coating can be seen. In this method, inorganic material is coated first and the substrate is dipped into methylammonium iodide solution after annealing. In two-step coating method, the reaction occurs at the second step and the key point is that the second solvent should be selected wisely in order to prevent dissolution of the inorganic material (Mitzi et al., 1998).

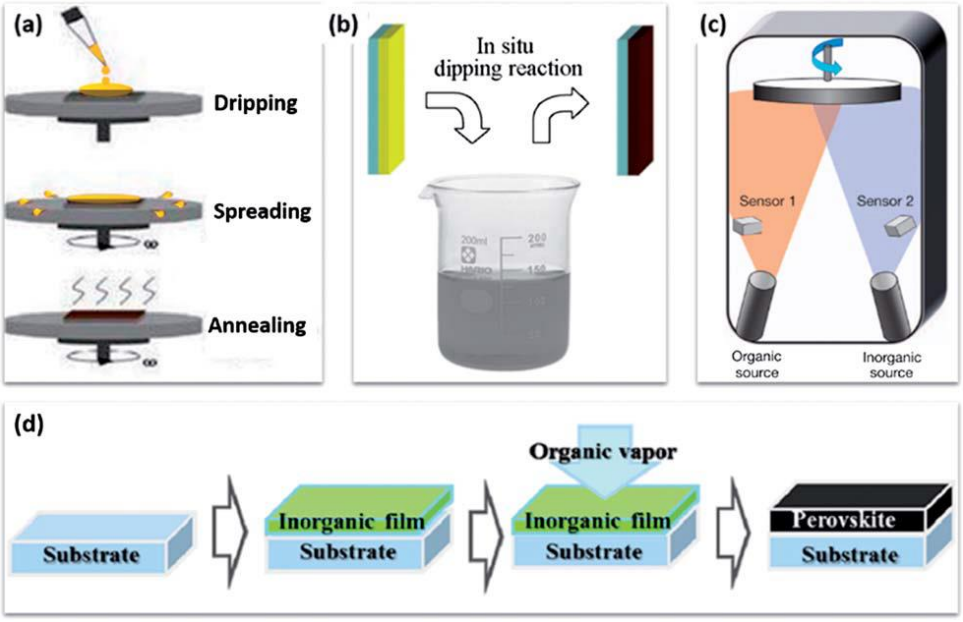

Figure 3.9. Different coating methods (Gao et al., 2014).

For the third coating method shown in Figure 3.9. (c), the precursors are pulverized on the surface at the same time and the reaction occurs on the surface. It is good for quick reactions, so that a homogenous film can be obtained and thickness can be adjusted easily. Its only disadvantage is the cost because of its sensors and autonomic system. The fourth coating method shown in Figure 3.9. (d) is similar to the method given in Figure 3.9. (b). Instead of dipping, chemical vapor deposition (CVD) method is used. Its reaction yield is very good because of its easily controllable reaction conditions for Perovskite (Gao et al., 2014).

In this research, coating methods (a) and (b) were used. Furthermore, deriving new coating methods was also investigated within the scope of this study as well.

When the homogenized Perovskite layer is obtained, next layers are coated by turns, which can be seen in Figure 3.10. (Grätzel, 2014).

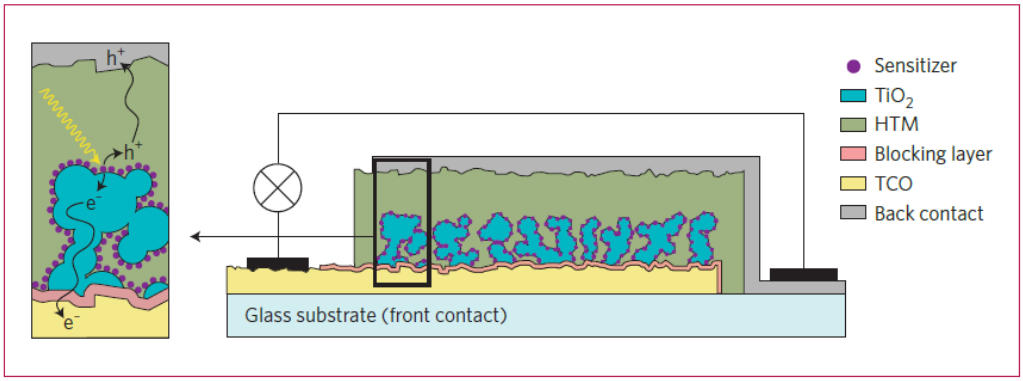

Figure 3.10. Layers of the Perovskite solar cell (Grätzel, 2014).

The purple dots are Perovskite crystals, which are coated on mesoporous titanium dioxide (TiO_2) surface. Yellow layer is transparent conductive oxide (TCO). In Perovskite case, the most common TCO is fluorine doped tin oxide (FTO). While green layer, which is the hole transport material (HTM) carrying the holes towards back contact, turquoise mesoporous TiO_2 and pink compact TiO_2 layers, which are blocking layers, carry electrons to the front contact in order to complete the circuit. Grey layer in the Figure 3.10. is back contact, which collects holes, and can be either silver or gold layer. Back contacts can be deposited by evaporation of these materials under very high vacuum in order to prevent

possible degradation of the other layers due to high melting point of these materials. The back contact evaporator can be seen in Figure 3.11.

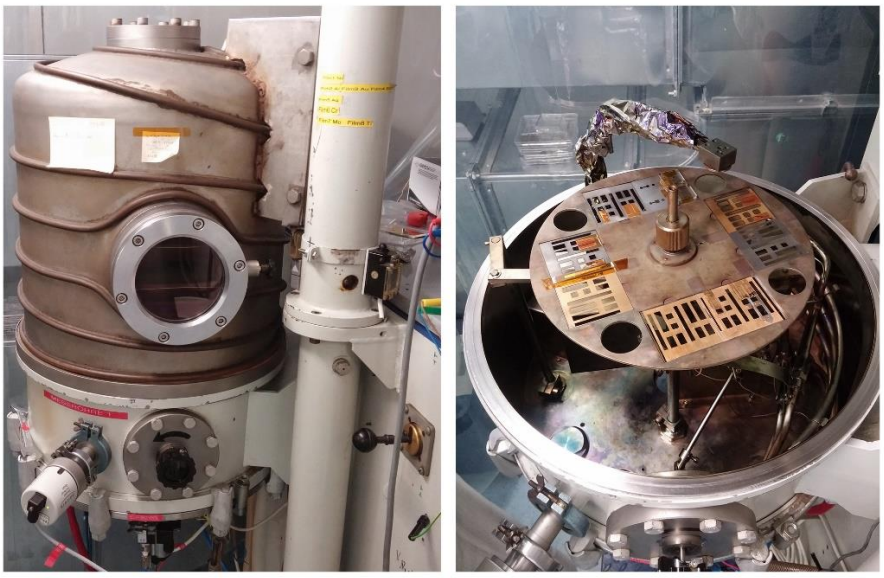

Figure 3.11. Back contact evaporator for gold or silver.

The back contact evaporator can evaporate gold at $3x10^{-5}$ mbar vacuum, which can be provided by a turbo pump. It is a custom made evaporator, however, its thin film deposition controller is Inficon XTC/2 model (Inficon, Switzerland). A gold layer with 200 nm thickness has been obtained for the samples using the back contact evaporator in this study.

3.3. Structural Characterization of the Materials

After standardizing the reaction conditions and coating methods in order to obtain the homogenized Perovskite layer, some measurements were conducted. The structural characterization was performed by using X-Ray Diffraction (XRD) in order to see what kind of material was obtained as a final product. When the desired final product was obtained, Scanning Electron Microscope (SEM) provided data about the crystallinity orientation and the coverage by the acquired visual images. Ultraviolet–Visible Spectroscopy (UV-Vis) and Photoluminescence (PL) analysis were used to show the band gap energy distribution of the material, which was the energy differences between ground and excited states. Thus, acquired band gap energy can be used in theoretical efficiency calculations, whereas it is another identification parameter for the materials whose band gap energies are known.

3.3.1. X-Ray Diffraction

An X-ray beam can undertake these conditions; reflection, absorption, refraction and diffraction. X-Ray Diffraction is one of the most significant methods in industrial laboratories for characterization, quality control and routine analyses, which uses diffraction property of the materials. It scans different 2-D diffraction planes as concentric rings of scattering peaks for various d spacings, thus the 3-D structural information of the crystalline material can be formed by applying Bragg's Law (Pandian, 2014).

Bragg's Law, which can be seen in Figure 3.12., involves with (n+1) equidistant atomic planes of spacing d and a X-ray beam, which is coming towards those planes with a glancing angle, θ (Ewald, 1962).

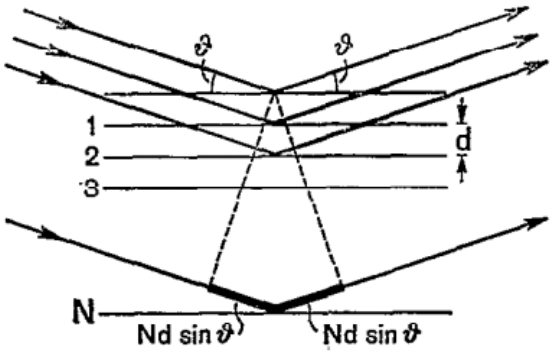

Figure 3.12. Bragg reflection according to his law (Ewald, 1962).

Bragg's Law is: $n\lambda = 2d \sin\theta$, where the integer n is the number of the plane intervals, λ is the wavelength of the incident X-ray beam, d is the distance between equidistant planes of atoms (the d-spacings), and θ is the angle of incidence of the X-ray beam. Since we know λ and we can measure θ, we can calculate the d-spacings (Ewald, 1962).

Since 95% of all solid materials are crystalline, it is possible to have diffraction patterns for them all with the help of the XRD. Those patterns are unique like a fingerprint for each pure substance. There are about 50,000 patterns for inorganic and 25,000 patterns for organic substances which are stored in its library as standards (ThermoARL, 1999).

In this work, X'Pert Pro model XRD device was used (PANalytical, Netherlands).

3.3.2. Scanning Electron Microscope

The SEM uses a focused beam of high-energy electrons instead of light to generate an image by applying a variety of signals at the surface of the solid samples. For thick samples, SEM has a distinct advantage over traditional transmission electron microscope because of the fact that the SEM measures by the help of the reflected electrons from the sample surfaces (Smith and Oatley, 1955).

In this experimental work, model 1530 Leo SEM device (Leo, Germany) was used for the visual characterization of the materials.

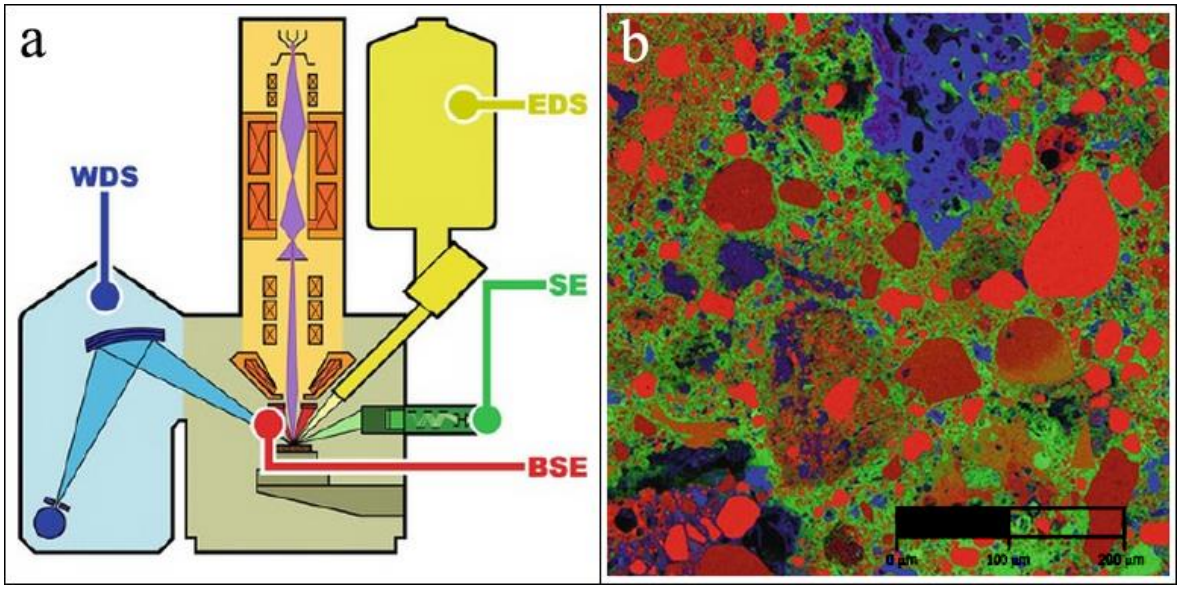

Figure 3.13. Schematic shown of the SEM (a), EDS mapping (b) (Frahm, 2014).

The SEM device configuration is given in Figure 3.13. Each color in Figure 3.13. (a) stands for a part of the SEM: purple for electron beam, orange for electron focusing column, brown for the specimen, tan for chamber, green for secondary electron detector (SE), red for back-scattered electrons (BSE), yellow for Energy-Dispersive Spectrometer (EDS). The microscope magnifies the sample area between 5X and 200,000X (Frahm, 2014).

The colors in Figure 3.13. (b) are representing the elemental composition for the specimen. The EDS (EDX, EDXA, or the trade name EDAX) can differ the selected

elements by the intensity of their X-ray energy correspondence. The shown specimen, which is a slag from an iron puddling furnace of Minneapolis, has excess carbon, silicon and other impurities from raw iron to make wrought iron. Thus, the glassy matrix of slag is dominated by iron (green), and includes carbon (blue) and silicon (red). The shown length of the specimen is 500 μm across (Frahm, 2014).

3.3.3. Ultraviolet-Visible Spectroscopy

Uv-Vis Spectroscopy is another important measurement device for the solar cells. There are mainly three phenomena, which are interested for solar cell designs: Reflectance, absorbance and transmittance. Although transmittance is enough to calculate absorbance (Absorbance = log (1/Transmittance) for liquids by applying the Beer-Lambert Law, one should measure reflectance and transmittance amounts in order to calculate absorbance amount of the solid materials (100%=%Absorbance+%Reflectance+%Transmittance) (Tams and Enjalbert, 2009). The process can be seen in Figure 3.14.

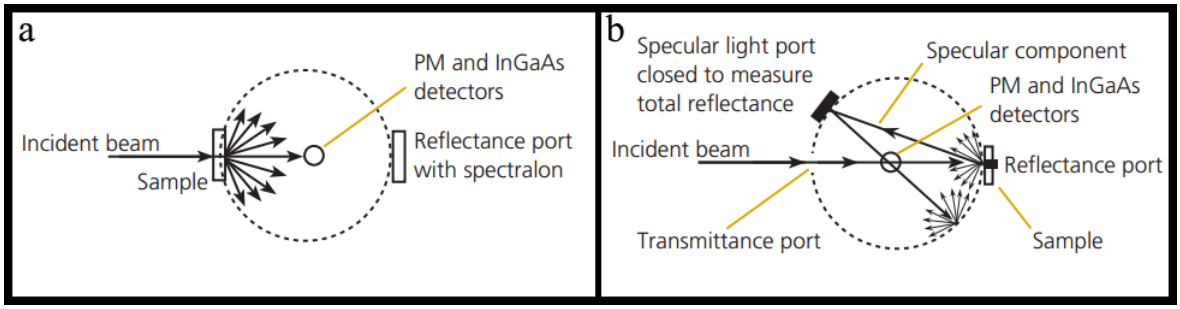

Figure 3.14. Transmittance (a), Reflectance (b) measurements of the Uv-Vis Spectroscopy (Tams and Enjalbert, 2009).

Uv-Vis measurements are very significant for photovoltaic solar cells, because one should know about which part of the solar irradiance spectrum can be absorbed by solar materials. The overlapped Uv-Vis spectrum on solar irradiance spectrum would be perfect match for the best efficiency. On the other hand, because of the tandem solar cells, if the material can absorb a part of the light spectrum economically, it is still useful. That means the proper combination of two materials can cover whole solar irradiance spectrum and convert solar energy to electricity or thermal energy.

In this study, Perkin Elmer Uv-Vis spectrometer Lambda 950 model was used (Perkin Elmer, USA).

3.3.4. Photoluminescence Imaging

Photoluminescence (PL) imaging is another characterization technique for the material science, which has been a standard method in recent years for photovoltaic solar cells. The PL imaging setup can be seen in Figure 3.15. (Trupke and Mcmillan, 2010).

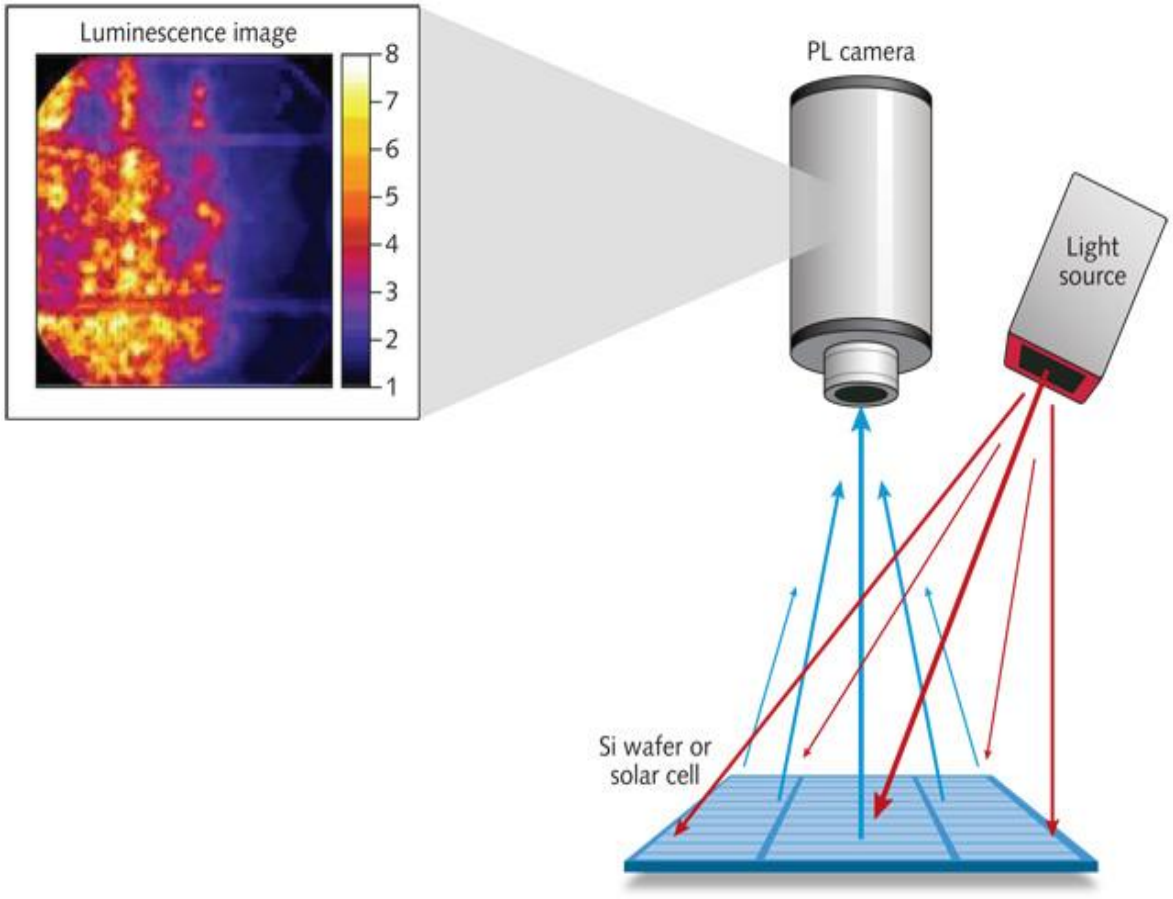

Figure 3.15. Schematic shown of the Photoluminescence Imaging (Trupke and Mcmillan, 2010).

The illuminated solar cell is excited by a high-power fiber-coupled infrared laser (red arrows) and a sensitive PL camera takes snapshots of the luminescence signals (blue arrows), which are emitted by the specimen (Trupke and Mcmillan, 2010).

PL measurement can be used for the detection of defects and impurities in semiconductors. However, the most important usage of the PL imaging is to determine the band gap energy of materials, which is distinctive for each material (Jayakrishnan, 2008).

Regarding the PL spectroscopy within this study, Andor Shamrock spectrometerSR 500 model was used (Andor Shamrock, Ireland). The PL set-up has various detectors and lasers. For the Perovskite samples, 660 nm diode laser was used. InGaAs detector for infrared region of the light spectrum and silisium based Charge-Coupled Device detector for the rest of the light spectrum were used.

3.3.5. Current-Voltage (I-V) Curves

Finally, in order to determine the efficiency of the solar cell, the current-voltage (I-V) curves are measured by using a solar simulator which provides an illumination similar to the natural sunlight. The solar simulator is used for indoor photovoltaic tests under a laboratory conditions and it has different types of lamps (Xenon arc or multiple metal-halide lamps) which can simulate sunlight with their combination. The standard solar simulator should have 1.5 air mass (AM), 25 °C temperature and 1 standard sunlight power property which is 1000 W/m^2 for the comparable results. The air mass value simulates the blockage level of the sunlight caused by the scatterings and absorptions of the water vapor in the atmosphere.

In this study, Steuernagel Lichttechnik EPS 1200S solar simulator was used (Steuernagel Lichttechnik , Germany).. The data was taken by Keithley, a high current source measure unit with 238 model number. Finally, LabView was used as a visualization software.

4. RESULTS AND DISCUSSION

All the acquired characterization results and problems in this experimental work will be discussed in five main sections in this chapter. Three sections present the results of each reaction method used, which have already been mentioned in chapter 3, one section present the results of the solvent changing trials, and one another section reporting the results for further investigations, which should be discussed separately than others.

4.1. One Step Method

This is the most widespread method for the methyl ammonium based Perovskite production. The procedure, which was already explained in Chapter 3, was used for all cells, while the various values of some parameters were tested to find the best conditions. With its easy preparation, one step method may be the most promising method for the industrial scale production of the tin based Perovskite as well. The only disadvantage of the one step method is lower coverage properties.

4.1.1. Tin (II) Iodide

In this section, the following data will be the results of the obtained pure iodine Perovskite by using one step Method. It was prepared at the beginning of this study by the help of the literature, in order to compare it with the other perovskites which were produced with the other tin salt precursors. Methyl ammonium tin triiodide ($MASnI_3$) Perovskite has the highest potential efficiency because of its lower band gap energy (E_g) and low cost production process compared to the first generation solar cells. But, efficiency-cost-stability triangle is still valid for this material, which means that the poor stability is still a disadvantage, while efficiency and production cost are advantageous.

The XRD result (left) for the experimental $MASnI_3$ Perovskite and the reference from the literature (right) (Kanatzidis et al., 2014) can be seen in Figure 4.1. The peaks, which are indexed as (100), (200) and (300), are characteristic peaks of Perovskites. The other peaks

depend on the orientation of the crystalline and they may stay behind of the characteristic ones when bigger crystalline structures are obtained.

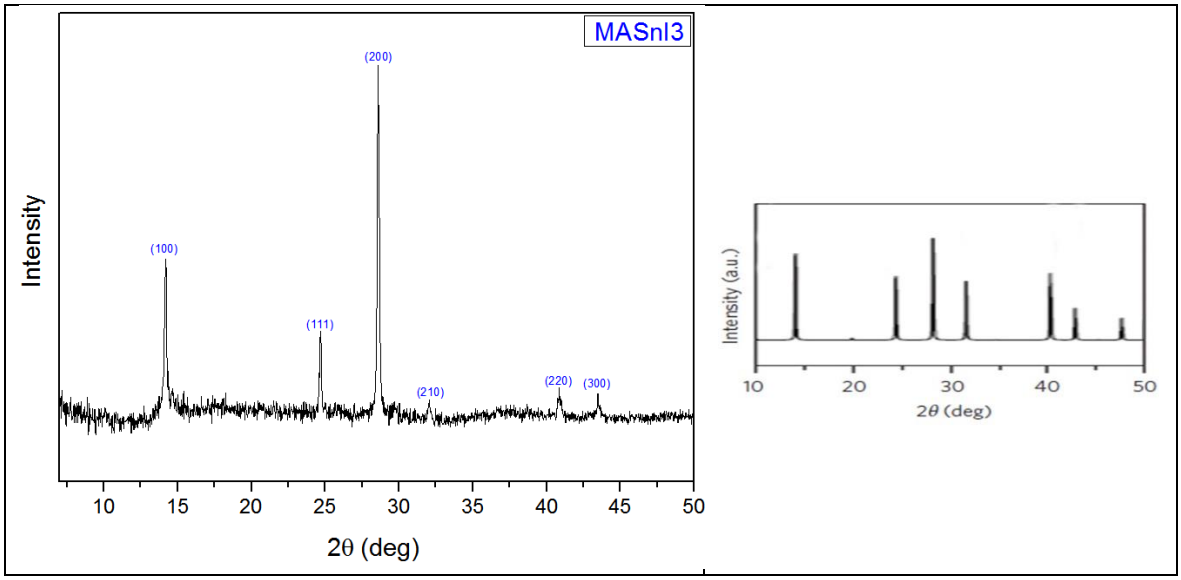

Figure 4.1. XRD patterns for the experimental $MASnI_3$ (left) and the reference (right) (Kanatzidis et al., 2014).

In Figure 4.2., the SEM images of the experimental $MASnI_3$ crystals are shown.

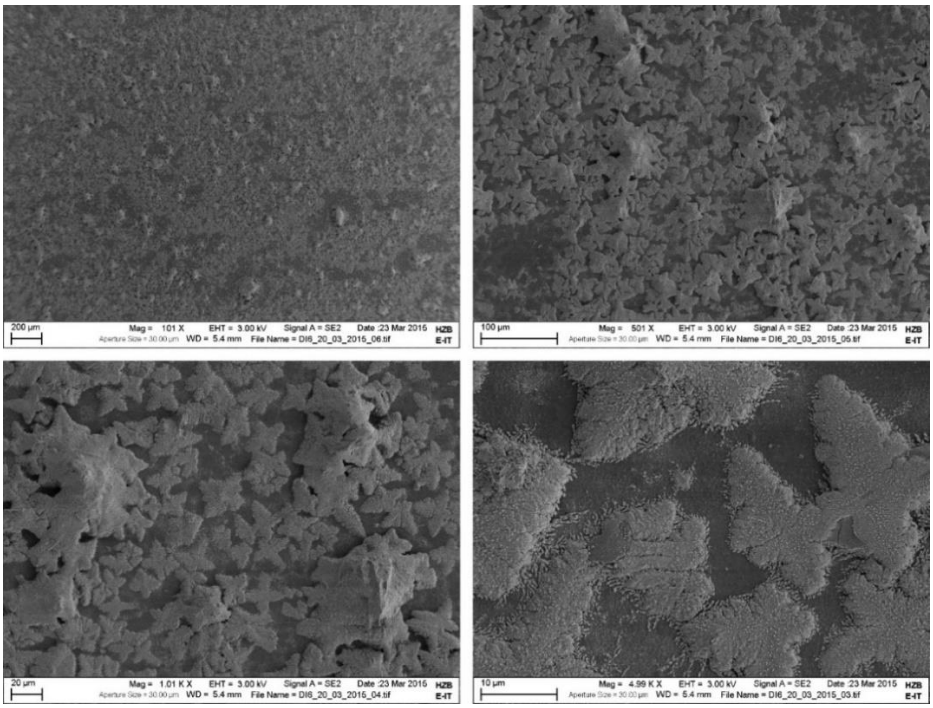

Figure 4.2. SEM images of the experimental $MASnI_3$ crystals (Around 100X, 500X, 1000X and 5000X, respectively).

As can be seen in Figure 4.2., Perovskite crystals were formed, but the coverage was not good enough to prevent shunting, which was due to manufacturing defects. Shunting is basically an unwanted short-circuit path between transparent conductive oxide (TCO) and back contact layer because of the low resistance due to poor coverage. As shunting increases on the solar cell, photovoltaic current decreases and even may cease depending on the shunt area extent.

4.1.2. Tin (II) Chloride

This section will provide data for the iodine-chlorine mixed tin Perovskites. After the pure iodine tin Perovskite was acquired with the identical properties of the one from the literature, the investigation of the iodine-chlorine mixed tin Perovskite was begun in order to obtain different tin Perovskites with useful band gap energies and better stability.

Because of methyl ammonium iodide (MAI) precursor and equimolar tin (II) chloride ($SnCl_2$), it was expected that the final product would be $MASnICl_2$.

There was no report encountered about iodine-chlorine mixed tin Perovskites in literature. Since the band gap energy tuning was possible by changing halogens of Perovskites, $MASnICl_2$ might have had a certain band gap energy between the band gap energy of $MASnI_3$ (1.3 eV) and $MASnCl_3$ (3.7 eV) (Kanatzidis, 2014). These mixed halide structures would not have low band gap energy like the triiodide tin perovskite, but they might have had better stability.

Though, as can be seen in Figure 4.3., the final Perovskite product was not $MASnICl_2$ as expected. The red indexed peaks belonged to pure tin chloride Perovskite, whereas the blue ones belonged to pure tin iodide Perovskite.

In other words, the structure in Figure 4.3. consists of the two crystalline of pure iodine Perovskite and pure chlorine Perovskite according to the reference patterns, which can also be seen in Figure 4.4.

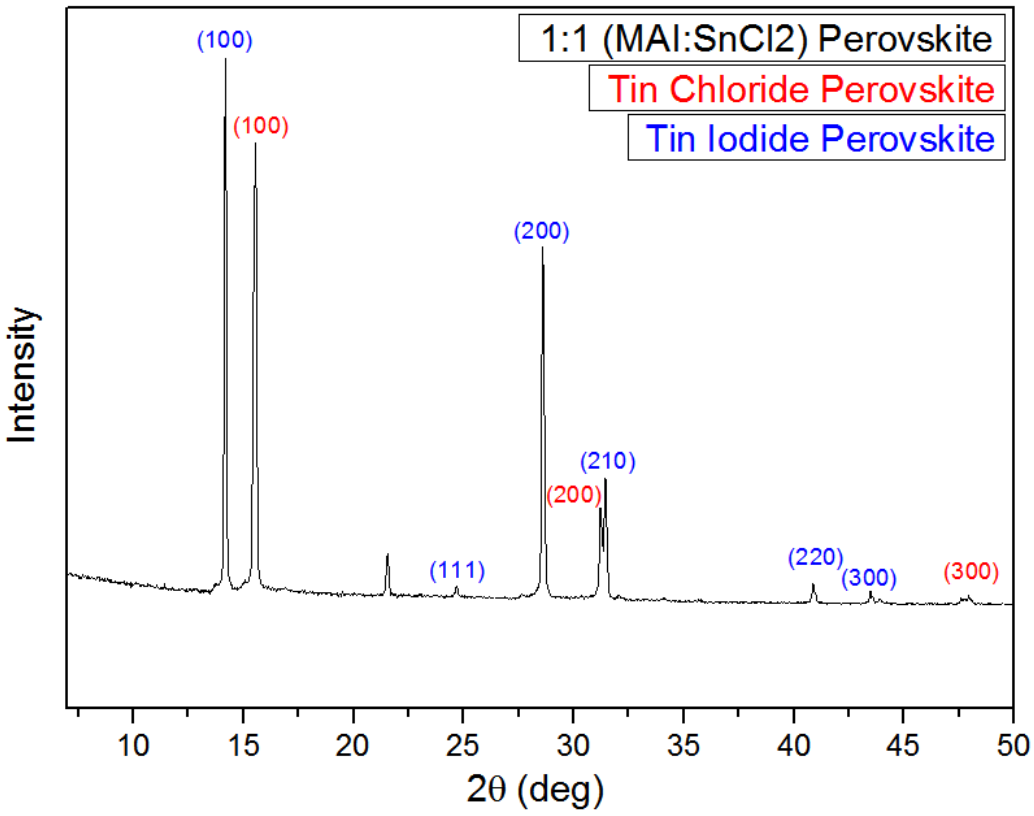

Figure 4.3. XRD pattern of the product from MAI and $SnCl_2$.

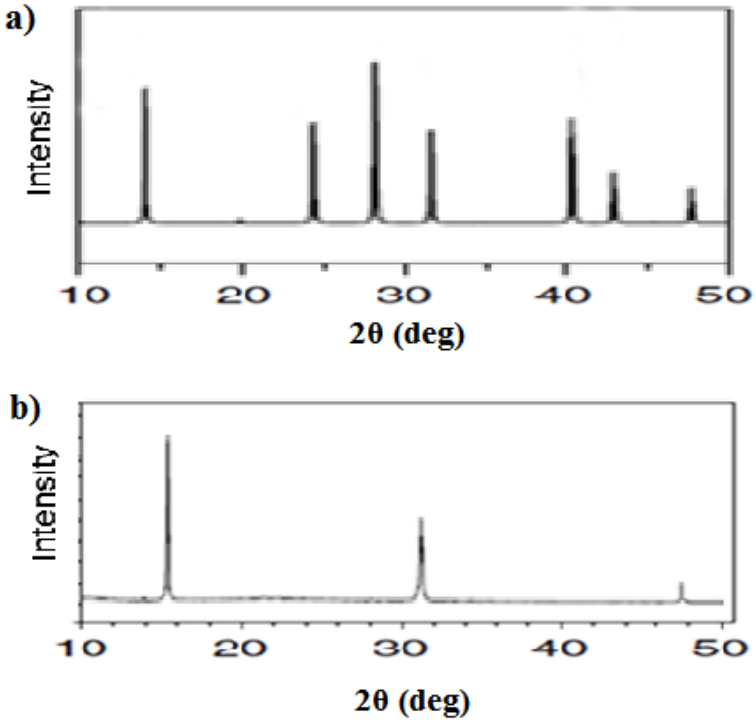

Figure 4.4. XRD patterns from the literature for different Perovskites: $MASnI_3$ (a) (Kanatzidis et al., 2014) and $MASnCl_3$ (b) (Chiarella et al., 2008).

Most probable reasons of the product separation are atomic diameter and different nucleophilicity of the halogen atoms.

Compared to bromine (1.9 Å) and iodine (2.1 Å), atomic diameter of chlorine (1.8 Å) may not be big enough to form proper cubic structure (Batsanov, 2001). Maybe, since the diameter of bromine atom is closer to iodine, the results for MAI and $SnBr_2$ mixture, which will be given in the next part, is not the same with this one.

Because of the fact that this is an SN_2 reaction, the nucleophilicity of the atoms are another important parameter to form a structure. As we go down at halogens group of the periodical table, we can observe that the nucleophilicity is increasing (nucleophilicity of halogens I>Br>Cl).

It has been reported that if one mixed a 3:1 ratio of MAI:$PbCl_2$ and annealed them for around 1 hour to produce lead based Perovskite, the chlorine substance leaved the material as methyl ammonium chloride (MACl) (Tidhar et al., 2014). Thus, the remaining product could be shown as $MAPbI_{3-x}Cl_x$ where the x was trace amount of chlorine since the most of chlorine was removed.

When it is considered that this is an SN_2 reaction which contains polar aprotic solvent and that the chlorine has lower nucleophilicity, the conception of iodine based Perovskite as a final product makes sense. Moreover, this behavior is the same for the tin Perovskite because of that it has similar structure with lead Perovskite.

Hull (1919) stated that every crystalline gave a specific XRD pattern, the same pattern was always found for the same substance, and each substance produced its own pattern independently of the others when they were mixed. He basically reported that ‘the summation of the XRD patterns’ in his research, whose one example can be seen in Figure 4.5. in our situation.

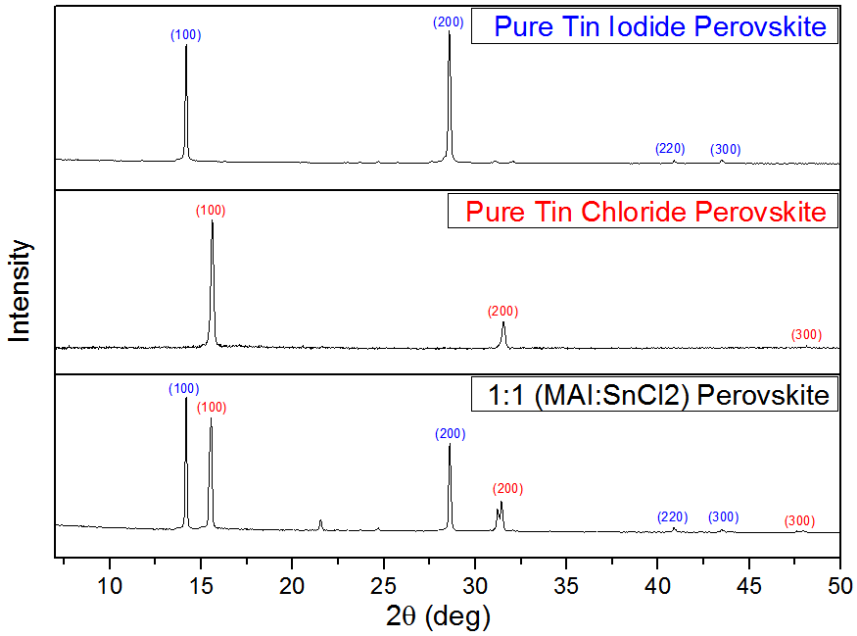

Figure 4.5. XRD patterns of the experimental polycrystalline Perovskite.

As can be seen in Figure 4.6., Perovskite crystals were formed again, but since the amorphous FTO layer could be seen between the crystals in the images as well, we could have clearly observed that the coverage was not good enough to prevent shunt and the structure was really unstable.

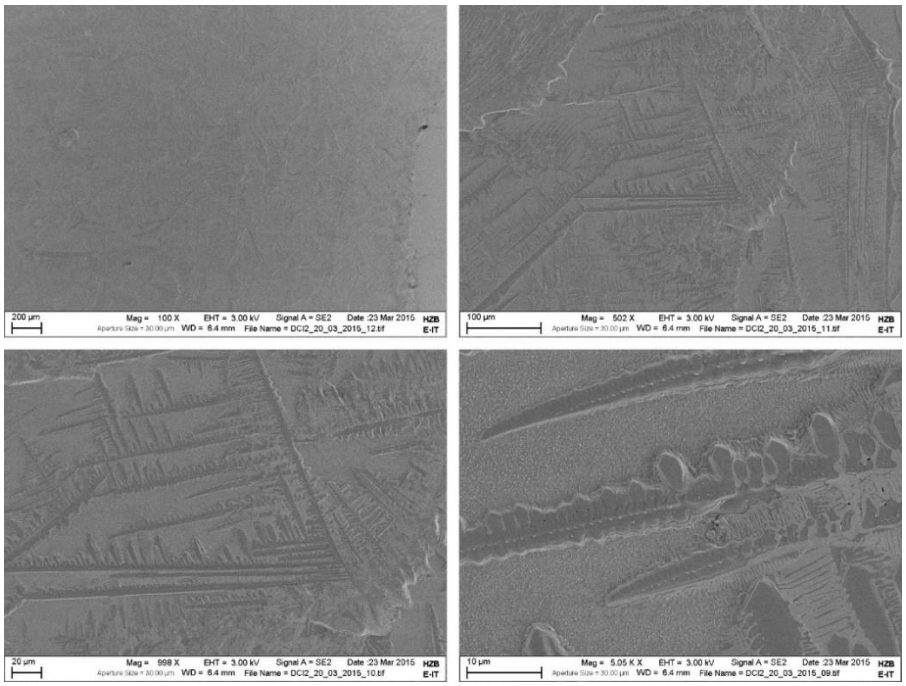

Figure 4.6. SEM images of the experimental polycrystalline $MASnI_{3-x}Cl_x$ crystals (Around 100X, 500X, 1000X and 5000X, respectively).

When the photoluminescence (PL) measurements were conducted, it was seen that there was a band gap energy at 1.3 eV (Kanatzidis, 2014), which belonged to pure iodine based tin Perovskite. Unfortunately, the band gap energy for pure chlorine based tin Perovskite could not have been measured with this PL setup because of that the excitation laser was not available in our set-up for that interval since that interval is not efficient for solar cells. The PL result of the sample, which is identical with the pure iodine, can be seen in Figure 4.7.

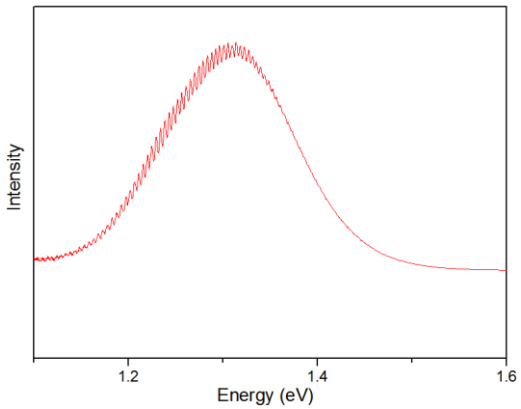

Figure 4.7. PL result for the mixed Cl-I based tin Perovskite sample.

Another important point was using glovebox during experiments in order to obtain specimens without any degradation. In Figure 4.8., the early production attempts without using glovebox can be seen. The yellow solution turned into red color in less than ten seconds because of moisture and oxygen contact, and thus, forming brown colored layers.

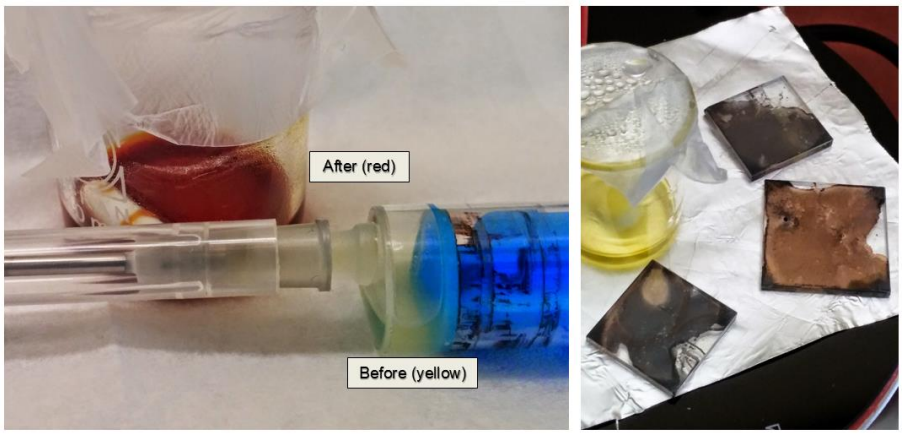

Figure 4.8. Degraded chlorine based tin Perovskite.

4.2. Two Step Method (Sequential Deposition)

The two step method is a good process for the lead halide Perovskites because of the comparatively low annealing time. The process needs annealing just for the crystal growth step, but not the forming step. But, as stated in the chapter 3, the selection of the second solvent is quite important. Unfortunately, the most of polar protic solvents dissolved tin (II) chloride and tin (II) bromide although they do not dissolve lead (II) chloride and lead (II) bromide. As can be seen in Figure 4.9., tin (II) chloride was washed away even though it was coated on mesoporous titania glass.

Figure 4.9. Image of tin (II) chloride for the sequential deposition method.

Even though tin (II) iodide (SnI_2) was partially soluble in polar aprotic solvents, the coating, which was on the bare glass, was totally washed away when it was dipped into second solution. Thus, it was seen that the two step method for tin Perovskites was not as applicable as the one for the lead Perovskites.

4.3. Solid State Reaction Method

Solid state reaction method is a promising method to prepare Perovskite crystals. Compared to other methods, the biggest Perovskite crystals were obtained as seen in XRD

images as higher intensity. Most probable reason why the bigger crystals were achieved was the intermediate Perovskite structure, which was the one before the nucleation step was already formed by this method. The specimen was observed even at the crystal formation step. Besides, when it is dissolved at lower temperatures than the formation temperatures, most of the intermediate Perovskite structures may preserve themselves from degradation.

4.3.1. Tin (II) Iodide

Since that pure iodide tin Perovskite was our verifiable material from the literature, the first trials of the solid state reaction method were conducted in order to acquire properly produced pure iodine tin Perovskite. As can be seen in Fig 4.10., as a consequence of the solid state reaction, the pure iodide Perovskite was obtained with its prominent XRD peaks.

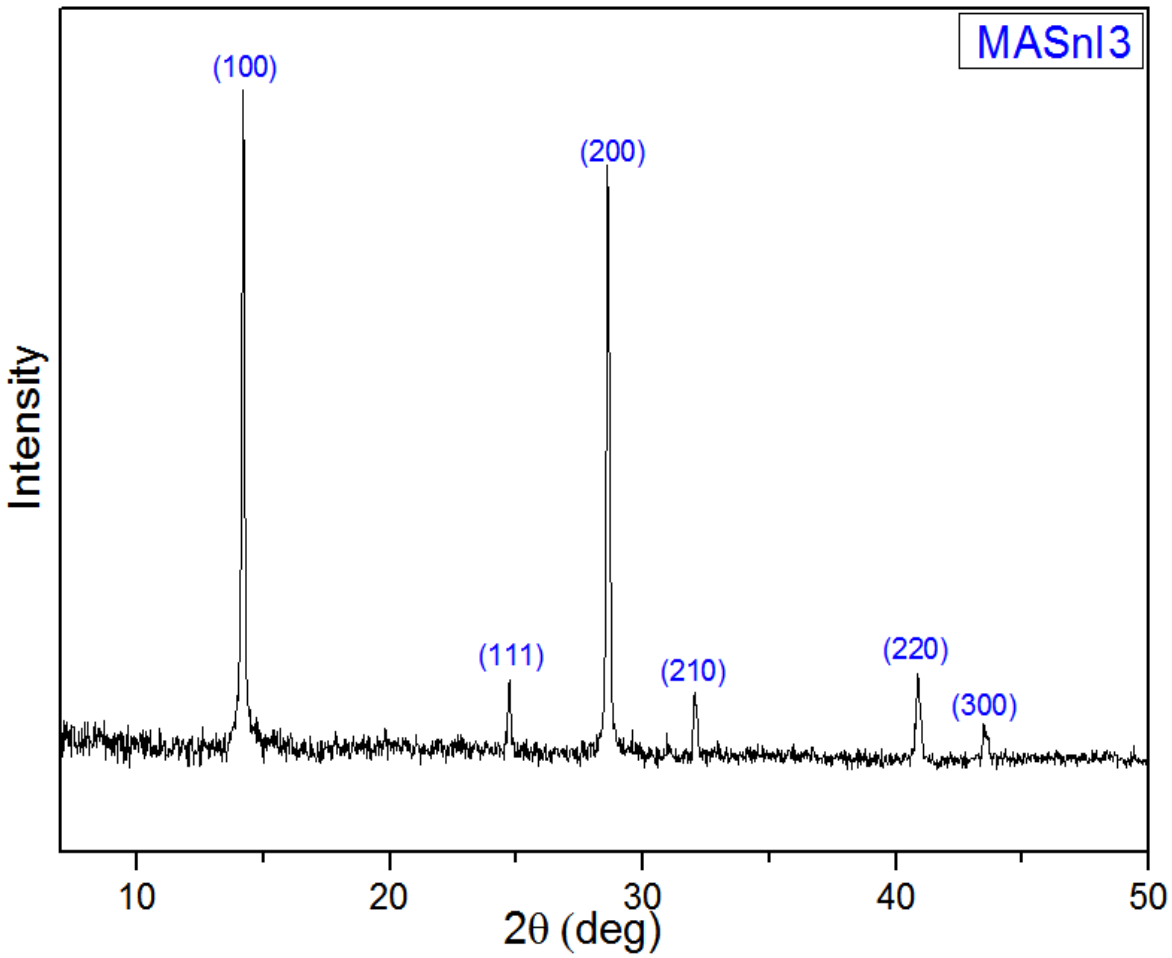

Figure 4.10. XRD pattern for the experimental $MASnI_3$ of solid state reaction.

Though, the coverage was still not good to prevent shunting because of that crystals did not grow to spread all over the surface (Figure 4.11.).

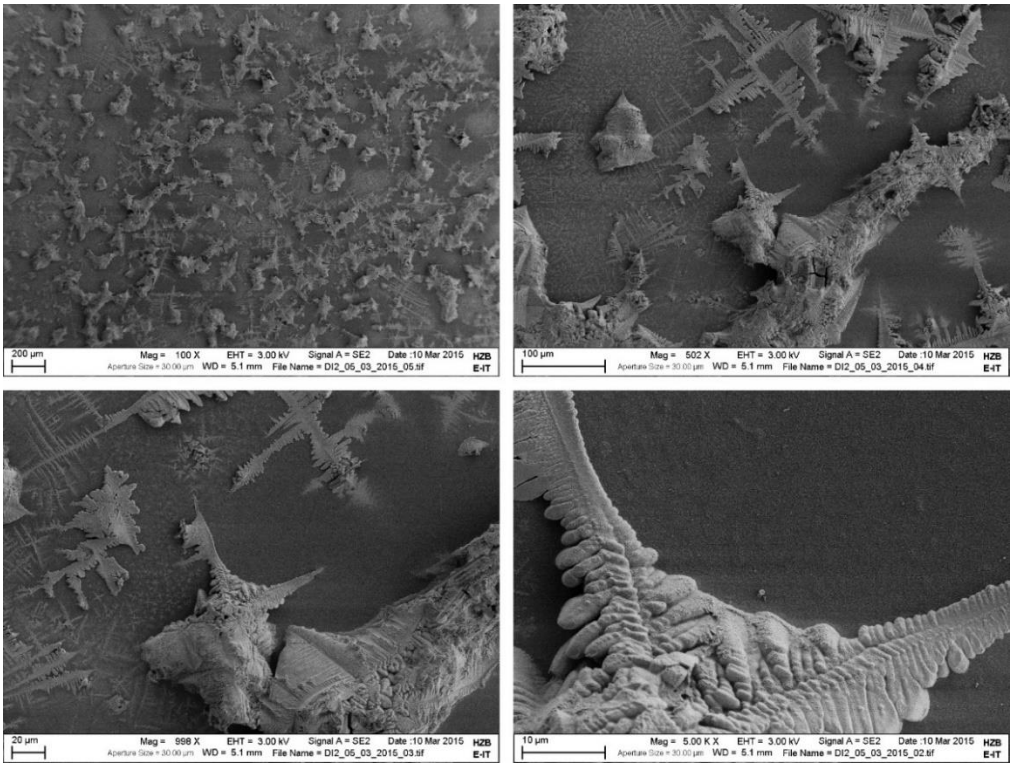

Figure 4.11. SEM images of the experimental $MASnI_3$ crystals of solid state reaction (Around 100X, 500X, 1000X and 5000X, respectively).

The colorless precursors turned into grey even while grounding. When they were heated at 120°C for around 20 minutes, the final color was black as seen in Figure 4.12.

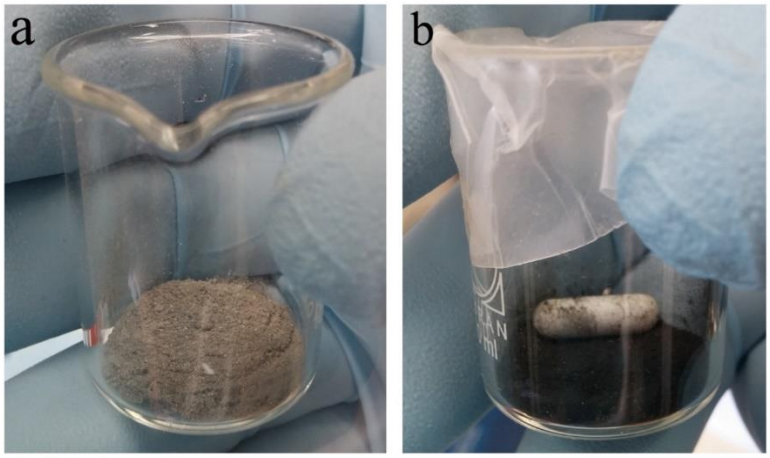

Figure 4.12. Prepared $MASnI_3$ by the solid state reaction method.

Although, the dissolved iodine Perovskite gave a dark yellow solution, the film of the Perovskite turned into black again as in Figure 4.13.

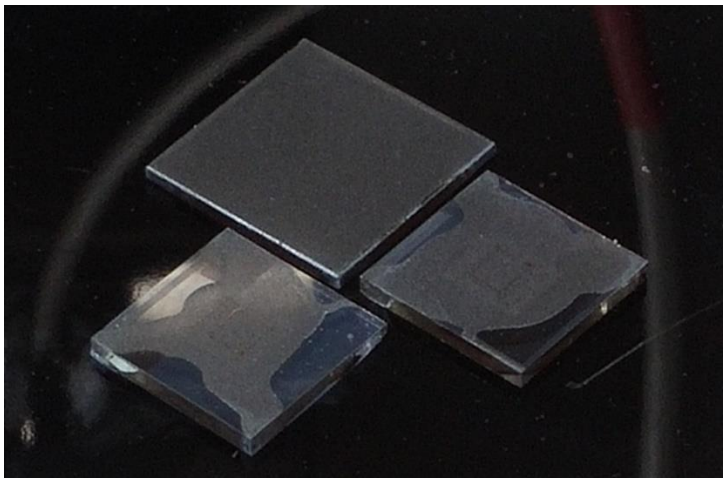

Figure 4.13. Prepared $MASnI_3$ crystals of solid state reaction while annealing.

The characteristic PL result for the pure iodine Perovskite of the solid state reaction, which can be seen in Figure 4.14, is identical with the one which produced by one step method. This result also proves that it is iodine tin Perovskite with its 1.3 eV band gap energy.

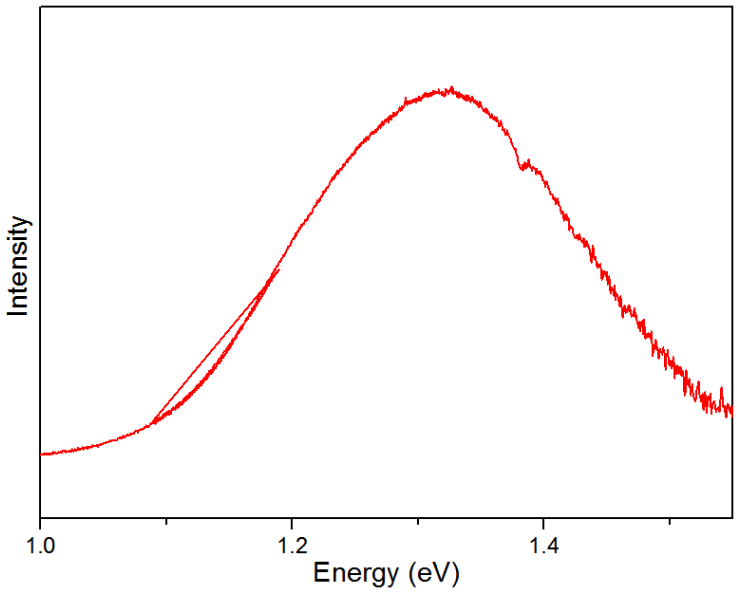

Figure 4.14. PL result for the pure iodine tin Perovskite of the solid state reaction.

4.3.2. Tin (II) Bromide

When pure iodine tin Perovskite was obtained, its method was used as a template for the next experiments. Since that pure bromine tin Perovskite has 2.15 eV band gap energy and pure iodine tin Perovskite has 1.3 eV band gap energy, the band gap energy of mixed iodine-bromine tin perovskite would be in this energy interval. Thus, in this section, data for mixed iodine-bromine tin Perovskite will be provided.

As can be seen in Figure 4.15., the produced mixed tin iodide-bromide Perovskite by using the solid state reaction had the same properties with the ones produced by using one step method, except their crystalline sizes.

The crystal sizes were improved in the solid state reactions as well as tin iodide Perovskite, which was discussed in the previous section.

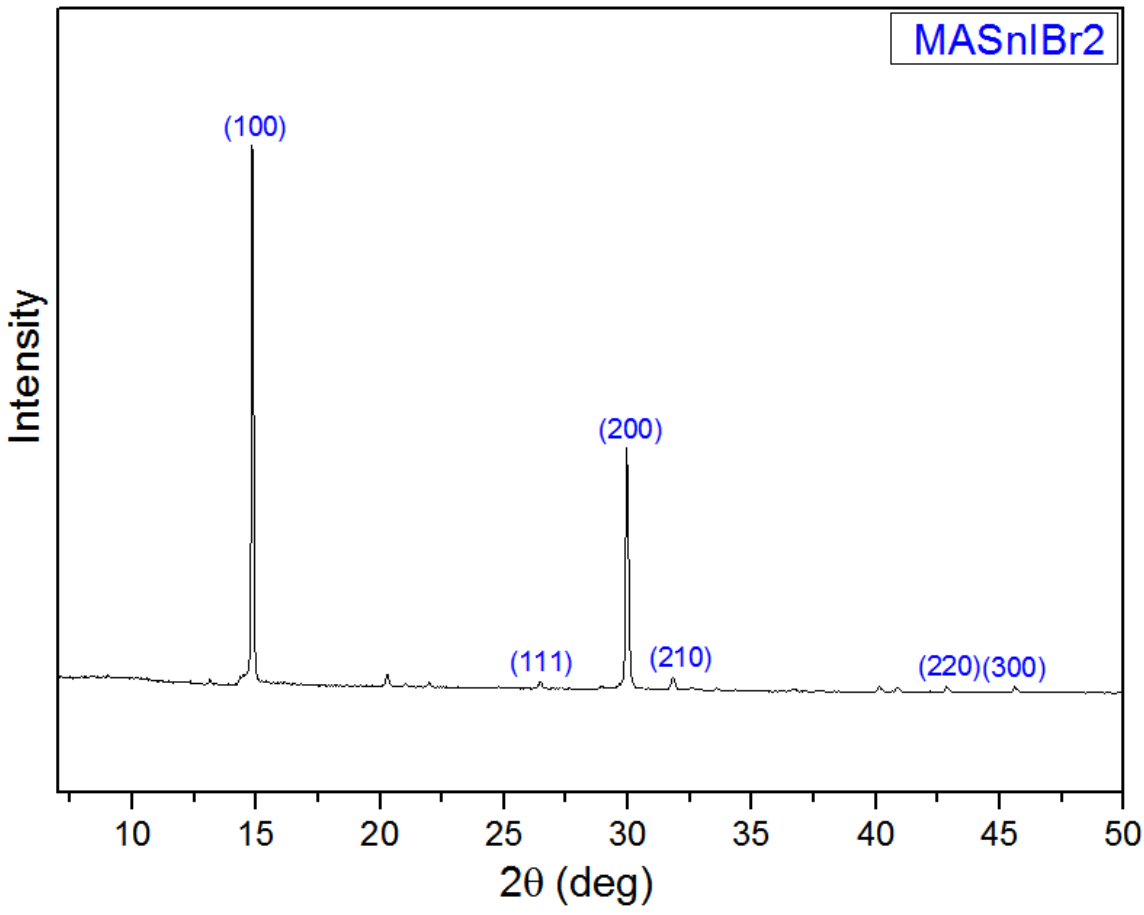

Figure 4.15. XRD pattern for the experimental $MASnIBr_2$ of solid state reaction.

Even though the crystalline sizes obtained by this method were bigger than the ones in other methods, there was no great advancement in the coverage.

The existing gaps between the crystals, which can be seen in Figure 4.16, are too wide to prevent shunting and keep the circuit closed.

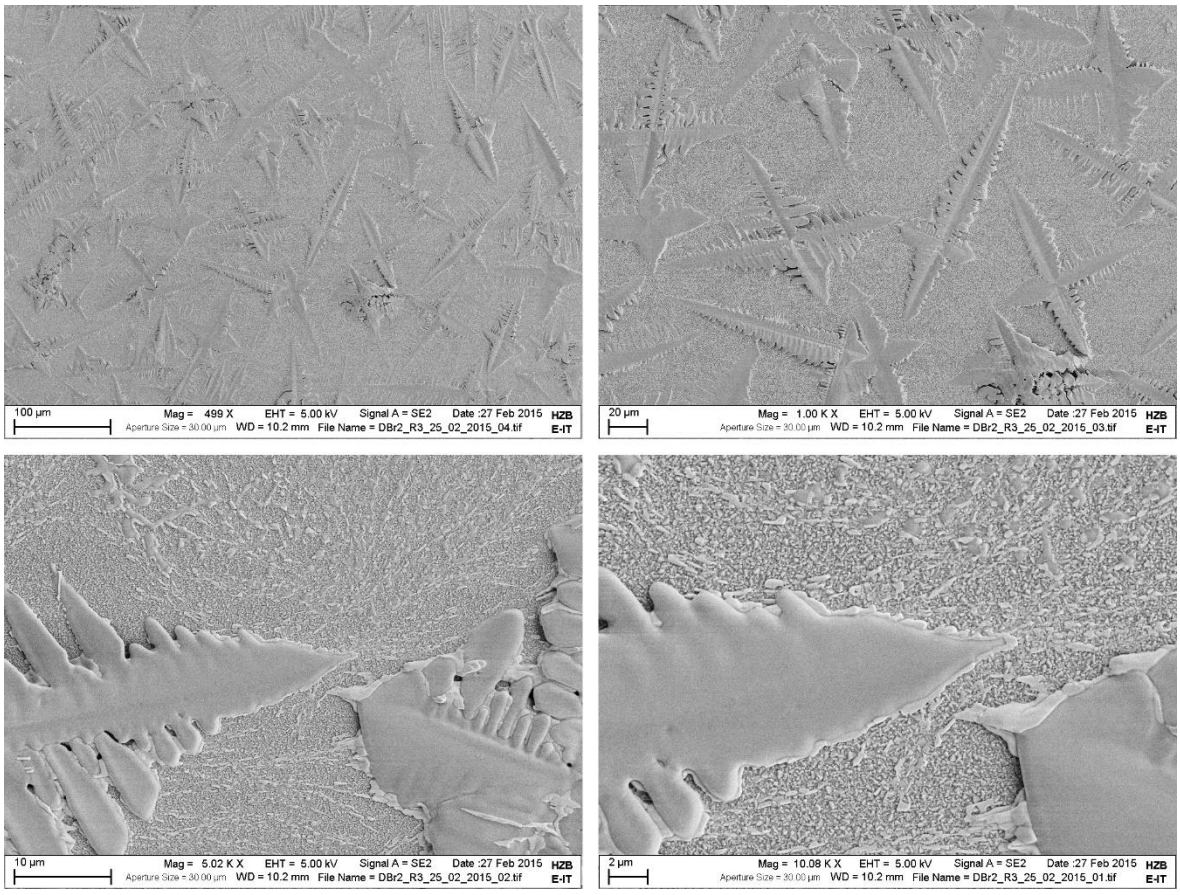

Figure 4.16. SEM images of the experimental $MASnIBr_2$ crystals (Around 500X, 1000X, 5000X and 10000X, respectively).

The PL and Uv-Vis results are given in Figures 4.17. and 4.18. for this specimen, respectively, showing that the iodine-bromide mixed tin Perovskite has around 1.75 eV band gap energy.

And the given data from the literature in Figure 4.19 shows the same result when they are compared.

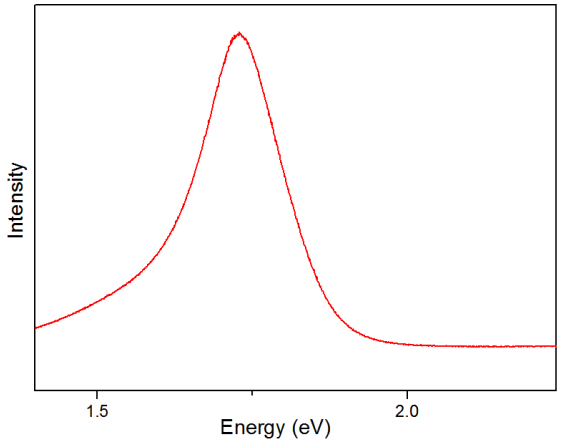

Figure 4.17. PL result for the Br-I mixed tin Perovskite of the solid state reaction.

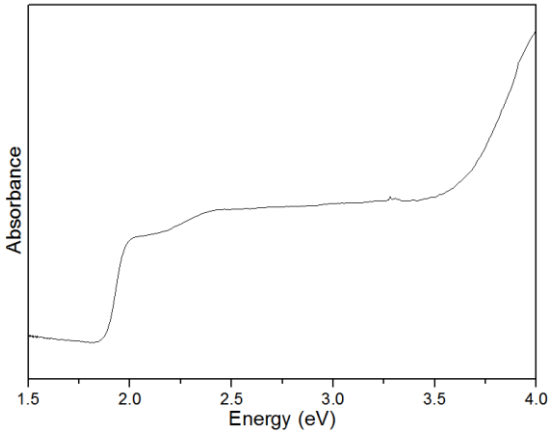

Figure 4.18. Uv-Vis pattern for the experimental $MASnIBr_2$ of solid state reaction.

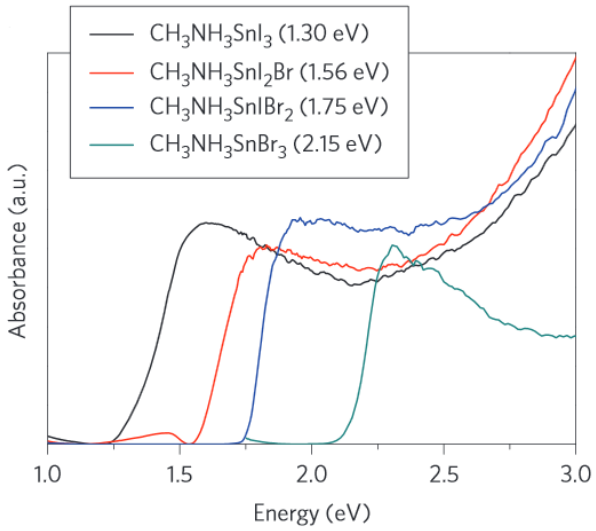

Figure 4.19. Uv-Vis pattern for the bromine-iodine mixed tin Perovskites (Kanatzidis et al., 2014).

All the data, which has been obtained until this point of the study, has shown that the mixed iodine-bromine tin perovskite might compete with the pure iodine tin Perovskite by relatively high band gap energy of the mixed one. Thus, the mixed iodine-bromine tin perovskite was worth investigating at the next steps of this study.

4.3.2.1. Tin (II) Bromide for Different Reaction Temperatures. Now that the reaction kinetic affected the final product and the coverage consequently, reaction temperature, which was one of the main parameters of reactions, was investigated. Due to time restriction for this study, the changed temperature intervals were large. However, there were some differences on the structures. When the experiments were completed for the tin (II) bromide based Perovskites, the one produced at 120°C was selected because of its comparatively better physical and chemical properties. The XRD patterns of the $MASnIBr_2$ for different reaction temperatures are given in Figure 4.20.

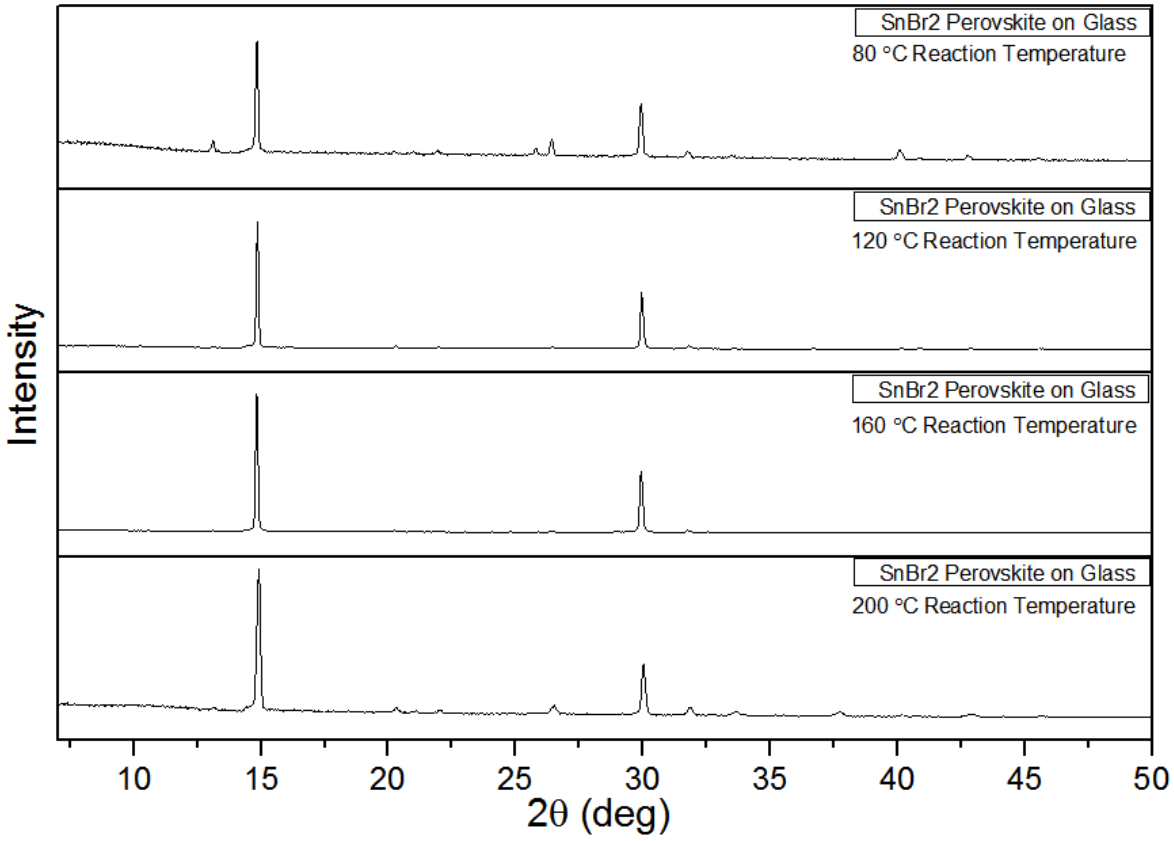

Figure 4.20. XRD patterns of the $MASnIBr_2$ for different reaction temperatures.

As can be seen in Figure 4.20., there were extra peaks, which did not belong to Perovskite structure at 80 and 200°C. Since the one produced at 160°C used more energy, the one formed at 120°C was chosen for further experiments.

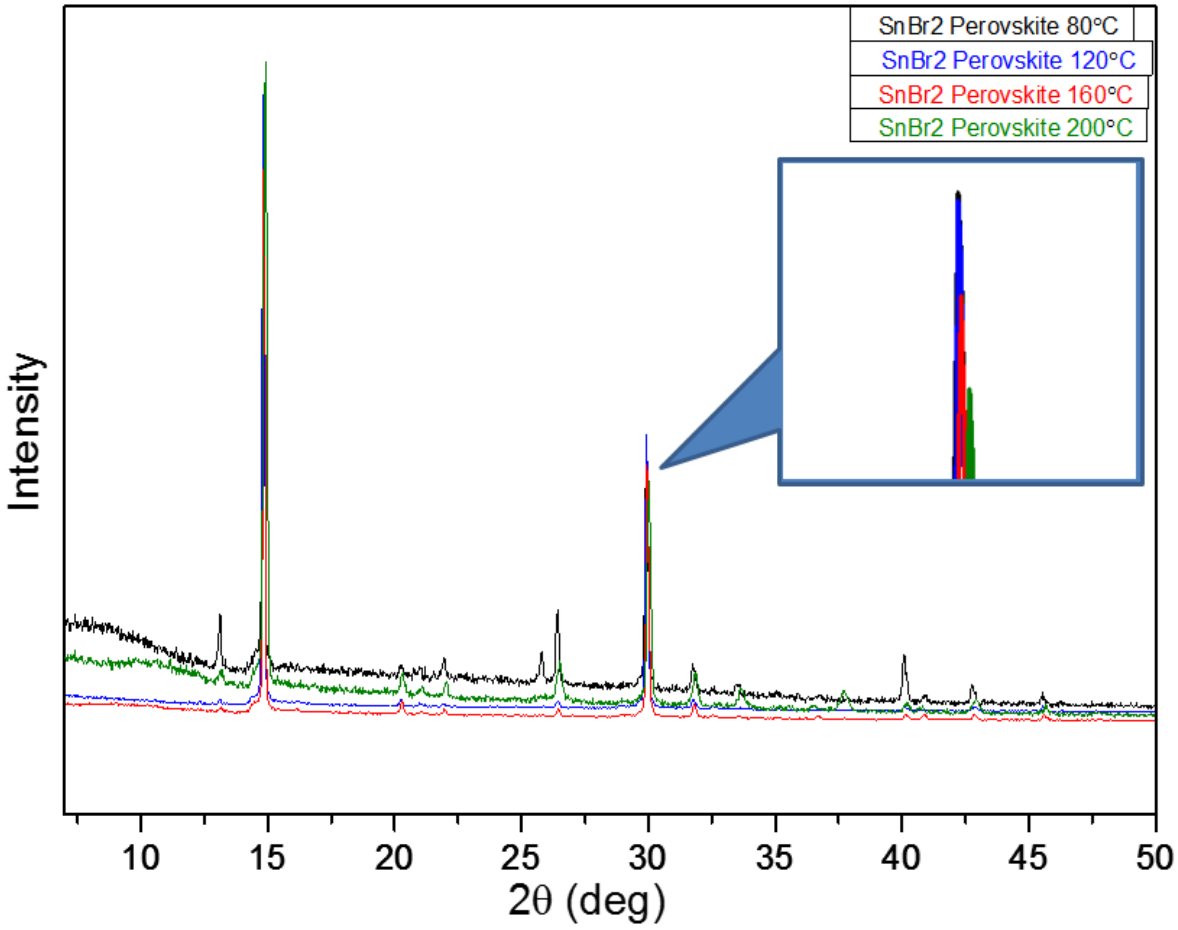

Figure 4.21. Final product selectivity due to the reaction temperature.

In Figure 4.21., it can be observed that there is shifting for the peaks, which show tendency towards lower nucleophilic halogen at higher temperatures in contrast to ordinary reaction tendency.

The product is yielding to the side of bromine, which can be seen in Figure 4.22. In other words, the bromine number of the Perovskite molecule was increasing. This may be a possible product selectivity due to the reaction temperature or may be just because of the removal of the MAI precursor by heat.

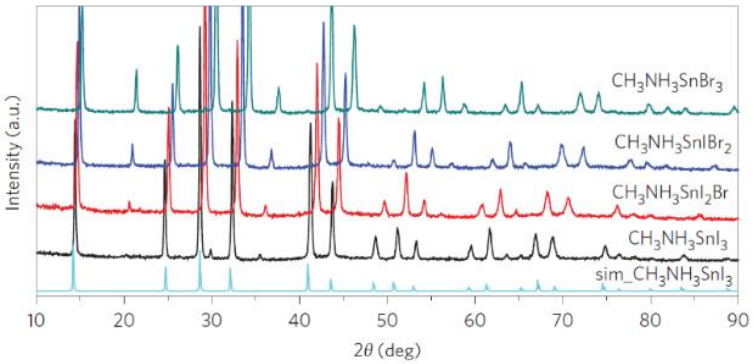

Figure 4.22. XRD patterns for the Br-I combinations of the tin Perovskite (Kanatzidis et al., 2014).

The shifting of the patterns continues to the same direction for the chlorine based Perovskites as well.

4.3.2.2. Tin (II) Bromide for Different Weight Concentrations. When the experiments were completed for the tin (II) bromide based Perovskites, the one produced at 120°C was selected because of its comparatively better physical and chemical properties, and it was used for the investigation of the different weight concentrations as a constant parameter. In Figure 4.23., another split of the pattern can be observed due to the concentration change.

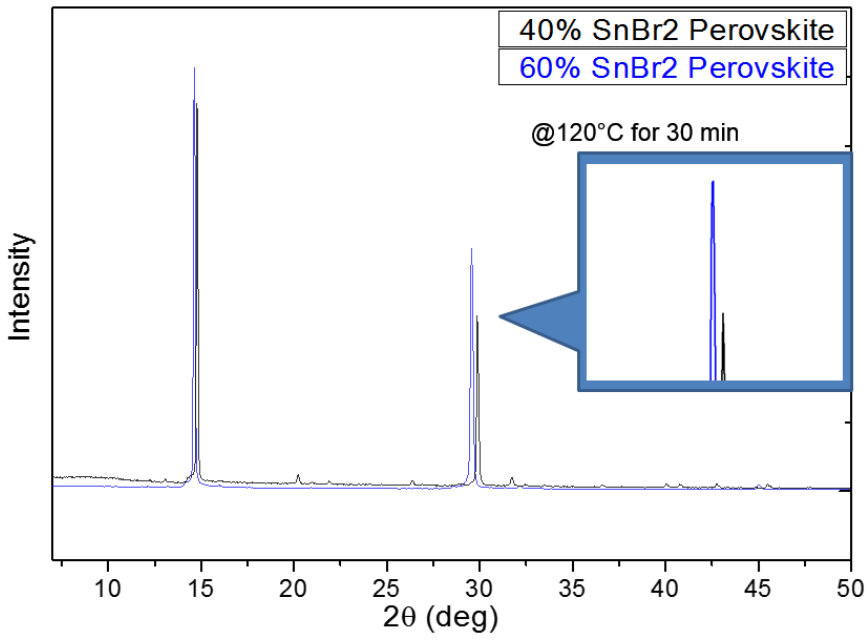

Figure 4.23. Final product selectivity due to the concentration of the precursors.

As we know, the reaction rate is proportional with the concentration of the reactant. Thus, increased concentration increases the rate of reaction. Now that there is tendency for iodine based Perovskite at further steps of the reaction as seen in Figure 4.22., the iodine ratio of the final product is higher for the higher concentrated solution.

Since high iodine ratio in the mixed Perovskite provided lower band gap energy and high efficiency consequently, 60 % mass concentration would be more beneficial for the solar devices. However, according to desired properties of the device or for higher stability, the concentration can further be optimized in another study.

4.3.2.3. Tin (II) Bromide for Different MAI Concentrations. Since one of the precursors could change the rate of the reaction, the investigation of the concentration change was applied to MAI since that the excess of MAI could be evaporated while annealing. In Figure 4.24., bromide based Perovskites for three different MAI ratio can be seen.

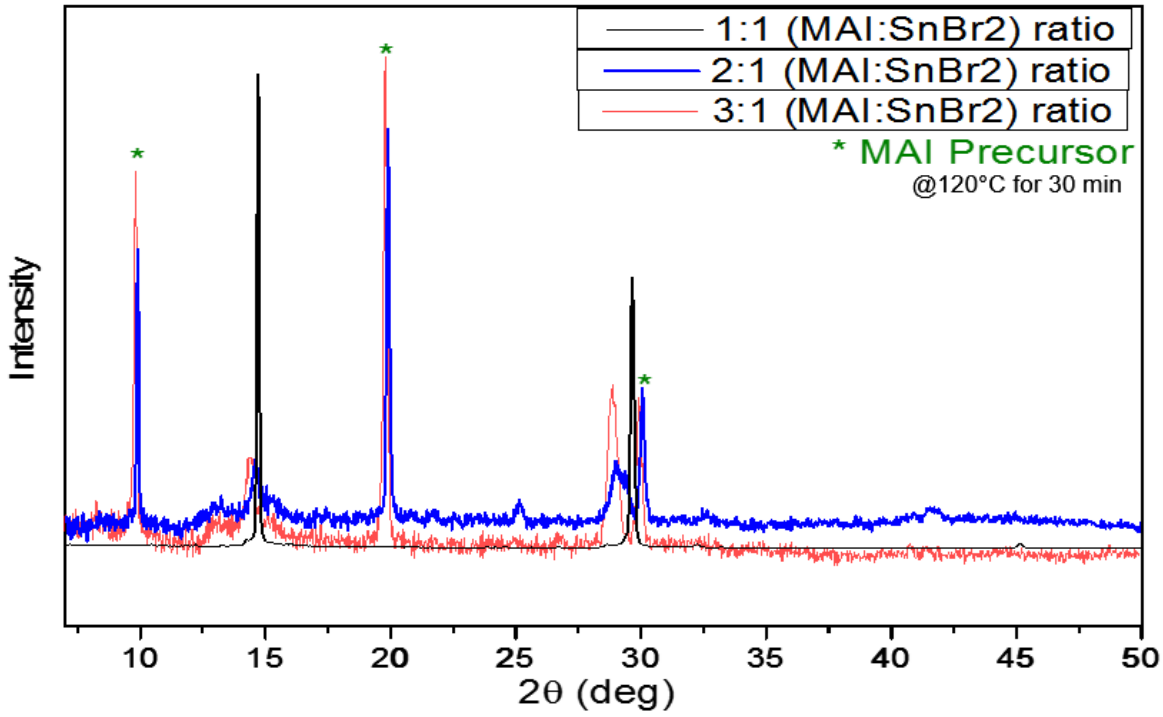

Figure 4.24. The investigation for the effects of different MAI concentrations.

The peaks denoted with stars show the presence of excess MAI. But the prominent split for the peak, which is at 30°, shows the sliding motion of the final product patterns towards

iodine side. This shows that there is a halogen exchange between MAI and the Perovskite. The split is wider as the MAI concentration increases.

4.3.3. Tin (II) Chloride

Prepared chlorine based tin Perovskite by using the solid state reaction has more prominent peaks, which can be seen in Figure 4.25. The presence of the tin chloride Perovskite is more visible, but the life-time of the tin chloride Perovskite is not too long.

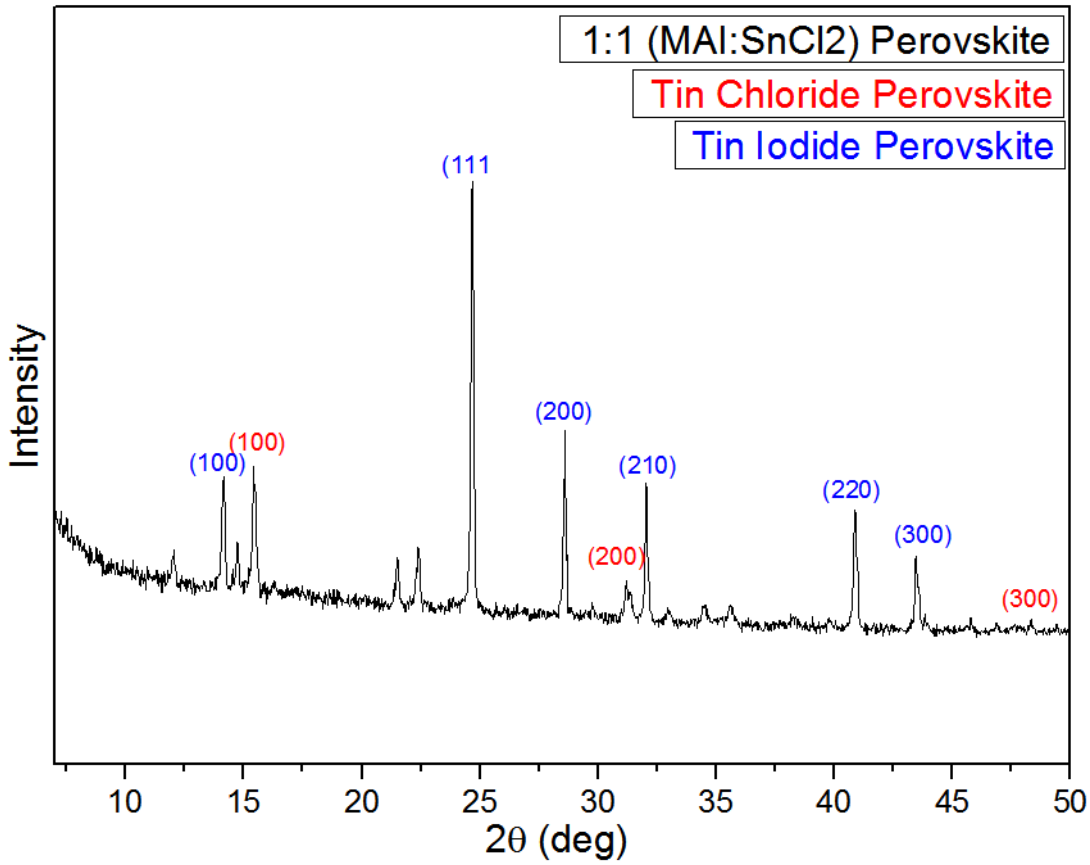

Figure 4.25. XRD patterns of the experimental $MASnI_{3-x}Cl_x$ for solid state reaction.

In Figure 4.26., the life-time of the mixed Cl-I based tin Perovskite can be seen. The specimen was sealed in the inert atmosphere full of nitrogen and brought out just for the measurements. Though, the degradation can easily be seen by the help of peak length comparison. Some of the peaks totally vanished and some other peaks appeared, which were not supposed to turn up.

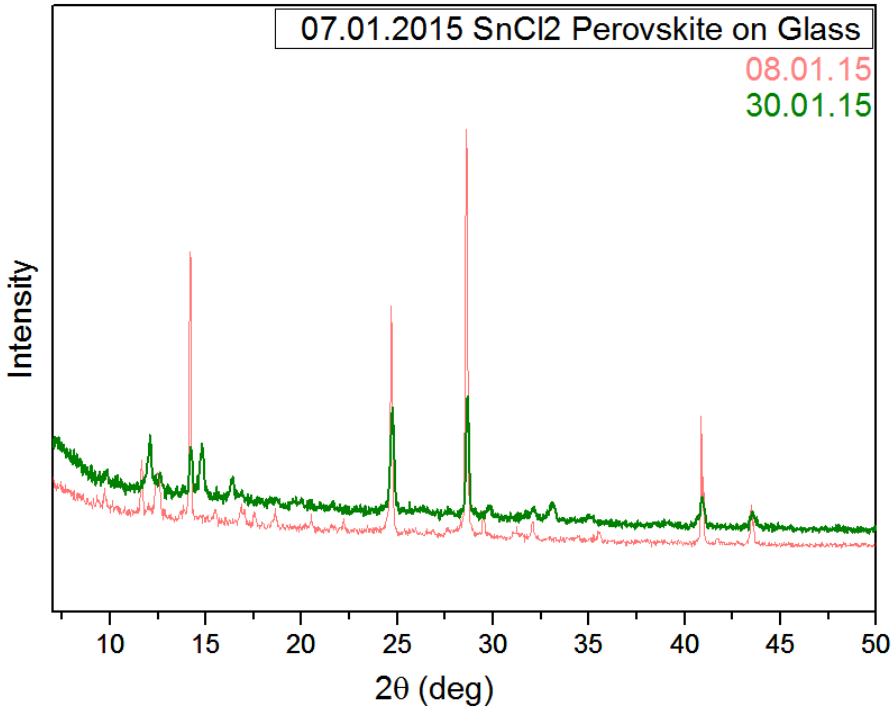

Figure 4.26. Life-time comparison of the same Cl-I mixed tin Perovskite sample.

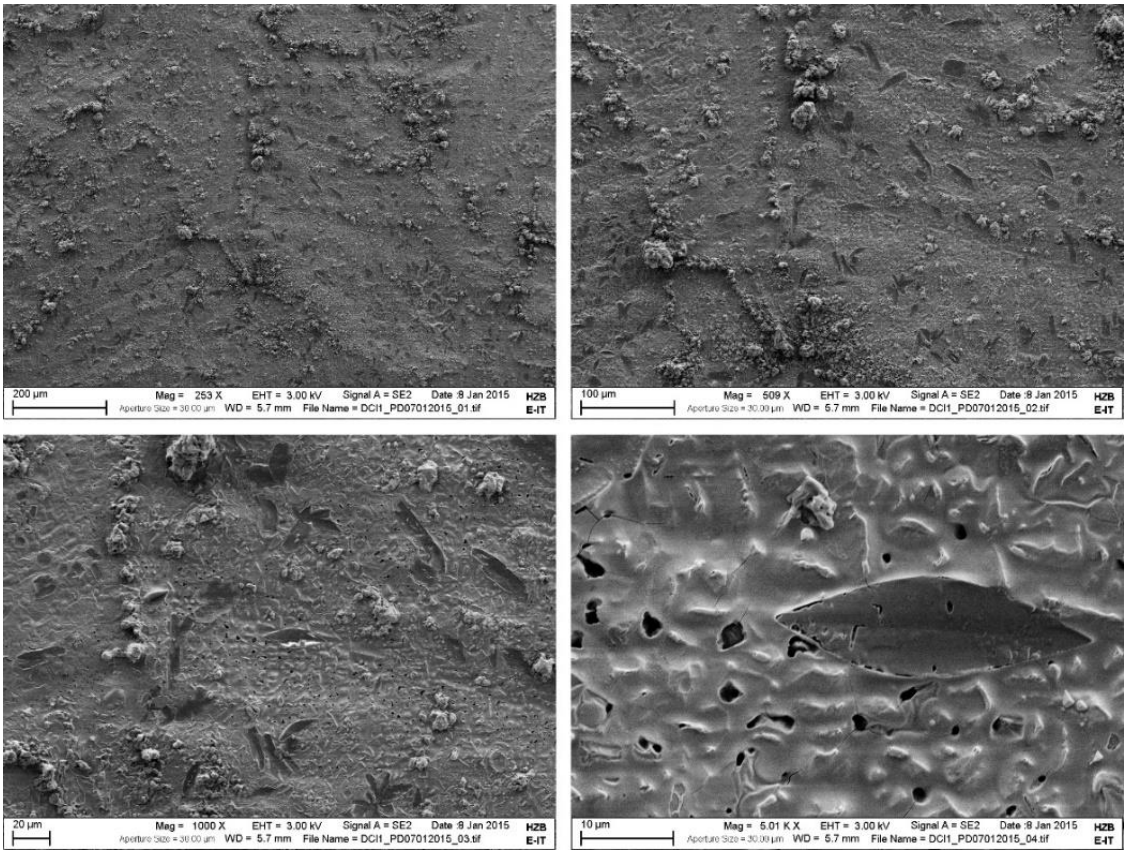

Figure 4.27. SEM images of the experimental $MASnI_{3-x}Cl_x$ crystals (Around 250X, 500X, 1000X and 5000X, respectively).

The SEM images of the mixed Cl-I tin Perovskite can be seen in Figure 4.27. While taking the SEM images, it was observed that there were still some reactions going on in the sample. Due to vacuum, some bubbles were coming through the leaf-like holes, which were present in the SEM pictures taken.

When EDX images were taken (Figure 4.28.), it was observed that those bubbles were coming from the chlorine part of the specimen as can be seen in the Cl part of the figure.

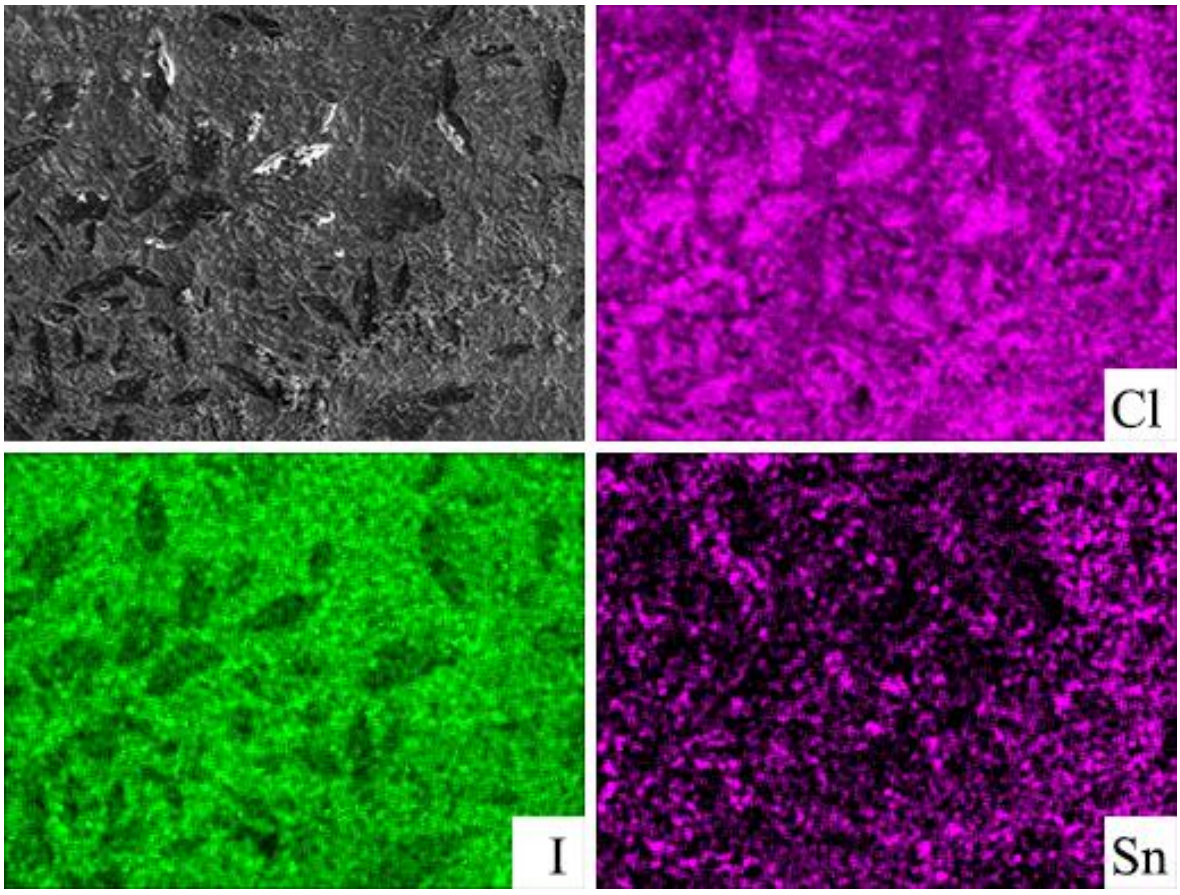

Figure 4.28. EDX images of the $MASnI_{3-x}Cl_x$ crystals of solid state reaction.

As seen in Figure 4.28., chlorine atoms were dense on some points of the sample and they had the poorest stability compared to the rest. The other elements looked like they were dispersed equally to the rest of the surface. With the help of high vacuum and electrons with high energy, chlorine abandoned the structure by evaporation.

4.4. Solvent Changing

Since that DMF was harmful not only for living beings but also for the environment, another solvent as substitute was considered. In this part of the research, we investigated two different solvent to exchange with DMF, namely DMSO and Acetone.

4.4.1. Acetone

Acetone is easy to find in every chemical laboratory and with its less harmful property, it is a good candidate for the solvent replacement. But unfortunately, it was not good enough to dissolve the precursors even though it was also from the same solvent group with DMF.

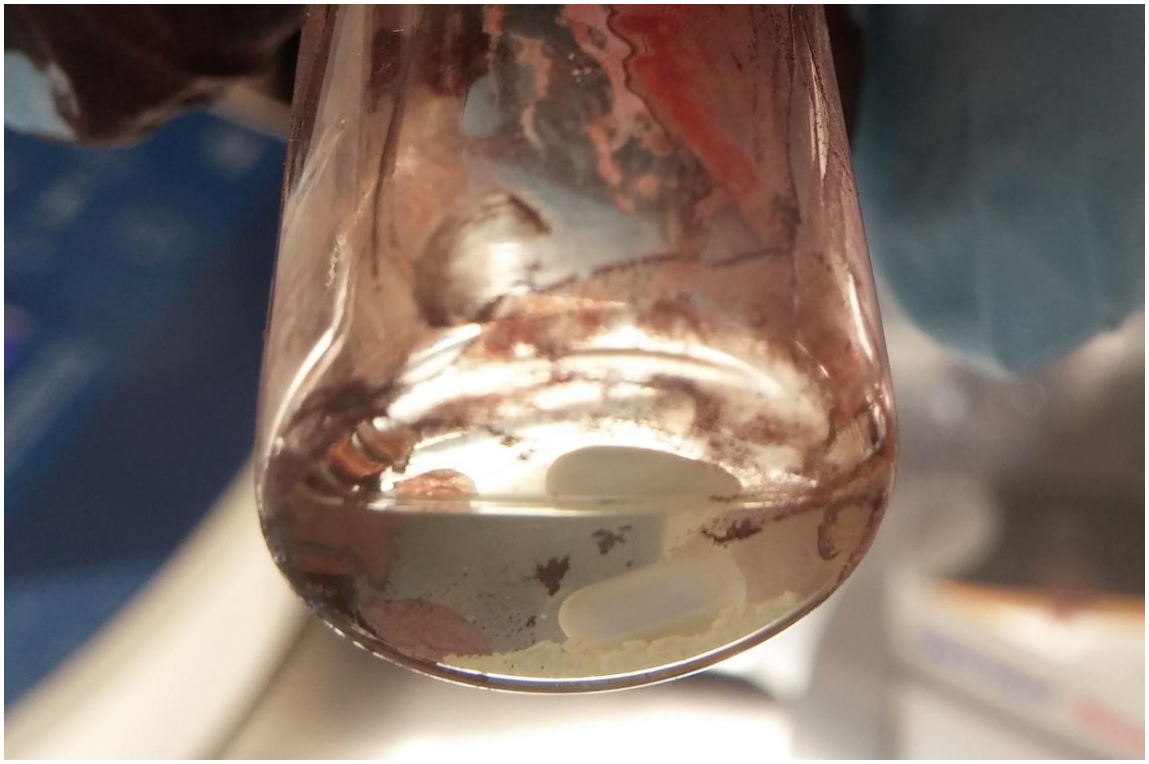

Figure 4.29. Undissolved precursor of the bromide based tin Perovskite.

In Figure 4.29., the undissolved part of the mixed bromide tin Perovskite precursors can be seen. Even though tin (II) chloride was partly soluble, it was a blurry solution, which was the indication of the partial dissolving and it did not spread on the glass properly (Figure 4.30.).

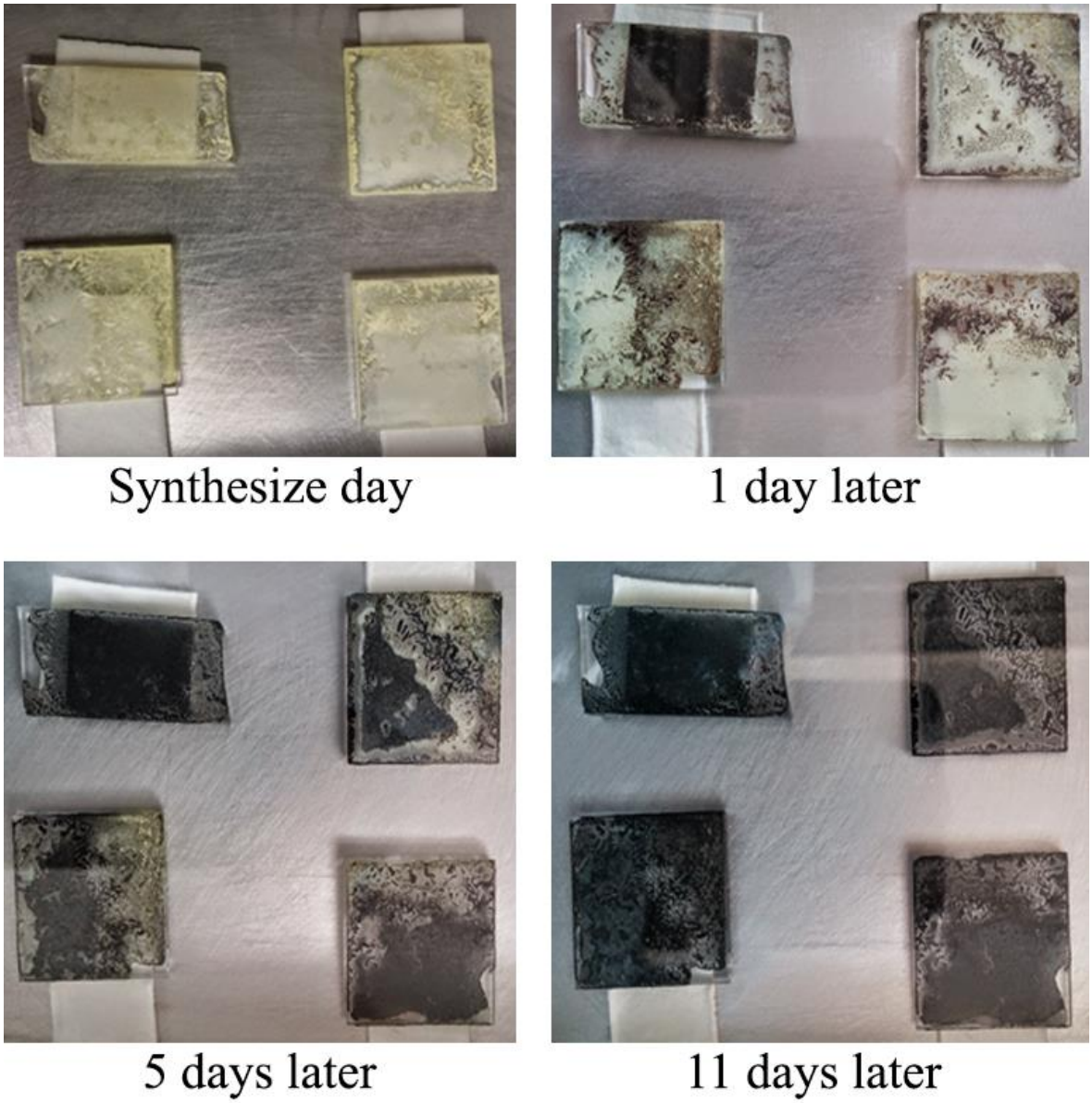

Figure 4.30. Partial solubility of the precursors in acetone.

Experiencing this reaction of the insoluble precursors gave us the idea of going with the solid state reaction method, because we observed that the solvent was not necessary for the reaction, but it was essential to obtain a high coverage of the material.

4.4.2. Dimethyl Sulfoxide (DMSO)

DMSO is also from the same solvent group, which is called polar aprotic solvents. Thus, they have similar chemical properties, except DMSO is less harmful than DMF. DMSO is

even used for cancer treatments, whereas DMF is carcinogenic. In this work, we report that it is possible to have same results when DMSO is used instead of DMF.

As can be seen in Figure 4.31., the identical tin bromide Perovskite peaks were present in the XRD pattern of the tin bromide Perovskite, which was produced with DMSO.

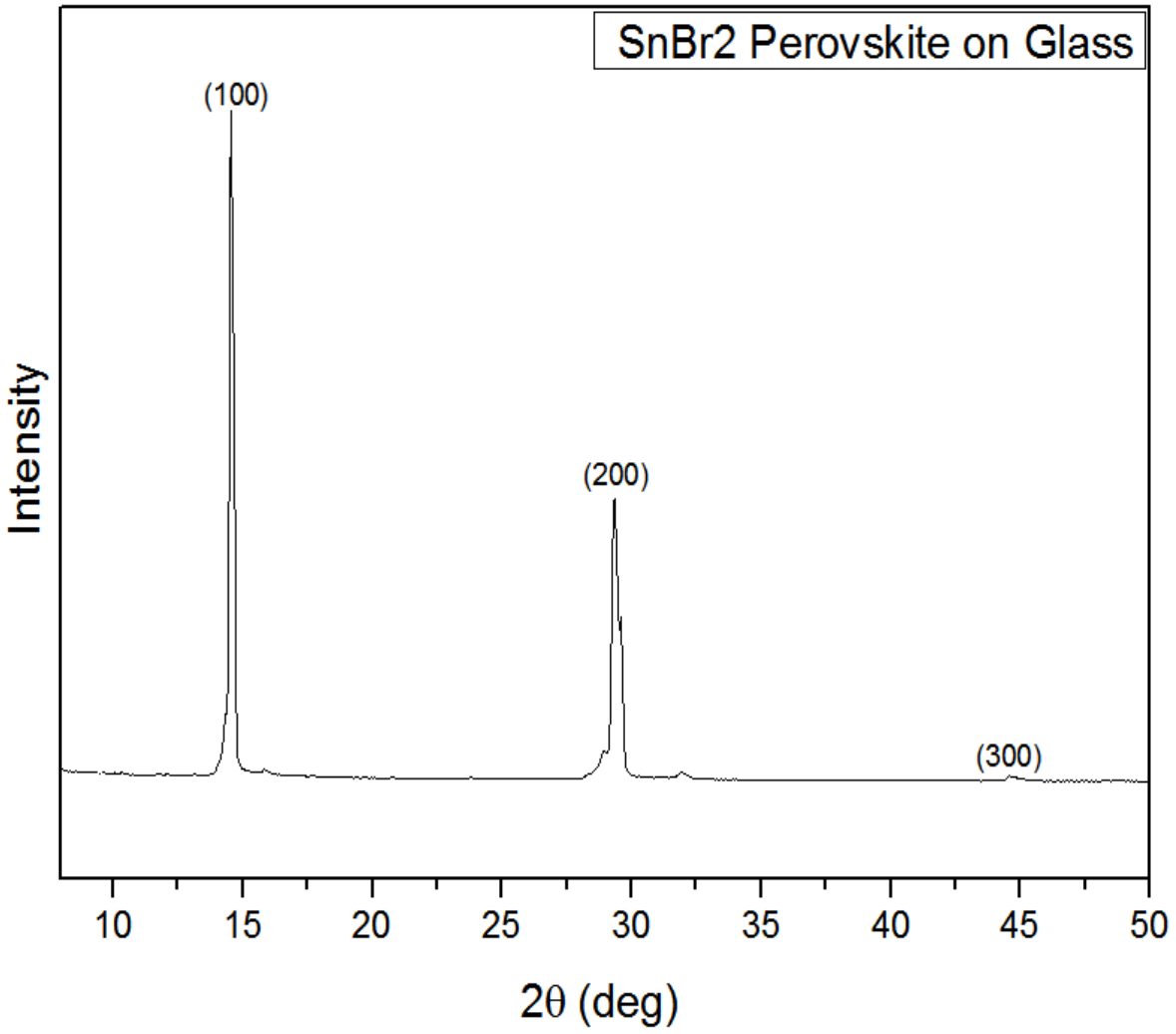

Figure 4.31. XRD pattern for the tin bromide Perovskite produced with DMSO.

We also observed that the response of the specimen to the concentration change of the precursors was the same with the one, which was done with DMF as previously discussed in this chapter. When the concentration of the precursors in the solvent increased, the product still preferred to go for more nucleophilic side as can be seen in Figure 4.32.

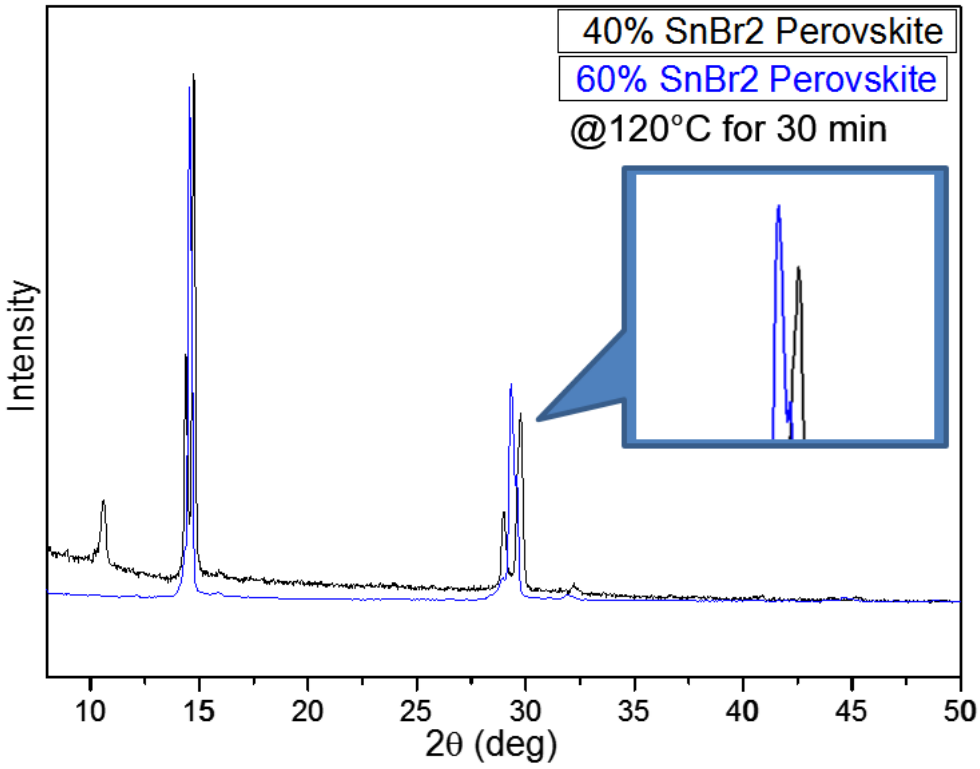

Figure 4.32. Final product selectivity due to the concentration of the precursors.

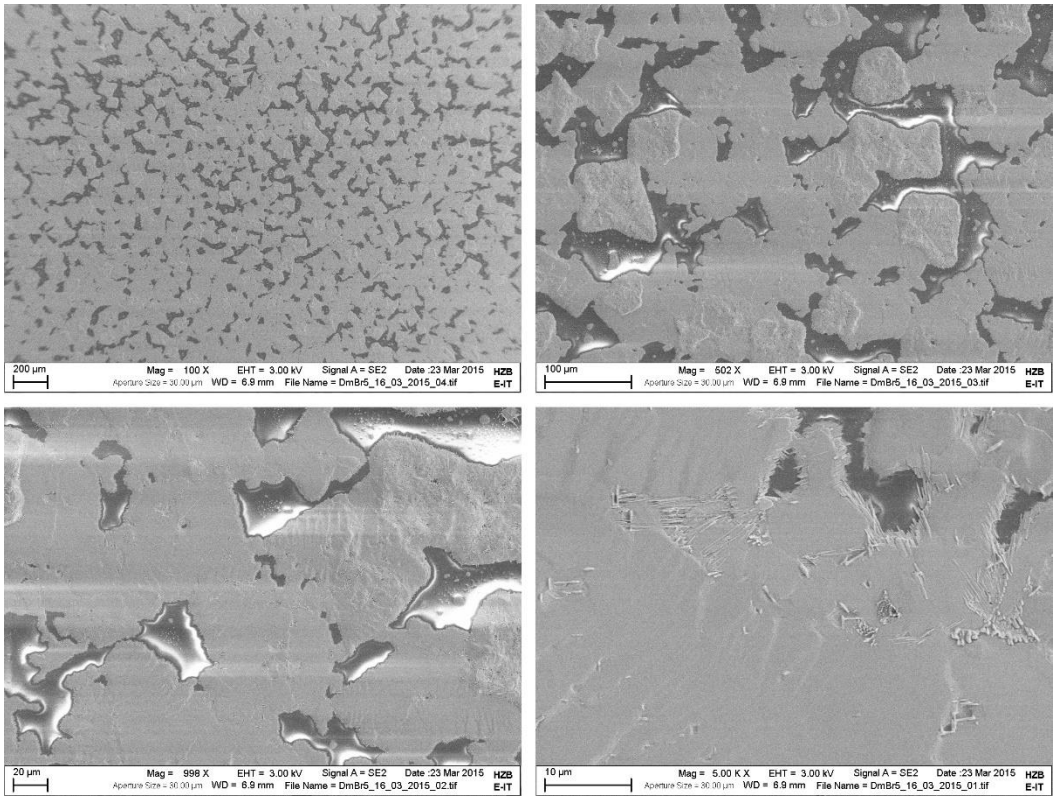

Figure 4.33. SEM images of the experimental $MASnIBr_2$ crystals (Around 100X, 500X, 1000X and 5000X, respectively).

According to the Figure 4.33., it could be stated that the coverage over the glass was even better than the one produced with DMF. Having the same band gap energy result with the PL measurement for bromine based tin Perovskite was still possible as seen in Figure 4.34.

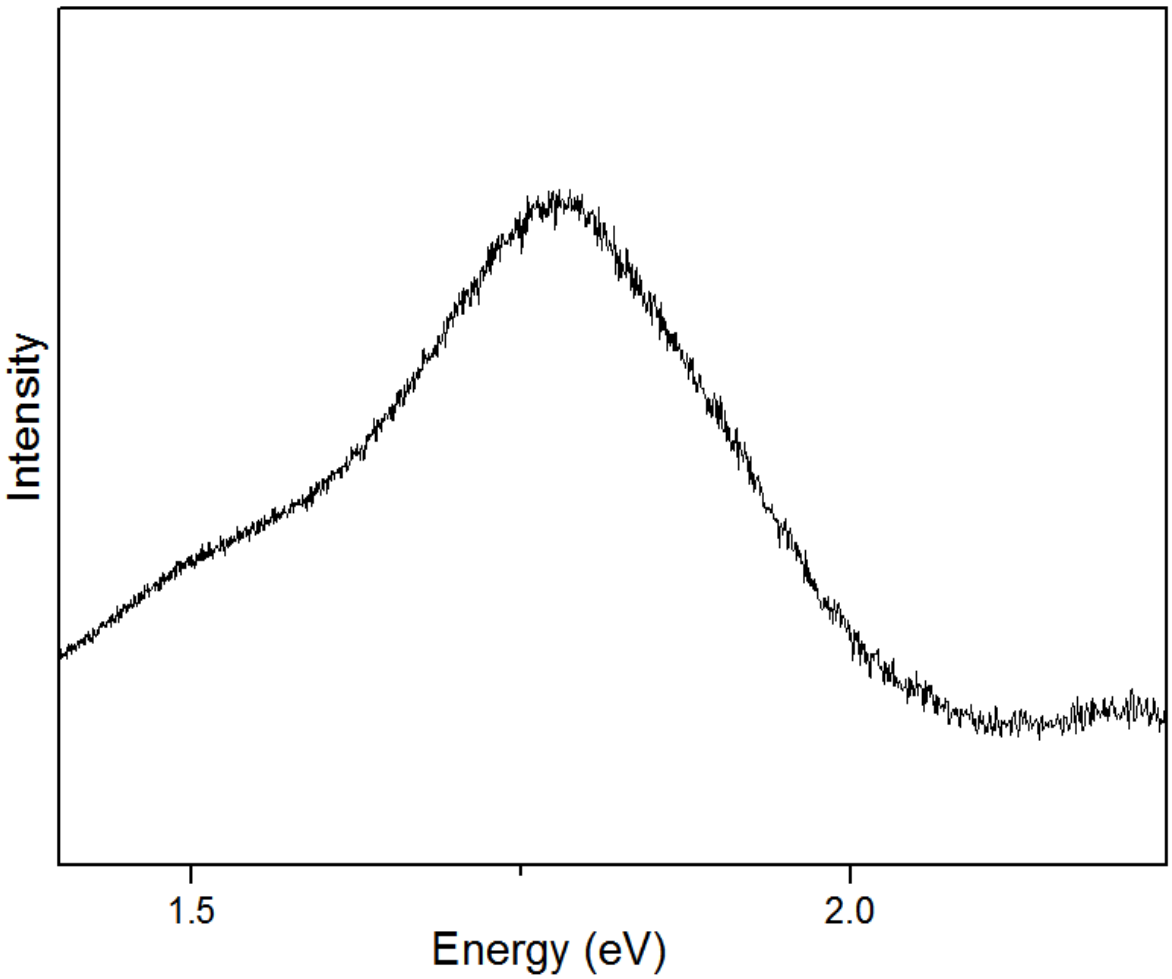

Figure 4.34. PL result for the Br-I tin Perovskite which is produced with DMSO.

4.5. Further Investigations

In this section, further investigations will be discussed, which cannot fit to the other sections. The effects of the glass surface on coverage, the simulation of low-budget chemical vapor deposition and the electrical characterization step will be discussed in subsections.

4.5.1. Effects of the Glass Surface

In order to increase the coverage of the material, there is commercial mesoporous titania coated glasses. The covered PV material can be held on pores by this type of glasses.

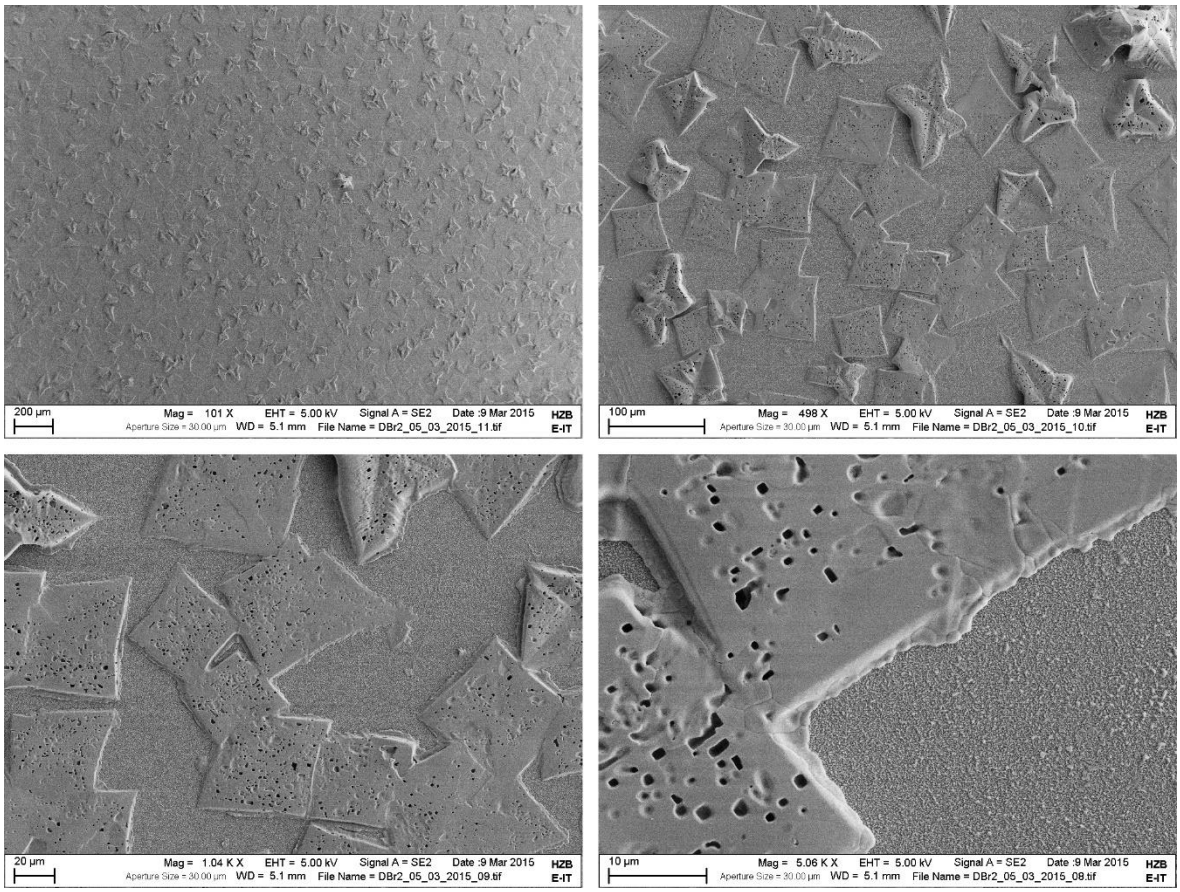

Figure 4.35. SEM images of the $MASnIBr_2$ crystals on FTO (Around 100X, 500X, 1000X and 5000X, respectively).

In Figure 4.35., there is no extra captivating coating on FTO glass. The amorphous FTO material can be observed between the crystals, which means the coverage is not so good. Nevertheless, the crystals looked like cubical as they were supposed to be.

On the other hand, there was scaffolding titania layer under the active PV material in Figure 4.36. Although the coverage was comparatively better, the crystals did not look like perfectly cubical.

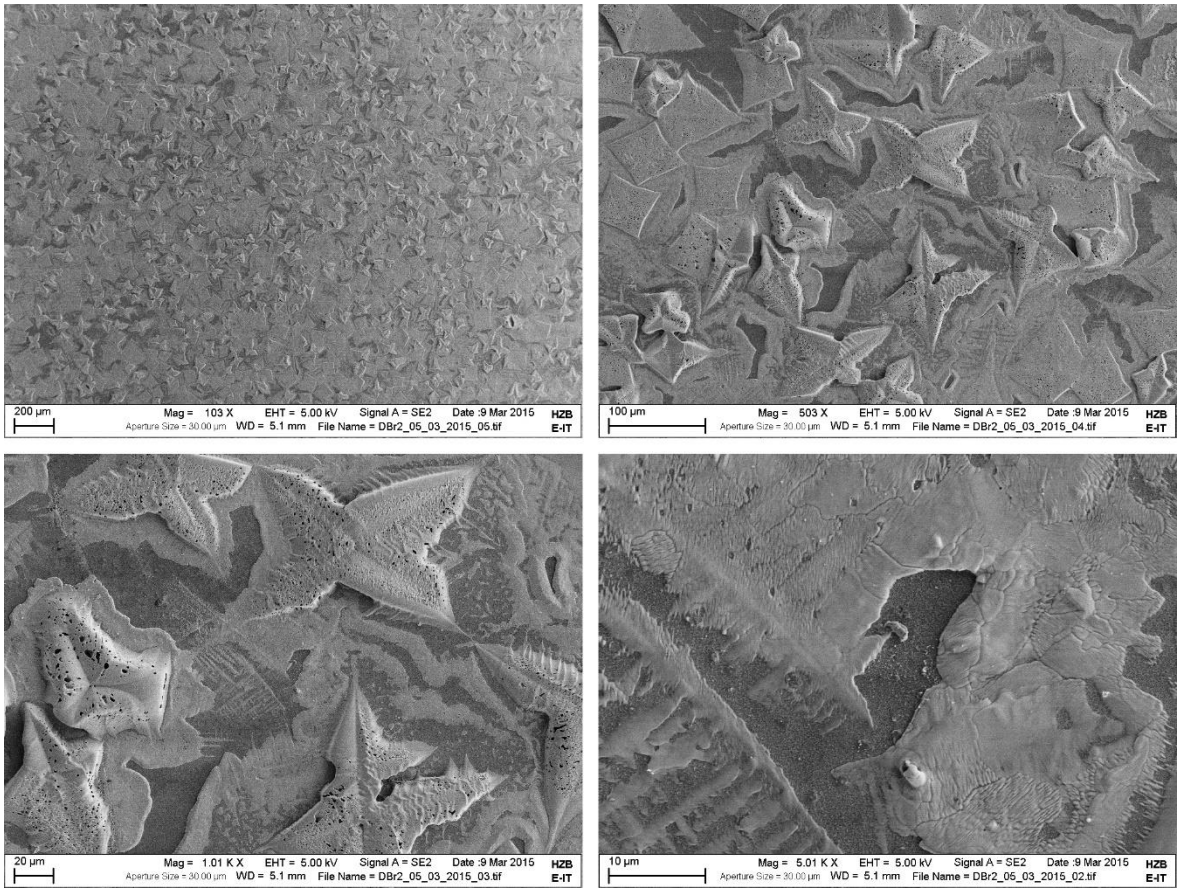

Figure 4.36. SEM images of the $MASnIBr_2$ crystals on titania (Around 100X, 500X, 1000X and 5000X respectively).

Due to the fact that both Perovskite layers in Figures 4.35. and 4.36. provide the identical XRD and PL results, there is no structural difference between them. However, the one, which is coated on titania as shown in the Figure 4.36., has a better coverage, therefore, it can offer a better selection.

4.5.2. Simulated Chemical Vapor Deposition

Chemical vapor deposition is a promising technique for the investigations of the thin film solar cells since controlling of layer thicknesses is easier than the other techniques. Moreover, it is likely to see the limits of the solar cells by producing the solar cells with optimum layer thicknesses.

On the other hand, the worst disadvantage of this process is the cost. Therefore, we tried to simulate it in a cheapest way to have a perception. The first step was similar to the two

step method, which meant that the glasses were coated with inorganic salts by using spin coater. Then, they were sealed in a petri dish to complete the reaction with evaporated MAI as seen in Figure 4.37.

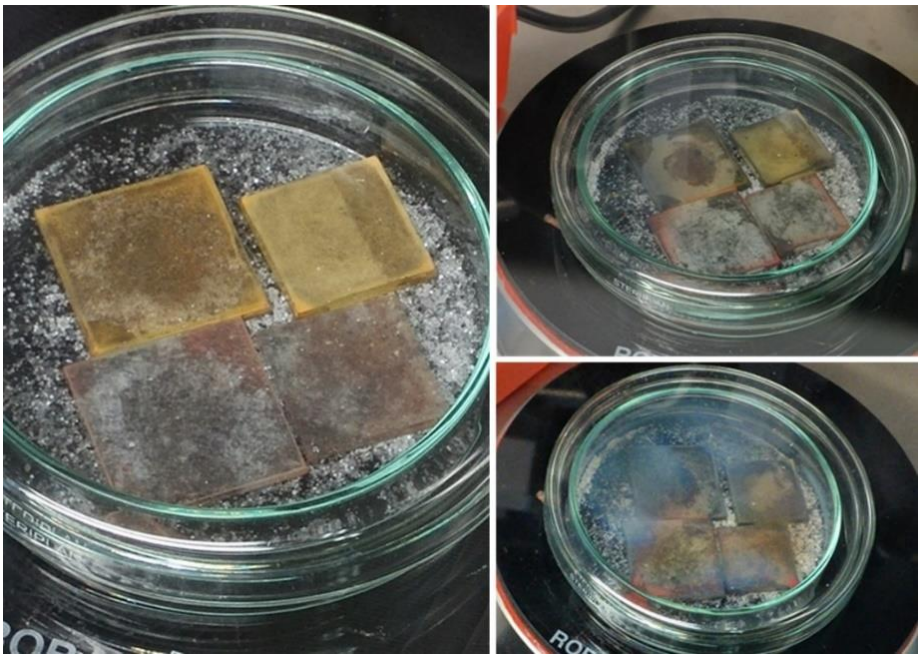

Figure 4.37. Low-budget CVD method simulation.

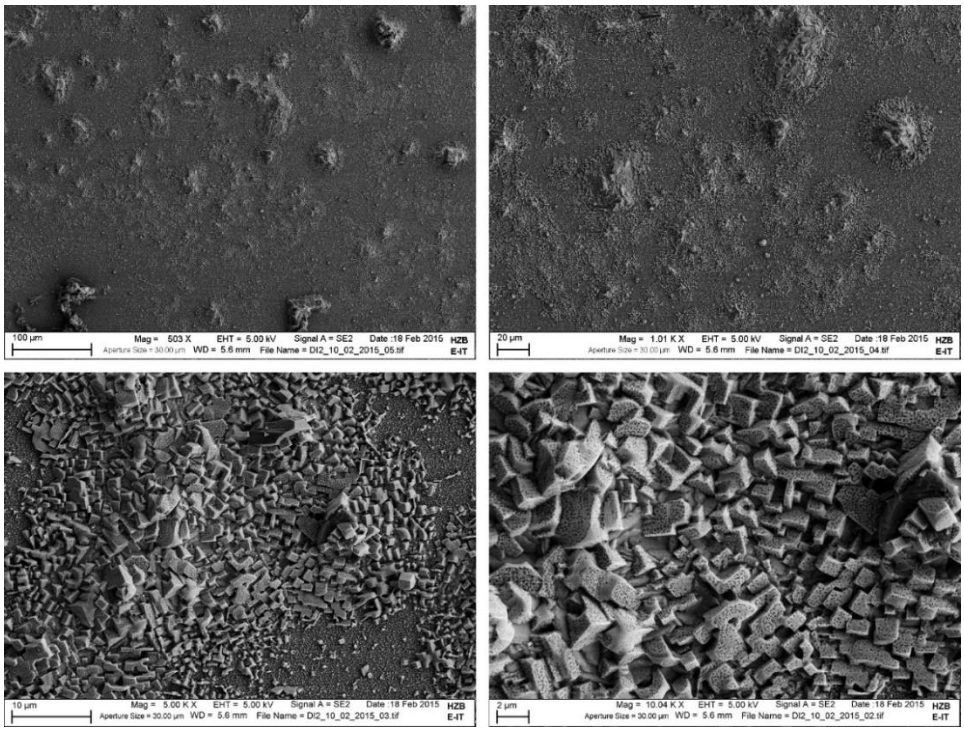

Figure 4.38. SEM images of the $MASnI_3$ crystals of simulated CVD.

As can be seen in Figure 4.38., the produced tin iodide Perovskites were shaped in cubical structure, as they were supposed to be. Though, the low-budget simulation of the CVD method could not provide the equal distribution for the crystals. They were gathered at some points as islands.

4.6. Overall Evaluation of the Experimental Work

The exchange of harmful lead content in Perovskite with tin was successfully conducted by both one step method and the solid-state method. Then, different tin Perovskites were produced with different halogens and they were compared with each other in terms of the obtained band gap energies from PL results of the specimens and the active layer coverage, since obtaining the material with higher coverage and useful band gap energy was the main objective of this work.

As instrumental characterizations, XRD, SEM, Uv-Vis and PL measurements were successfully conducted for the material characterization.

When the experimental materials were obtained, they were verified by XRD and PL if their band gap energy was known. If the band gap energy was not known, then PL and Uv-Vis were used to find it out. The found band gap energies, which can be seen in Table 4.1., were verified with each of the one step method and the solid-state reaction method.

Table 4.1. Experimental band gap energy results

Material	**Band Gap Energy (eV)**
$MASnI_3$	1.3
$MASnIBr_2$	1.76
$MASnICl_2$	Material could not be obtained.
$MASnCl_3$	E_g is higher than the efficient solar cell range.

Moreover, the band gap energies were identical for replaced DMSO solvent instead of DMF. Acetone could have been another option for solvent replacement, since it was also a polar aprotic solvent like DMF and DMSO, but it just partially dissolved the precursors due to its weak solvent properties. The occurred reaction of partially dissolved precursors

showed that solid-state reaction could be used for the process as well, because all the solvent vaporized during the annealing, however, the reaction was completed anyway.

SEM was used for observing the coverage of active materials. Different reaction methods were investigated in order to acquire higher coverage ratio, and consequently higher efficiency due to lower band gap energies of the materials. Since the vapor deposition method was not cost-effective for Perovskite production due to its high vacuum, high temperature and high initial investment costs, it was not used in this work. The two step method (the sequential deposition method) was implemented for each tin salt materials, and it was seen that the two step method was not applicable for tin salts, due to their high solubility in polar protic solvents, which were used in second layer solutions. When the vapor deposition and the two step methods were eliminated, the parameters were examined for the one step and the solid-state methods. Although the one step method was widespread in literature, the solid state reaction was the most efficient one for the coverage. Now that it resulted in bigger crystal production and increase in the number of the crystals due to the seed formation during the solid-state reaction, the coverage increased visibly around by 10 %.

Consequently, the solid-state reaction was selected as the optimum reaction type for further works. When the proper reaction type was selected, another investigation for the optimum reaction temperature and the optimum annealing time were carried out. For the solid state reaction, 120°C was selected as the optimum reaction temperature and 2 hours annealing time was set according to the optimum annealing time investigation.

When the parameters (e.g. optimum reaction temperature and optimum annealing time) were fixed, production attempts of the novel perovskite materials were initiated. Whereas the chlorine-iodine mixed tin Perovskite production was not possible due to the big difference between iodine and chlorine nucleophilicity, it was possible to produce mixed bromine-iodine one, since the nucleophilicity of these two halide were closer. If the stability condition can be provided, 1.7 eV band gap energy for the bromine-iodine mixed tin Perovskite may be very useful to obtain high efficiency with its low cost. With the help of band gap engineering, it may even be possible to have lower band gap energy by using methylammonium bromide and tin (II) iodide salt as precursors for further researches.

Different concentrations of the precursors and different precursor ratios were also investigated. When 60 % (wt) and 40 % (wt) precursor to solution concentrations were used for the mixed halide tin Perovskite, it was observed that iodine ratio of the mixed Perovskite was higher in the structure. So that high concentration of the precursors increased the rate of the reaction, they drove the reaction to the more stable side, which had a higher iodine ratio. High concentration provided comparatively better coverage as well. However, 60 % was not the highest concentration that could be achieved, therefore, concentration optimization could be done according to the desired final product.

Another investigation for different substrate usage to obtain high coverage ratio was held. Fluorine doped tin oxide (FTO) coated layer was used for the first experimental group since FTO was former layer in the solar cells. For the second group, substrates which have mesoporous titania layer on FTO were used. The task of titania was holding materials inside the pores on the substrate while spin coating. Thus, the coverage would be higher after the annealing procedure. With the usage of titania, the coverage was improved as expected. However, it was seen that the Perovskite crystal shapes on titana were not cubic on SEM images while the Perovskite crystal shapes on the bare FTO glass were perfectly cubical. Though, XRD results of both groups verify that they all have cubic structure. Thus, it was just a physical appearance and post-annealing can be used in further investigations to observe whether it can be handled or not.

Even though the aim of the experimental work was obtaining different mixed halide tin Perovskites with higher coverage ratio and lower band gap energies in order to have higher theoretical efficiencies, the electrical device characterization, which can be seen in the appendix, was held. As electrical device characterization, the measurement for current-voltage (I-V) curve was done, but it was not successful, since the HTM layer optimization needed a longer period of time.

5. CONCLUSIONS AND RECOMMENDATIONS

The following conclusions can be drawn from the experimental work conducted within the scope of this study;

Due to the low stability of the active PV material, all the tin Perovskite experiments should be done in a glovebox, which provides better working conditions in an inert atmosphere. Otherwise, all the samples degrade in seconds. Moreover, the precursors should be kept in an inert atmosphere due to their hygroscopic properties.

During the experimental work, the crystal sizes of the selected materials were improved for each material, but they were not good enough to cover all the surface. Pure iodine tin Perovskite or bromine-iodine mixed tin Perovskite should be chosen in order to be focused on, since chlorine-iodine mixed tin Perovskite production was not possible.

Commonly used, harmful DMF solvent was substituted with the environmental friendly DMSO. Acetone was found out not to be a good medium for the reaction, but it might still be used for some small experiments, since the reaction did not require any solvent. At our limited trials, we could not manage to have good coverage results for acetone. On the other hand, DMSO was a good replacement with its environmentally friendly properties. Moreover, DMSO is not harmful to health which is good for non-automatic production lines.

HTM layer optimization should be done as a future investigation. Spiro-MeOTAD is the best HTM option for lead-Perovskites. However, Spiro-MeOTAD needs to be oxidized to work properly as an HTM, and tin Perovskites are too hygroscopic to stay without degradation during the oxidation process of Spiro-MeOTAD. For this reason, Spiro-MeOTAD may be considered to replace. When the HTM optimization is done separately, the electrical characterization can be done as a further investigation.

REFERENCES

Abrahams, I., Demetriou, D.Z., 2000. Inert pair effects in tin and lead dihalides: Crystal structure of tin (II) bromide, Journal of Solid State Chemistry, 149, 28-32.

Akyüz, E., Bayraktar, M., Oktay, Z., 2009. A feasibility study on hybrid renewable energy systems for the industrial broiler sector: An application, Balıkesir Üniversitesi FBE Dergisi, 11, 2, 44-54.

Appleyard, D., 2012. PV Technology: Swapping Silver for Copper, Renewable Energy World International, http://www.renewableenergyworld.com/articles/print/volume-15/issue-3/solar-tech/pv-technology-swapping-silver-for-copper.html.

Batsanov, S.S., 2001. Van der Waals radii of elements, Inorganic Materials, 37, 9, 871-885.

Brabec, C.J., Durrant, J.R., 2008. Solution-processed organic solar cells, Material Research Society Bulletin, 33, 670-675.

Burn, P.L., Meredith, P., 2014. The rise of the Perovskites: The future of low cost solar photovoltaics?, Nature Publishing Group Asia Materials, 6, 79-79.

Burschka, J., 2013. High Performance Solid-state Mesoscopic Solar Cells, Ph.D. Dissertation, École polytechnique fédérale de Lausanne.

Chiarella, F., Zappettini, A., Licci, F., Borriello, I., Cantele, G., Ninno, D., Cassinese, A., Vaglio, R., 2008. Combined experimental and theoretical investigation of optical, structural, and electronic properties of $CH_3NH_3SnX_3$ thin films (X=Cl,Br), Physical Review B, 77, 045129.

Chung, I., Lee, B., He, J., Chang, R.P.H., Kanatzidis, M.G., 2012. All-solid-state dye-sensitized solar cells with high efficiency, Nature, 485, 486–489.

Dağdaş, A., 2005. Energy cost of geothermal power plants, Sigma Journal of Engineering and Natural Sciences, 2, 84-94.

Dennler, G., Brabec, C., 2008. Organic Photovoltaics, Wiley-VCH, Weinheim, 531-566.

Energy Market Regulatory Authority (EMRA), 2013. Electricity Production without Licence, http://www.epdk.org.tr/documents/elektrik/mevzuat/yonetmelik/elektrik/lisanssiz_elektrik_uretimi/Elk_Ynt_Lisanssiz_Elektrik_Uretimi_ilkhali.docx.

Ewald, P.P., 1962. 50 Years of X-ray Diffraction, N.V.A. Oosthoek's Uitgeversmaatschappij, Utrecht, Netherlands.

Etgar, L., Gao, P., Xue, Z., Peng, Q., Chandiran, A.K., Liu, B., Nazeeruddin, M.K., Grätzel, M., 2012. Mesoscopic $CH_3NH_3PbI_3/TiO_2$ heterojunction solar cells, Journal of the American Chemical Society, 134, 17396–17399.

Frahm, E., 2014. Scanning Electron Microscopy (SEM): Applications in Archaeology, Encyclopedia of Global Archaeology, 6487-6495.

Feltrin, A., Freundlich, A., 2008. Material considerations for terawatt level development of photovoltaics, Renewable Energy, 33, 180–185.

Fraunhofer Institite for Solar Energy Systems, 2013. Levelized Cost of Electricity Renewable Energy Technologies Study, 36-37.

Gao, P., Nazeeruddin, M.K., Grätzel, M., 2014. Organohalide lead Perovskites for photovoltaic applications, Energy & Environmental Science, 7, 2448-2463.

Green, M.A., Ho-Baillie, A., Snaith, H.J., 2014. The emergence of Perovskite solar cells, Nature Photonics, 8, 506-514.

Gong, X.G., Xiang, H.J., Liu, H.R., Yang, J.H., Lang, L., 2013. First-principles study on the electric and optical properties of cubic ABX_3 halide Perovskites, Physics Letters A, 378, 290-293.

Goswami, D.Y., Kreith, F., Kreider, J.F., 2000. Principles of Solar Engineering, 2nd ed., Taylor & Francis Group, New York.

Grätzel, M., 2014. The light and shade of Perovskite solar cells, Nature Materials, 13, 838-842.

Hull, A.W., 1919. A new method of chemical analysis, Journal of the American Chemical Society, 41, 8, 1168–1175.

Jacobson, M.Z., Delucchi, M.A., 2010. Providing all global energy with wind, water, and solar power, Part I: Technologies, energy resources, quantities and areas of infrastructure, and materials, Energy Policy, 39, 1154–1169.

Jayakrishnan, R., 2008. Defect Analysis of Semiconductor Thin Films for Photovoltaic Applications Using Photo-luminescence and Photo-conductivity, Ph.D. Dissertation, Cochin University of Science and Technology.

Joskow, P.L., 2011. Comparing the costs of intermittent and dispatchable electricity generating technologies, American Economic Review: Papers & Proceedings, 100, 3, 238-241.

Jørgensen, M., Norrman, K., Krebs, F.C., 2008. Stability/Degradation of Polymer solar cells, Solar Energy Materials & Solar Cells, 92, 686–714.

Kamp, M., Bartsch, J., Nold, S., Retzlaff, M., Hörteis, M., Glunz, S., 2011. Economic evaluation of two-step metallization processes for silicon solar cells, Energy Procedia, 8, 558–564.

Kanatzidis, M.G., Chang, R.P.H., Cao, D.H., Stoumpos, C.C., Hao, F., 2014. Lead-free solid-state organic–inorganic halide Perovskite solar cells, Nature Photonics, 8, 489-494.

Kanatzidis, M.G., 2014. Novel Luminescent Materials for a Concentrator Approach to Enhanced Efficiency Solar Energy Conversion, https://isen.northwestern.edu/doc/pdf/Booster_MKanatzidis.Oct11_Final.Narrative.Report.pdf.

Kim, H.S., Lee, C.R., Im, J.H., Lee, K.B., Moehl, T., Marchioro, A., Moon, S.J., Humphry-Baker, R., Yum, J.H., Moser, J.E., Grätzel, M., Park, N.G., 2012. Lead iodide Perovskite sensitized all-solid-state submicron thin film mesoscopic solar cell with efficiency exceeding 9%, Scientific Reports, 2, 591.

Krebs, C.F., 2008. Polymer Photovoltaics: A Practical Approach, SPIE, Washington.

Lee, M.M., Teuscher, J., Miyasaka, T., Murakami, T.N., Snaith, H., 2012. Efficient hybrid solar cells based on meso-superstructured organometal halide Perovskites, Science, 338, 643–647.

Lee, M.M., Ball, J.M., Hey, A., Snaith, H.J., 2013. Low-temperature processed meso-superstructured to thin-film Perovskite solar cells, Energy & Environmental Science, 6, 1739–1743.

Mitzi, D.B., Liang, K., Prikas, M.T., 1998. Synthesis and characterization of organic-inorganic Perovskite thin films prepared using a versatile Two-step Dipping technique, Chemistry of Materials, 10, 403-411.

Miyasaka, T., Shirai, Y., Teshima, K., Kojima, A., 2009. Organometal Halide Perovskites as visible-light sensitizers for photovoltaic cells, Journal of American Chemical Society, 131, 6050-6051.

Møller, C.K., 1957. A phase transition in Caesium Plumbochloride, Nature, 180, 981-981-982.

Nara, J., Adachi, S., 2011. Optical properties of $SnCl_2$ phosphor, Journal of Applied Physics, 109, 083539.

Ogomi, Y., Morita, A., Tsukamoto, S., Saitho, T., Fujikawa, N., Shen, Q., Toyoda, T., Yoshino, K., Pandey, S.S., Ma, T., Hayase, S., 2014. $CH_3NH_3Sn_xPb_{(1-x)}I_3$ Perovskite solar cells covering up to 1060 nm, The Journal of Physical Chemistry Letters, 5, 1004–1011.

Pandian, M.S., 2014. X-ray Diffraction Analysis: Principle, Instrument and Applications, Pondicherry University, India, http://www.academia.edu/6371935/X-ray_Diffraction_Analysis_Principle_Instrument_and_Applications.

Park, N.G., Im, J.H., Lee, C.R., Lee, J.W., Park, S.W., 2011. 6.5% efficient Perovskite Quantum-Dot-Sensitized solar cell, Nanoscale, 3, 4088−4093.

Park, N.G., 2013. Organometal Perovskite light absorbers toward a 20% efficiency low-cost Solid-state mesoscopic solar cell, The Journal of Physical Chemistry Letters, 4, 2423-2429.

Peplow, M., 2014. The Perovskite revolution, IEEE Spectrum, 51, 7, 16-17.

Pivrikas, A., 2011. Relation between Nanomorphology and Performance of Polymer-Based Solar Cells. In Kosyachenko, L.A., (Ed.), Solar Cells: New Aspects and Solutions, InTech, Rijeka, 124.

Rehman, A., Lee, S.H., 2014. Review of the potential of the Ni/Cu plating technique for crystalline silicon solar cells, Materials, 7, 1318-1341.

Service, R.F., 2014. Perovskite solar cells keep on surging, Science, 344, 458-458.

Shaheen, S.E., Ginley, D.S., Jabbour, G.E., 2005. Organic-based photovoltaics: toward low-cost power generation, Material Research Society Bulletin, 30, 10-15.

Smith, K.C.A., Oatley, C.W., 1955. The scanning electron microscope and its fields of application, British Journal of Applied Science, 6, 391-399.

Snaith, H.J., Herz, L.M., Petrozza, A., Johnston, M.B., Pathak, S.K., Eperon, G.E., Sadhanala, A., Haghighirad, A.A., Guarnera, S., Wehrenfennig, C., Abate, A., Stranks, S.D., Noel, N.K., 2014. Lead-free organic–inorganic tin halide Perovskites for photovoltaic applications, Energy & Environmental Science, 7, 3061-3068.

Solaronix SA, Swiss supplier for solar cell materials, shop webpage for Perovskite cell kits. http://www.solaronix.com/documents/solaronix_materials.pdf

Tams, C., Enjalbert, N., 2009. The Use of UV/Vis/NIR Spectroscopy in the Development of Photovoltaic Cells, Application Note, PerkinElmer, Massachusetts, USA, http://www.perkinelmer.com/pdfs/downloads/APP_UseofUVVisNIRinDevelopmentPV.pdf.

Teleke, S., Baran, M.E., Bhattacharya, S., Huang, A.Q., 2010. Rule-based control of battery energy storage for dispatching intermittent renewable sources, IEEE Transactions on Sustainable Energy, 1, 3, 117-124.

ThermoARL, 1999. Basics of X-Ray Diffraction, Ecublens, Switzerland, http://old.vscht.cz/clab/RTG/dokumenty/thermo/xrd/Introduction%20to%20powder%20diffraction.pdf.

Tidhar, Y., Edri, E., Weissman, H., Zohar, D., Hodes, G., Chaen, D., Rybtchinski, B., Kirmayer, S., 2014. Crystallization of Methyl Ammonium Lead Halide Perovskites: Implications for photovoltaic applications, Journal of the American Chemical Society, 136, 13249−13256.

Trupke, T., Mcmillan, W., 2010. Photovoltaics: Photoluminescence Imaging Speeds Solar Cell Inspection, Laser Focus World, 46, 12, http://www.laserfocusworld.com/articles/print/volume-46/issue-12/features/photovoltaics-photoluminescence-imaging-speeds-solar-cell-inspection.html.

UK Trade & Investment, 2012, Renewables Sector in Turkey, http://www.ukti.gov.uk/export/countries/europe/southerneurope/turkey/sectorbriefing/360320.html, 2013.

Wadia, C., Alivisatos, A.P., Kammen, D.M., 2009. Materials availability expands the opportunity for large-scale photovoltaics deployment, Environmental Science and Technology, 43, 2072–2077.

Wang, L., Niu, G., Guo, X., 2015. Review of recent progress in chemical stability of Perovskite solar cells, Journal of Material Chemistry A, 2015, 3, 8970-8980.

Yang, Y., Liu, Y., You, J., Hong, Z., Duan, H.S., Song, T., Luo, S., Li, G., Chen, Q., Zhou, H., 2014. Interface engineering of highly efficient Perovskite solar cells, Science, 345, 542-546.

Yin, W.J., Yang, J.H., Kang, J., Yan, Y., Wei, S.H., 2015. Halide Perovskite materials for solar cells: a theoretical review, Journal of Material Chemistry A, 3, 8926-8942.

Yüksel, A., 2011. Turkey Moves to Boost Renewable Energy; new feed-in tariffs and other incentives for renewable energy, Project Finance Newswire, http://www.chadbourne.com/Turkey_Renewable_Energy_projectfinance.

Yüksel, A., Şahbaz, D., İnal, E., 2013. Sunny days ahead for solar in Turkey, Infrastructure Journal, 1-4.

APPENDIX:

ELECTRICAL CHARACTERIZATION

Electrical characterization is another characterization tool employed for the solar devices, but this characterization is an advanced level. It needs all the layers to be perfectly coated and the solar device was ready to measure.

Since the scope of this research was about the active material synthesis and characterization, the electrical characterization was not exactly applicable, because of the fact that another study could be conducted in order to optimize the next layer, which was a hole transport layer (HTM). However, a recipe for HTM layer, which was optimized for lead Perovskite, was used in order to have a chance to apply the electrical characterization as a trial.

After the coating process of the active PV material, which was called tin Perovskite, the spiro-MeOTAD as a hole transport material (HTM) was coated and gold was coated as a back contact. The spiro-MeOTAD is transparent, but the gold contact can be seen in Figure A.1.

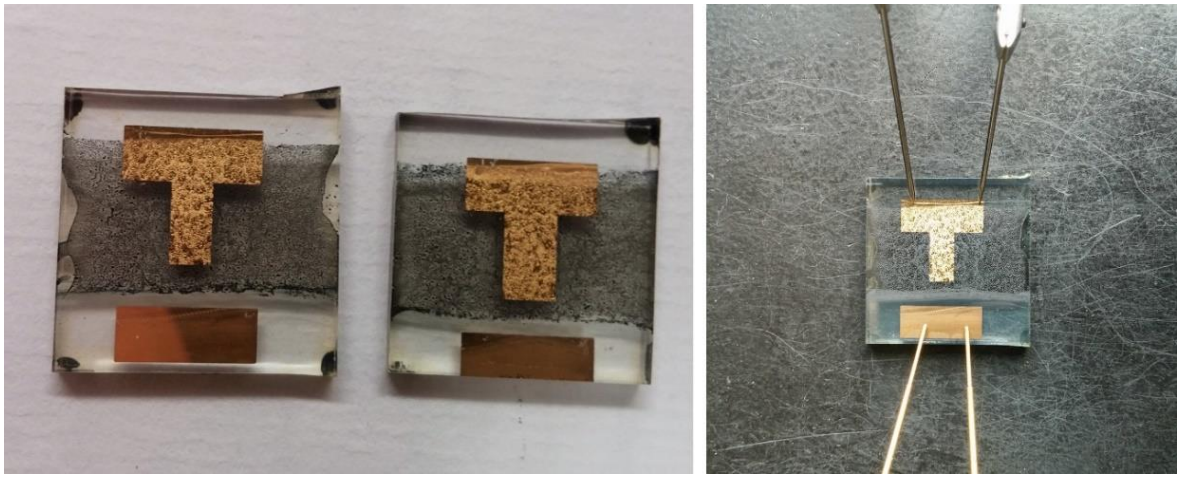

Figure A.1. Spiro-MeOTAD and gold back contact coatings.

Thus, the solar cells, which were coated with tin Perovskite, turned into the solar devices. As can be seen in Figure A.2., the devices were measured under the solar simulator which provided light having the identical sunlight spectrum.

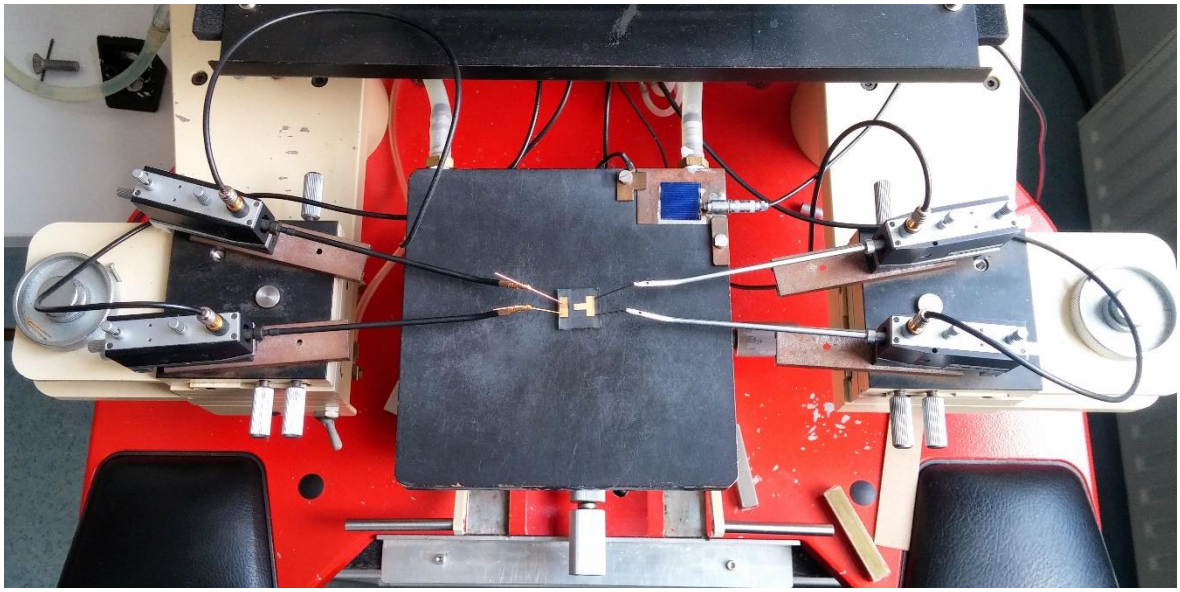

Figure A.2. Electrical characterization under the solar simulator.

Unfortunately, the devices could not produce any noteworthy current and voltage even though the material was totally photovoltaic. This could be a consequence of unoptimized HTM layer or short-circuit due to the poor coverage of active material.